Development and Analysis of WSR-88D Hydrometeorological Algorithms

James A. Smith
Mary L. Baeck
Matthias Steiner

Department of Civil and Environmental Engineering
Princeton University
Princeton, NJ 08544

September 2002

1. Introduction

Work during the year 2001-2002 has centered on analyses of WSR-88D rainfall rate estimates for warm season, high rainfall rate events. Much of the effort has involved analyses of observations from the Sterling WSR-88D, with special focus on the Baltimore metropolitan region. This focus is due to availability of unique ground validation data for the Baltimore region. A significant part of these analyses, which are presented in Section 2, has been assessment of rainfall estimates at space and time scales relevant to urban flash flood forecasting. Analyses of WSR-88D rainfall estimates have also been carried out for the 21-22 September 1998 Puerto Rico storm (Hurricane Georges) and 23 July 1997 Charlotte storm. These analyses are summarized in Sections 3 and 4.

A new element of WSR-88D rainfall rate assessments involves the use of U. S. Geological Survey (USGS) discharge measurements. The Baltimore District office of the USGS has provided "unit values" discharge data from 26 drainage basins in the Baltimore metropolitan region. Many of these stations are part of the Baltimore Ecosystem Study (BES) and were deployed in the late 1990s. Drainage area for the 26 basins ranges from 0.08 km^2 to 171 km^2. The time increment of the discharge data ranges from 1 minute to 15 minutes. Land use ranges from forested to urban with high impervious cover. We have selected 7 of the stations (see Section 2), each with drainage area less than 25 km^2 and significant urban/suburban development, as basins for "gage-radar" intercomparisons. USGS discharge observations also play an important role in the Puerto Rico and North Carolina analyses presented in Sections 3 and 4.

In many urban settings, flash flood hazards are characterized by basin scales smaller than 10 km^2 and response times less than 1 hour. We examine the utility of WSR-88D rainfall estimates for quantitative flash flood forecasting in small urban basins. The Baltimore (Section 2) and Charlotte (Section 4) analyses provide strong support for the utility of flash flood procedures like AMBER and the extension of flash flood forecasting procedures to site-specific quantitative discharge forecasts.

Stream gage observations also play a central role in analyses of WSR-88D rainfall estimates from Hurricane Georges and the 23 July 1997 storm in Charlotte. For Hurricane Georges, the focus is radar estimation of catastrophic, flood-producing rainfall from a tropical storm in complex terrain. Beam blockage, partial beam blockage and orographic amplification of rainfall are all important elements of the rainfall estimation problem.

2. Baltimore Hydrometeorological Analyses

We have obtained and processed Archive II data from the Sterling radar for a number of storm events during the period 1996 – 2002. In this report, we present analyses for 12 events during the warm season of 2000. The dates for these events are: 21 April, 13 May, 15 June, 22 June, 25-26 June, 26 June, 14 July, 15 July (storm 1), 15 July (storm 2), 16 July, 27 August, and 28 August. These 12 storm periods include all of the significant flash flood events in the Baltimore metropolitan region during the warm season of 2000.

As noted in the Introduction, we will use USGS discharge observation for intercomparison with Sterling rainfall estimates. Basins used for "gage"-radar intercomparisons (see Fig. 2.1) are: White Marsh Run at Fullerton (7.1 km^2), North Fork White Marsh Run (3.5 km^2), Minebank Run (7.5 km^2), Moores Run (9.1 km^2), Moores Run tributary (0.54 km^2), Dead Run (14.2 km^2) and Rognel Heights storm sewer (0.08 km^2). For each of the basins larger than 1 km^2 the basin has been extracted from 30 meter USGS DEMs. For these basins, we have determined the 1 km radar pixels for the Sterling WSR-88D that are contained within the basin (including the fractional coverage of pixels that are partially contained in the basin). This mapping of radar pixels to basin area is used to construct basin-averaged rainfall rate time series for each of the basins. For basins smaller than 1 km^2, we determine the 1 km radar pixel containing the basin.

Rainfall estimates were computed using the default Z-R relationship, $Z = 300R^{1.4}$ and a 55 dBZ reflectivity threshold. Time series of basin-averaged rain rates were developed by averaging rainfall rates over the drainage basin. For each 1 km radar bin,

we determine the fraction of the bin which is contained within the basin. The basin-averaged time series represent the fractional coverage of individual bins. It should be noted that the range of the radar from Baltimore is approximately 100 km so that the polar resolution of reflectivity observations is somewhat larger than 1 km. The polar to Cartesian mapping algorithm is a nearest neighbor algorithm.

Two principal analyses are presented for each event. Storm total rainfall maps were developed for each event and summarized as contour maps (Figure 2.2) with basin boundaries and the boundary of the city of Baltimore. Paired time series of basin-averaged rainfall rate were developed and are presented at 1 minute time interval for radar and 5 minute time interval for discharge (Figure 2.3). Volume scan rainfall estimates (at 5 – 6 minute time interval) were interpolated for each 1 km bin to produce rainfall estimates on a regular 1 minute interval. All rainfall products are then obtained by time and/or space averaging of the regular 1 minute rain products. USGS discharge observations have time intervals ranging from 1 minute to 15 minutes. For graphical purposes, 1 minute time series were aggregated to 5 minute time interval and 15 minute time series were interpolated to 5 minute time interval. All discharge observations are expressed as a "unit discharge", that is discharge in $m^3 s^{-1}$ divided by drainage area in km^2. This facilitates comparison of discharge properties for basins with differing drainage area (note too, that $m^3 s^{-1} km^{-2}$ can be converted to mm h^{-1} by multiplying unit discharge by 3.6). Movie loops are included as electronic supplements (on CD-ROM) for the 21 April, 15 July, 16 July, 27 August and 28 August storm events. Prior to summarizing these analyses, we introduce the major themes of these analyses through a closer examination of four events.

The flood of record for the Moores Run tributary station at a drainage area of 0.54 km^2 was produced by the 21 April 2000 storm (Fig. 2.2a; see also Fig. 2.4 for a reflectivity image at 2153 UTC). The peak unit discharge of 12 $m^3 s^{-1} km^{-2}$ was more than 4 times larger than the peak discharge of the downstream Moores Run station at 9.1 km^2 drainage area (Fig 2.2). The contrasting discharge properties between the Moores Run tributary and Moores Run gaging stations are represented in strong gradients in storm total rainfall over the Moores Run basin (Fig 2.3). The total rainfall period over the Moores Run tributary basin was approximately 15 minutes A major conclusion of

this study is that WSR-88D rainfall estimates can resolve flash-flood producing rainfall at basin scales finer than the 9.1 km^2 scale of the Moores Run basin and the 15 minute time scale of flood –producing rainfall for the 21 April storm over Moores Run.

The 16 July 2000 storm (see Fig.2.5 for Sterling reflectivity image at 1719 UTC) produced the flood of record at the Whitemarsh Fullerton gaging station with a unit discharge of 14 $m^3 s^{-1} km^{-1}$ at 7.1 km^2 scale (note that the 27 June 1995 Rapidan flood peak had a unit discharge peak of only 10 $m^3 s^{-1} km^{-2}$). Storm total rainfall estimates for the 16 July 2000 storm (Fig.2.2 and Fig 2.6 for a blowup over the Whitemarsh Run basin; we include an additional downstream gaging station, Whitemarsh Run at Whitemarsh in Fig. 2.6) over the 20 km^2 Whitemarsh Run watershed ranged from 60 mm along the western margin of the basin above the Fullerton stream gage to 0 mm at the Whitemarsh stream gage. Flood-producing rainfall over the upper Whitemarsh Run basin was concentrated in a period of approximately 60 minutes. The large gradients in rainfall accumulation (Fig. 2.6) over the 20 km^2 Whitemarsh basin for the 16 July storm resulted in striking contrasts in flood response (see Fig. 2.7 for comparative discharge plots for the three Whitemarsh stations). Once again, the key message is that WSR-88D rainfall estimates can resolve flood-producing rainfall at the time and space scales relevant to urban flash flood forecasting.

The 27 and 28 August storms (see Figs. 2.8 and 2.9 for reflectivity images at 2323 UTC on 27 August and 0240 UTC on 28 August) were separated by only a matter of hours but resulted in striking contrasts in flood response. The contrasts are best seen in Moores Run, the basin in which flooding from the 28 August storm was isolated. The 28 August storm was a rapidly-moving Low Echo Centroid (LEC) storm for which the storm total rainfall was 11.9 mm in Moores Run tributary and 12.1 mm in Moores Run at Radeke Avenue. The 28 August storm resulted in the largest runoff ratio (storm total runoff divided by storm total rainfall) of any event during the 2000 warm season with values of 61 % in both Moores Run and Moores Run tributary (7.2 mm / 11.9 mm in Moores Run tributary and 7.4 mm / 12.1 mm in Moores Run). Runoff ratios for the 27 August storm were more typical of analyses for other events with Moores Run tributary having a runoff ratio of 12 % (3.97 mm / 31.8 mm) and Moores Run having a runoff ratio of 13 % (3.5 mm / 26.2 mm).

The 27 and 28 August analyses for Moores Run highlight several issues. Bias correction is an important element of rainfall estimation for flash flood forecasting. The

28 August rainfall estimates, like many LEC storms, are very likely biased low relative to the 27 August rainfall estimates. We have not integrated rain gage observations into a bias correction procedure, in part to illustrate the properties of radar rainfall estimates absent additional rain gage information and in part because there were not adequate rain gage observations for bias correction in the Baltimore region. It should also be noted that for the 27 August rainfall runoff analyses in Moores Run, as with analyses in other basins and for other events, a large fraction of the storm total rainfall is partitioned to infiltration and storage (in particular, detention basins). These storage processes are illustrated in Fig. 2.10 for Whitemarsh run through scatterplots of storm total rainfall and runoff for all events (note the different scales for the two axes). Both Moores Run and Whitemarsh Run have relatively large fractions of the basin in impervious cover (approximately 30%), yet runoff ratios, especially for smaller storm total accumulations, are often smaller than the impervious fraction of the basin. Interpretation of radar rainfall – discharge analyses (Fig. 2.3) and development of flash flood forecasting procedures that utilize WSR-88D rainfall estimates need to account for these storage processes. We summarize below inferences that can be drawn from the gage-radar time series plots in Figure 2.3.

The agreement in timing and relative magnitudes between the Rognel Heights discharge observations and rainfall rates estimates is excellent (recall that Rognel Heights has a drainage area of 0.08 km^2 and is completely drained by storm sewers). For the 13 May storm, the rainfall rate and discharge time series overlap. For the 15 June event, the initial peak is followed by two smaller discharge peaks, each associated with a short burst of moderate intensity rainfall. For the 22 June event, the initial discharge peak is followed by a second peak for which there is no associated pulse of rainfall. In the stratiform rainfall that follows during the next 2 hours, each small peak in rainfall is followed by a discharge peak. The most striking relationship between rainfall and discharge in the Rognel Heights area is for the first 26 June storm. Four short pulses of rainfall are followed by four sharp peaks in discharge. Runoff ratios for the Rognel Heights observations range from less than 5 % to no more than 14 %.

The Moores Run analyses, like the Rognel Heights observations, show excellent agreement in timing and relative magnitude of rainfall and discharge (see, for example,

the first 26 June storm; the drainage area of the Moores Run tributary gage is 0.54 km^2 and the downstream Radeke Avenue gaging station has an upstream area of 9.1 km^2). As noted above, the contrasts in runoff and peak discharge between the two Moores Run gaging stations is clearly related to the spatial distribution of rainfall (as illustrated in Fig. 2.2).

The 14 July event produced the largest storm total accumulation of any event during the warm season of 2000. The peak rainfall accumulation of more than 250 mm (Fig. 2.2) was east of the Moores Run basin. The Moores Run gaging stations were rendered inoperative by the flood. There are no discharge observations from the Radeke Avenue station for the entire series of flood events during the period 14 – 16 July. The tributary gage was functioning after 14 July.

The timing and magnitude of flood response varies widely across the Baltimore draingage basins. Minebank Run has slower response times, lower flood peaks and smaller runoff ratios than basins of comparable size. Similar conclusions can be drawn concerning Dead Run. There is also a notable contrast in hydrograph shape between Dead Run and Minebank Run. Although response times in Minebank Run are on the order of 30 minutes, the rise to peak is very rapid. For the 15 June storm, Minebank Run increases from baseflow to peak discharge in a single time period. The Dead Run response is characterized by a more gradual hydrograph rise to peak. For Dead Run, detention storage plays a major role in flood response properties.

CONCLUSIONS:

WSR-88D rainfall estimates for the Baltimore metropolitan region resolve rainfall variability at time scales (less than 60 minutes) and spatial scales (less than 4km) that are characteristic of urban flash flooding. Even for small drainage basins (less than 1 km^2), the agreement in timing and relative magnitudes of radar rainfall estimates and discharge is exceptional. Analyses of discharge and storm total rainfall illustrate the capability of resolving gradients in flash flood producing rainfall on length scales of 1 – 10 km. Water balance analyses indicate that even for basins with relatively large impervious cover, infiltration losses and abstractions for detention storage are a major component of the water budget. Bias in radar rainfall estimates was not directly examined, but the relative

contrasts in rainfall – discharge analyses between the 27 August and 28 August storms demonstrate the importance of bias correction for quantitative flash flood assessments in urban drainage basins.

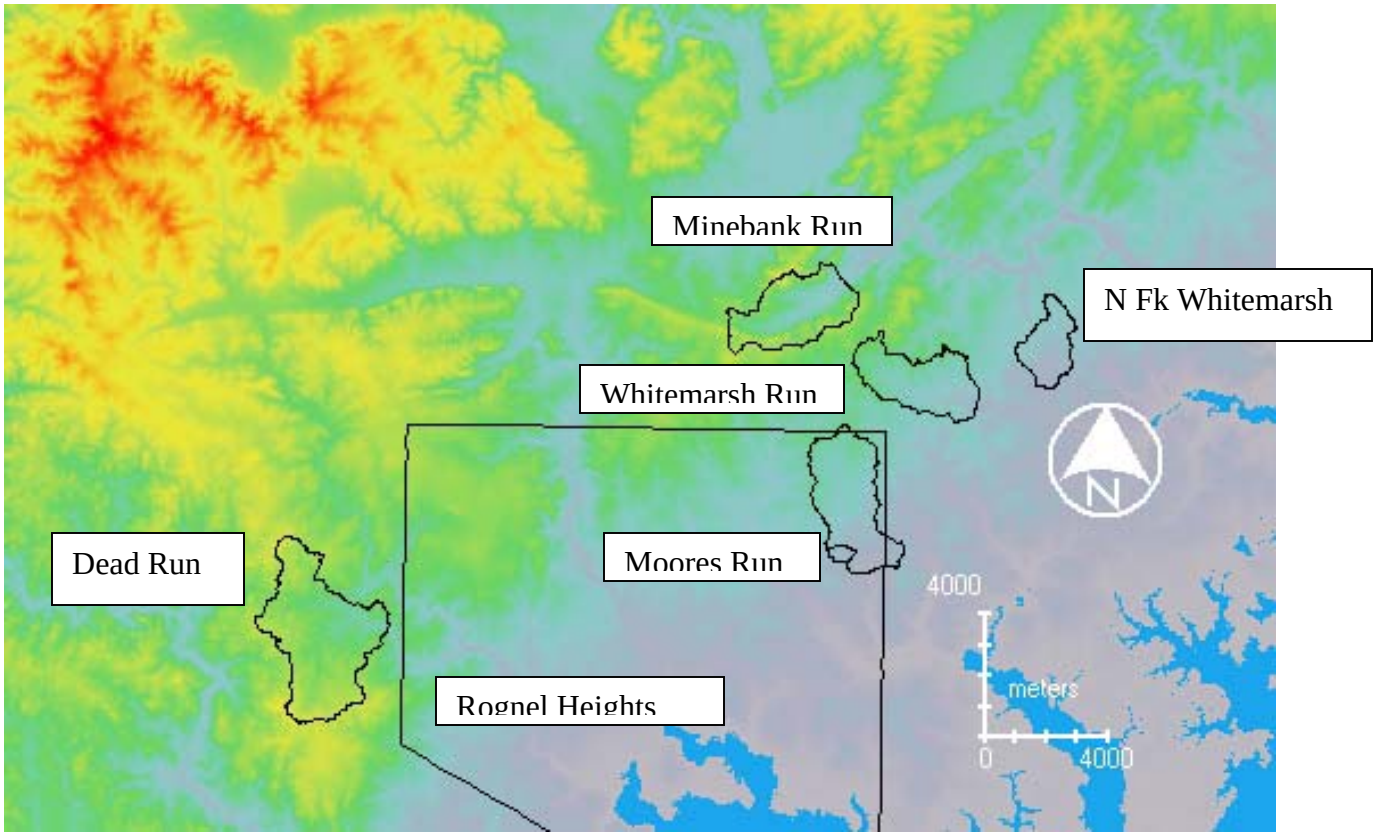

Figure 2.1 Location map for the Baltimore study region. The Baltimore City boundary is outlined in black. Basin boundaries for drainage basins are identified.

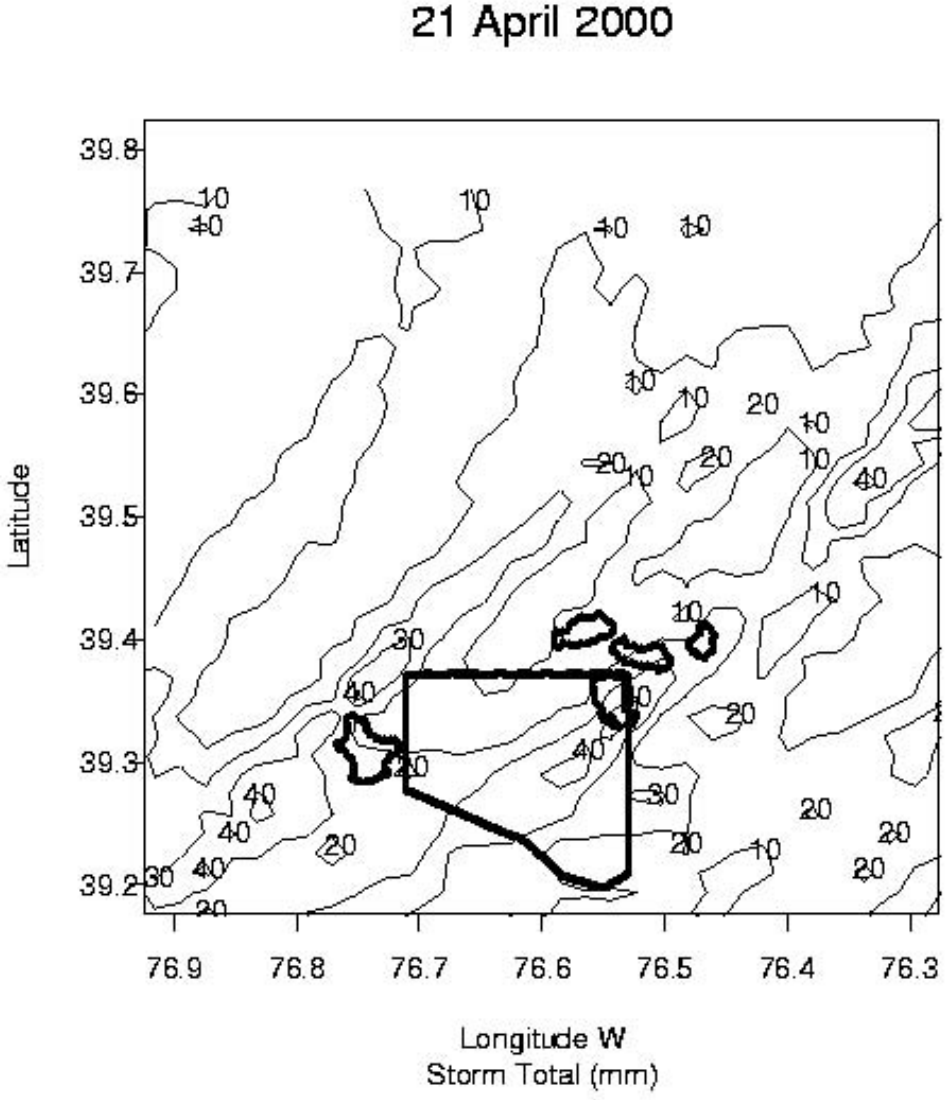

Figure 2.2a. Storm total rainfall map for the 21 April storm.

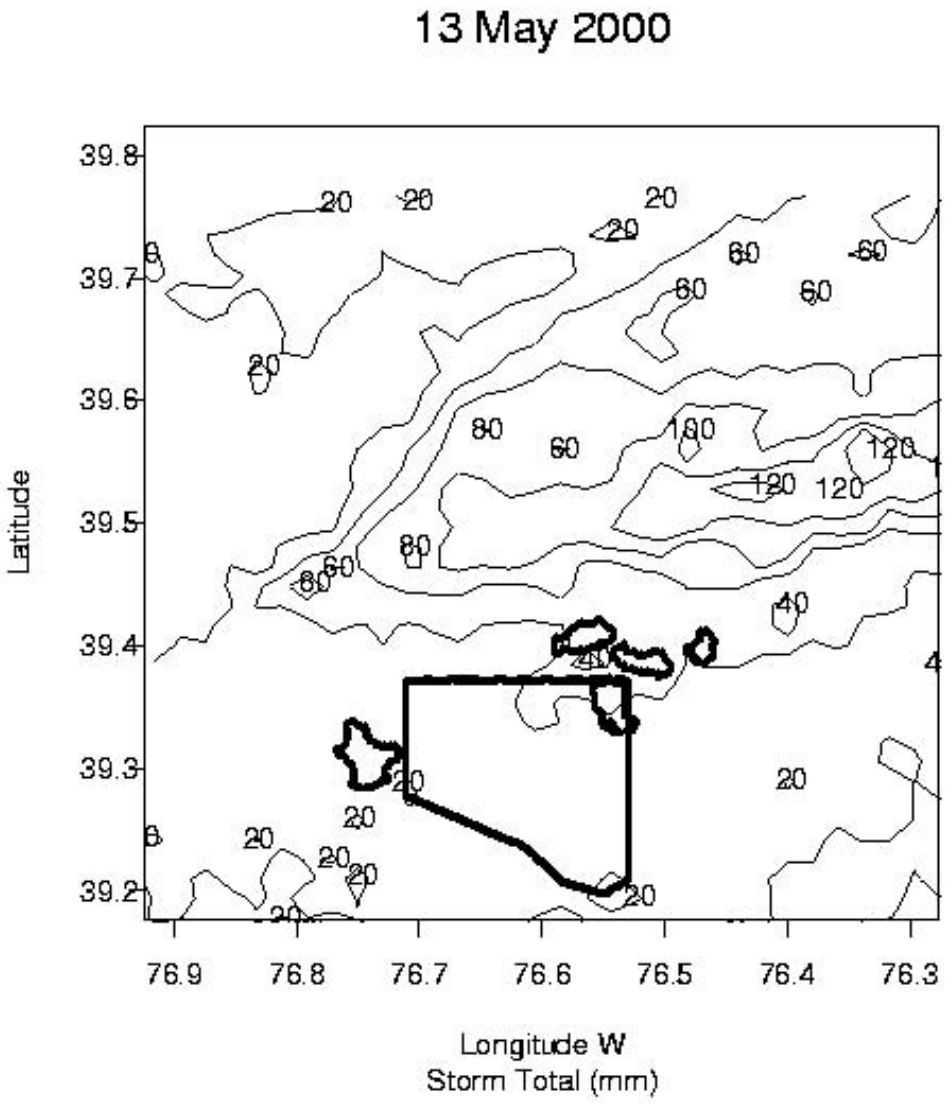

Figure 2.2 b. Storm total rainfall map for the 13 May storm.

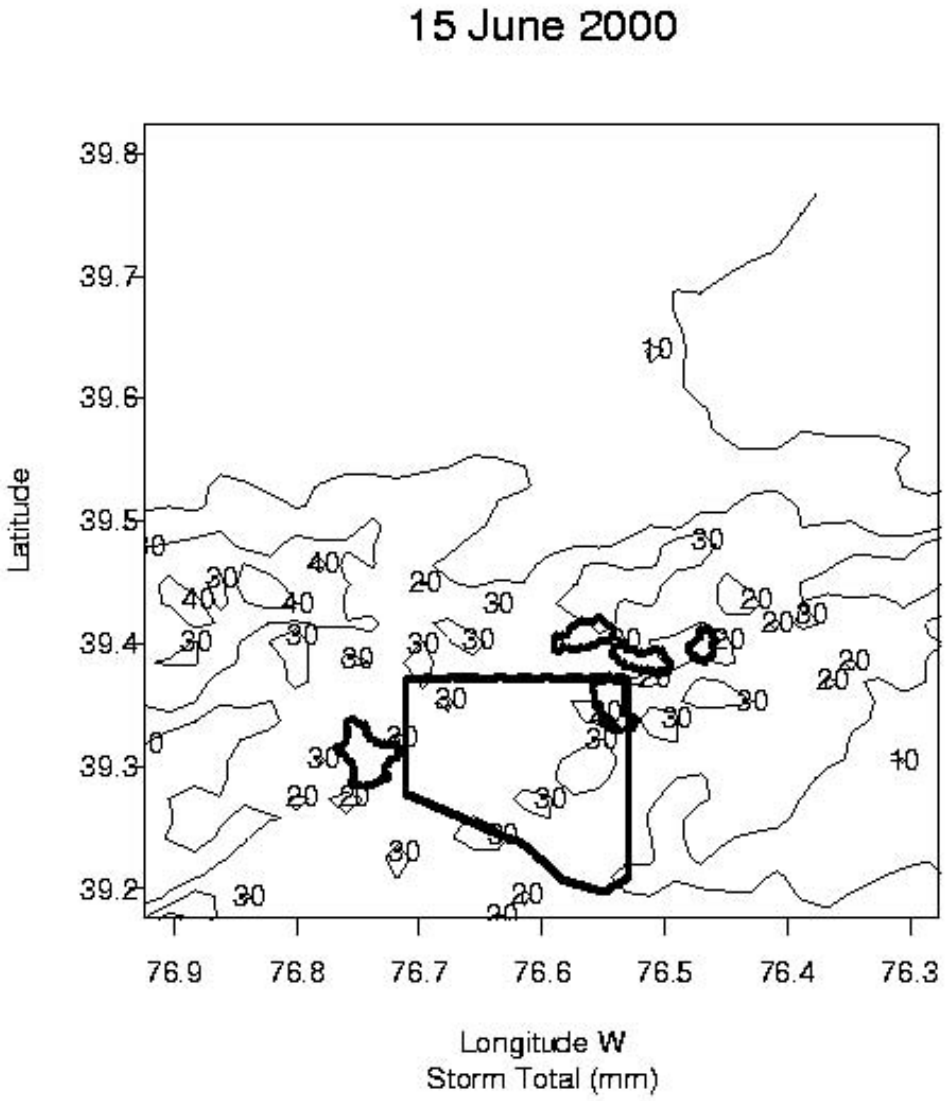

Figure 2.2 c. Storm total rainfall map for the 15 June storm.

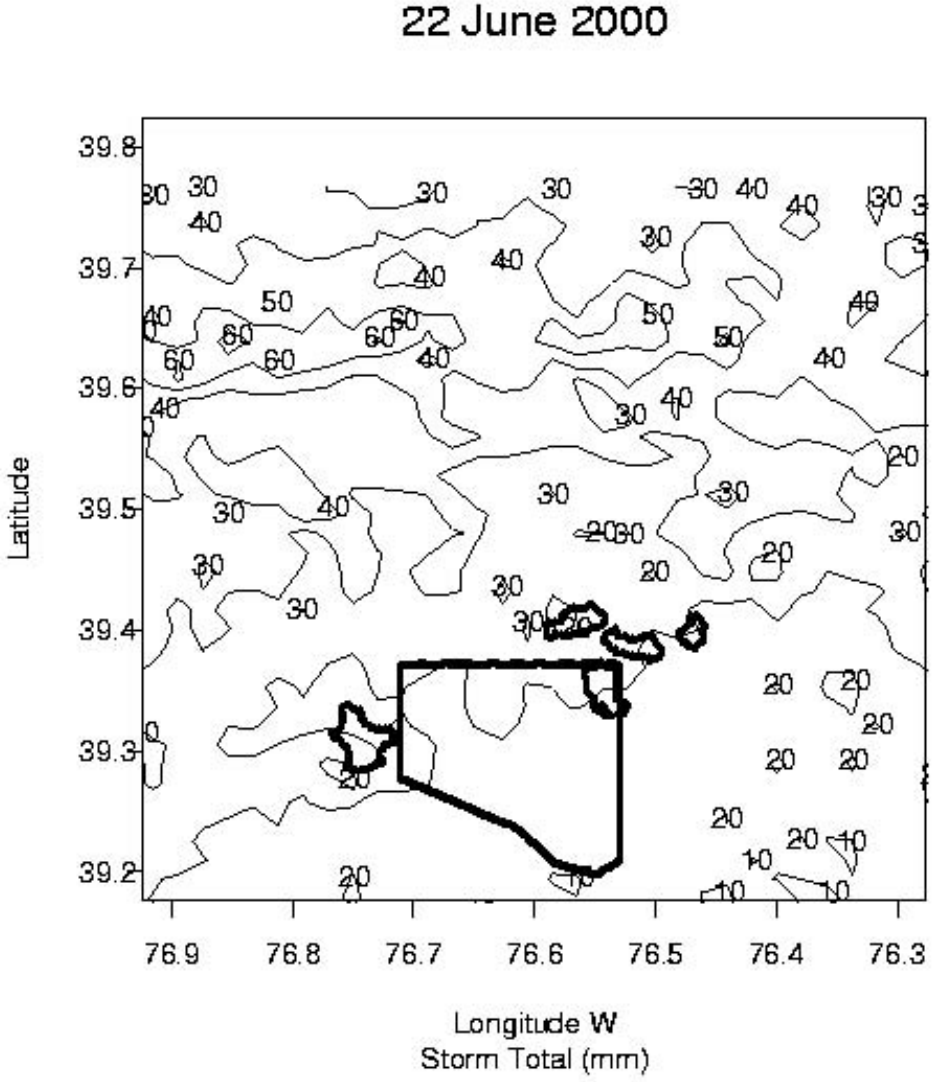

Figure 2.2 d. Storm total rainfall map for the 15 June storm.

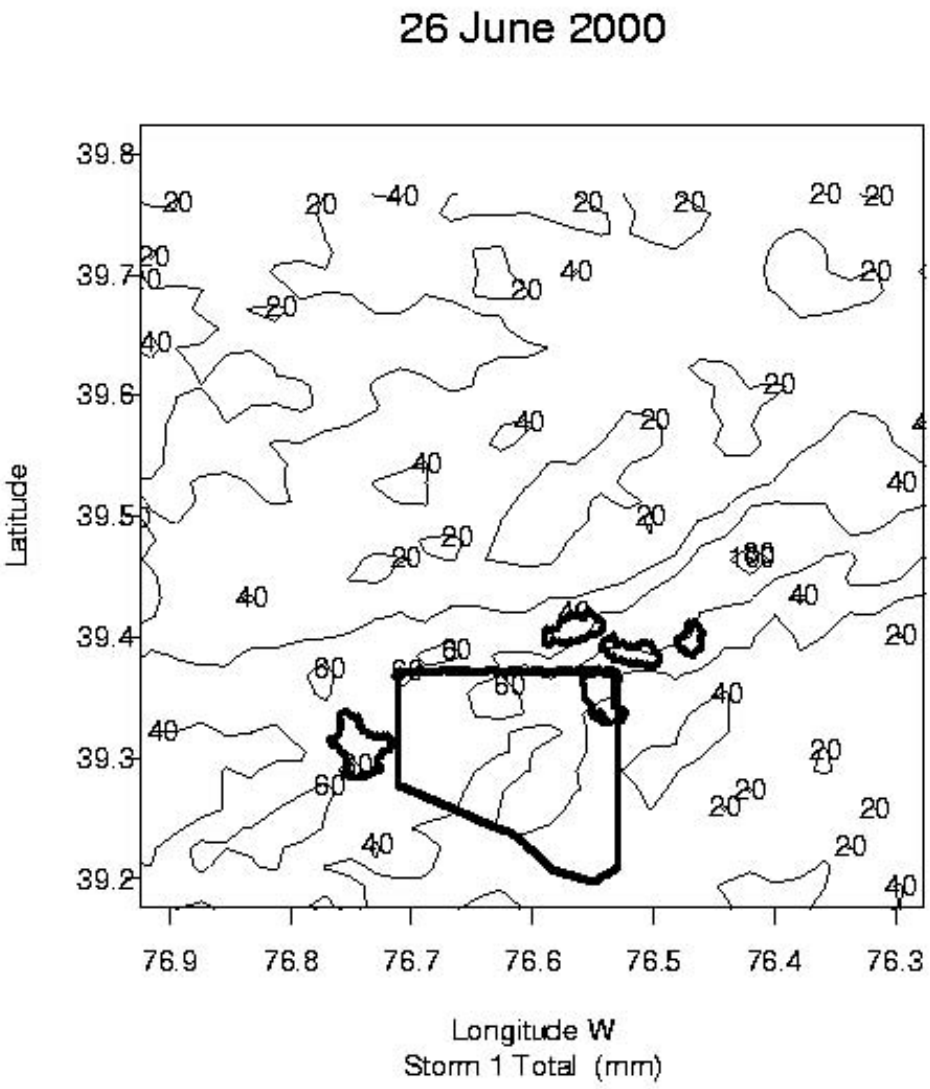

Figure 2.2 e. Storm total rainfall maps for the first 26 June storm.

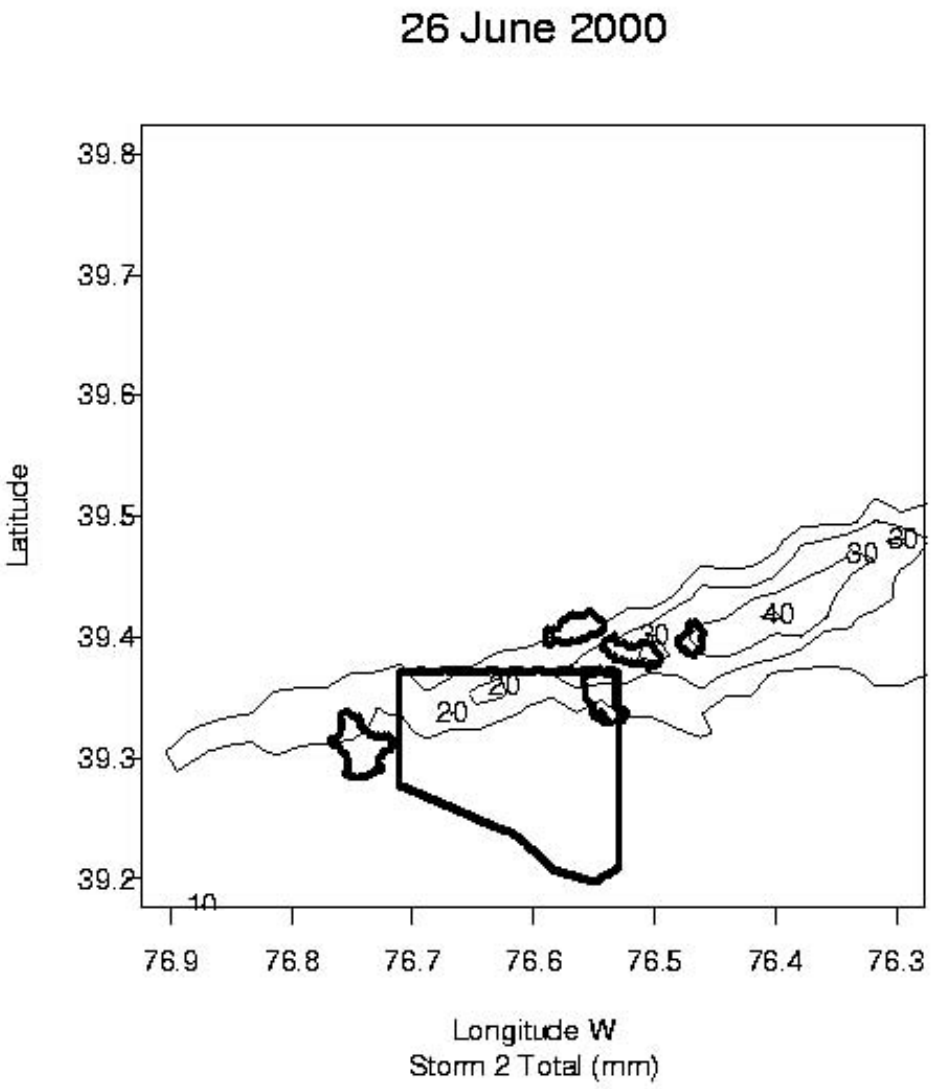

Figure 2.2 f. Storm total rainfall for the second 26 June storm.

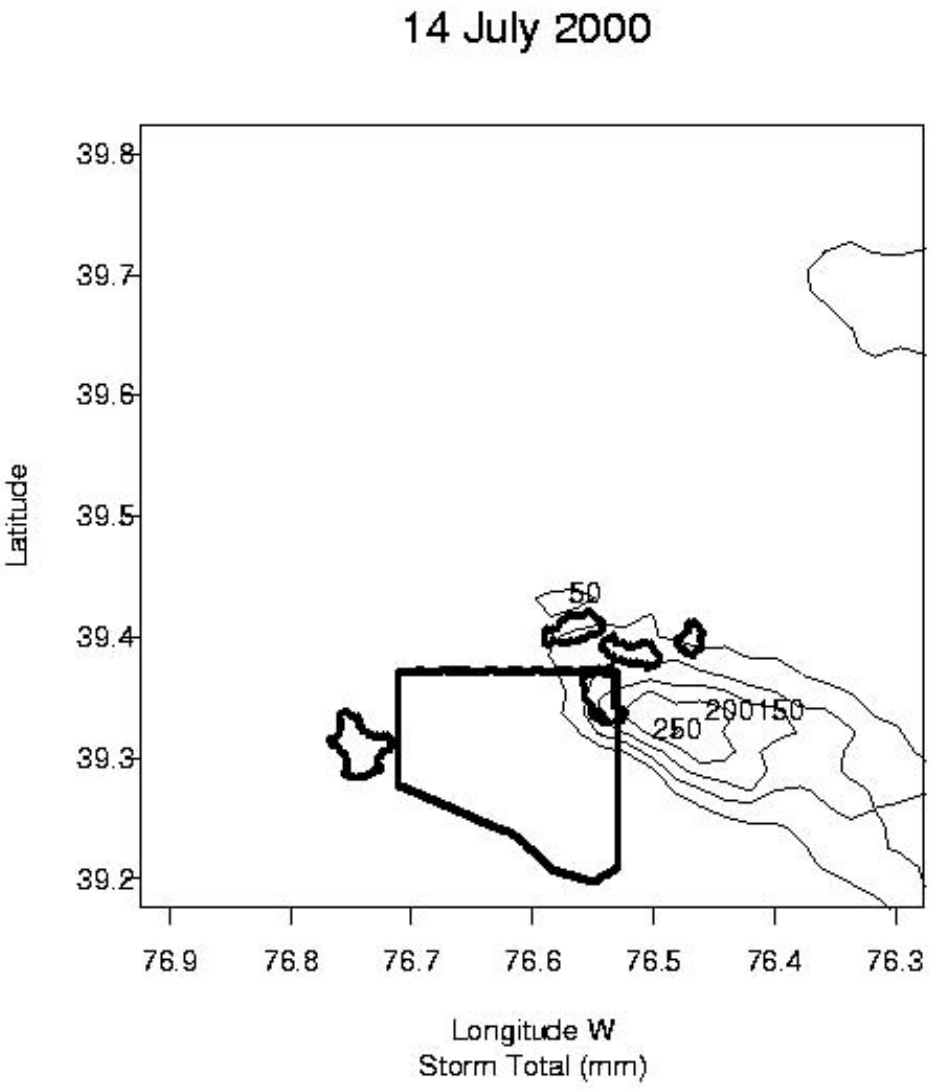

Figure 2.2 g. Storm total rainfall for the 14 July storm.

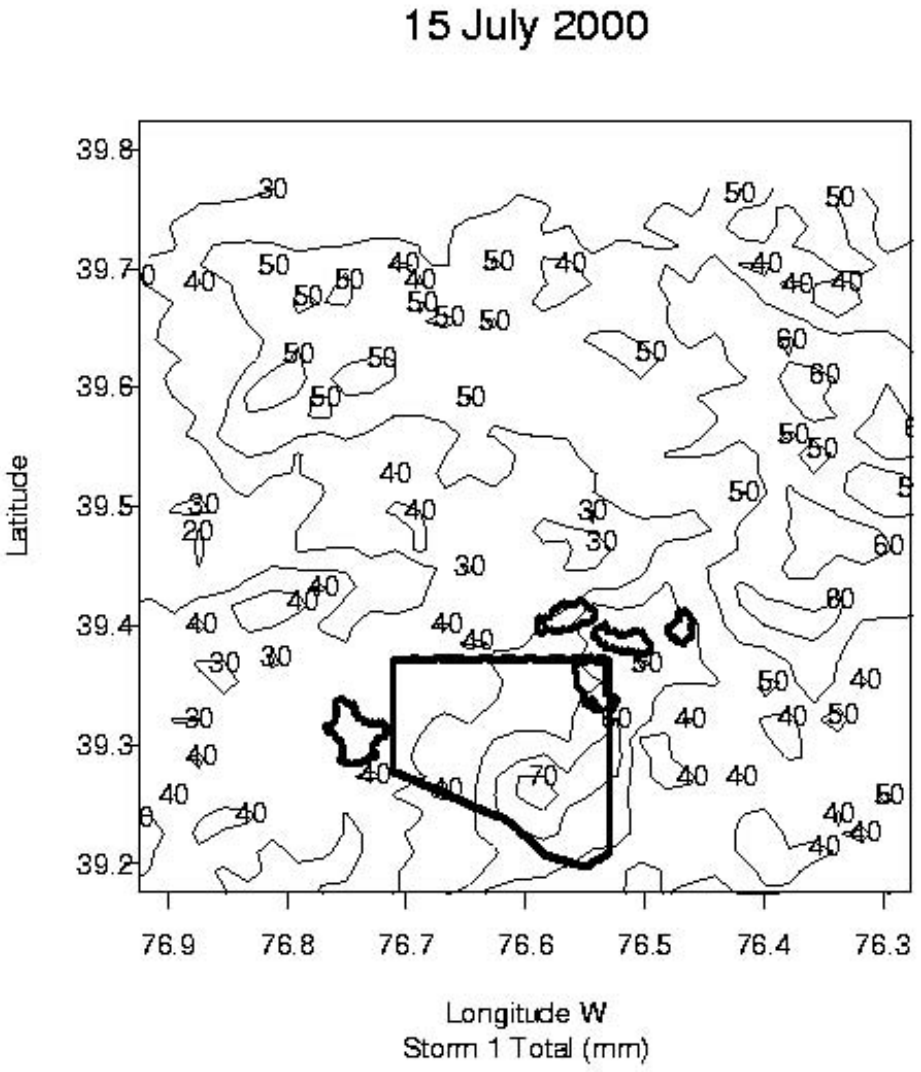

Figure 2.2 h. Storm total rainfall for the first 15 July storm.

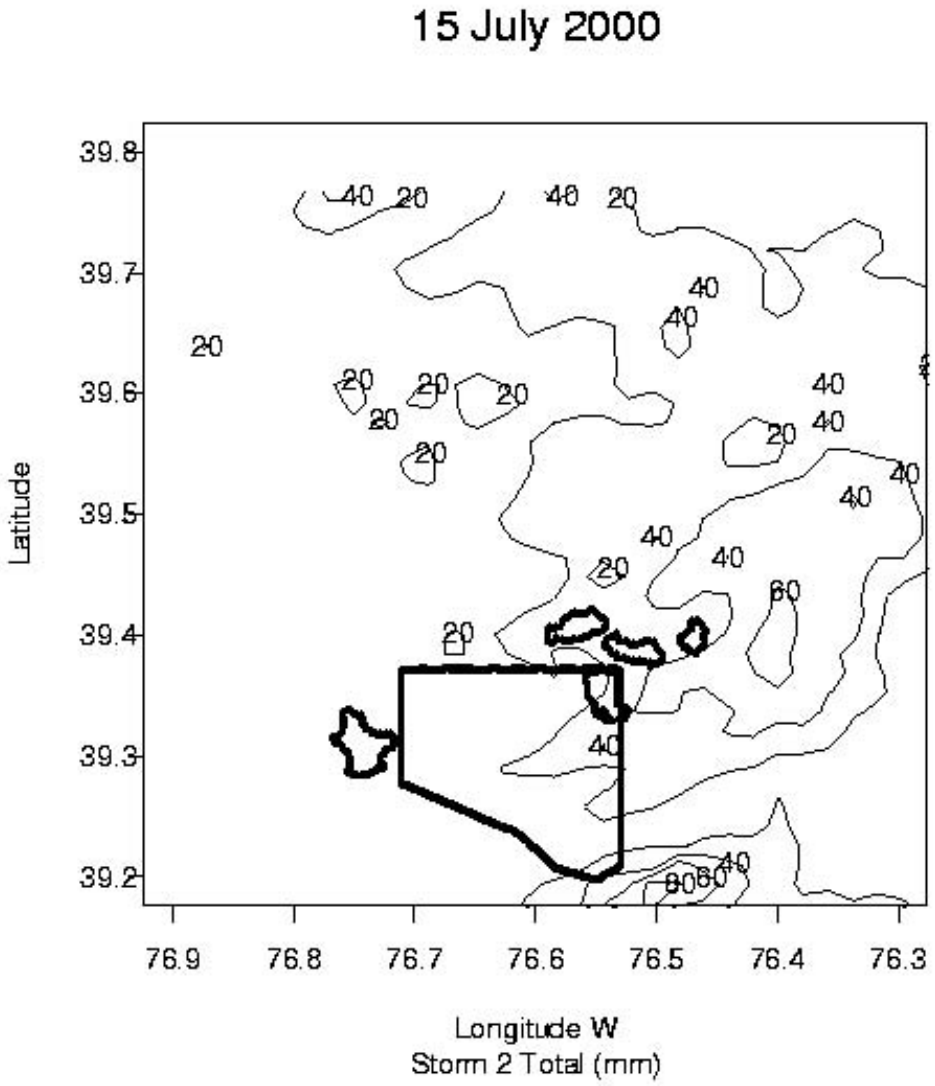

Figure 2.2 i. Storm total rainfall for the second 15 July storm.

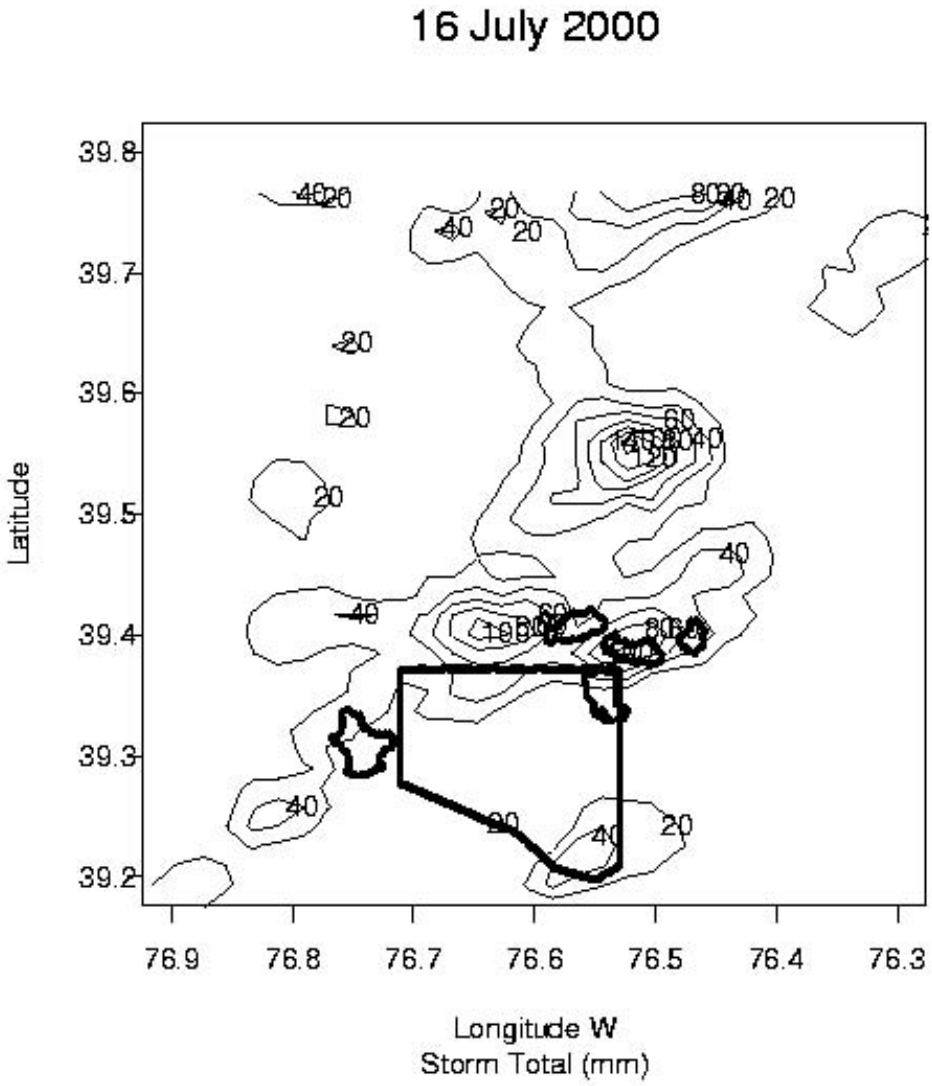

Figure 2.2 j. Storm total rainfall for the 16 July storm.

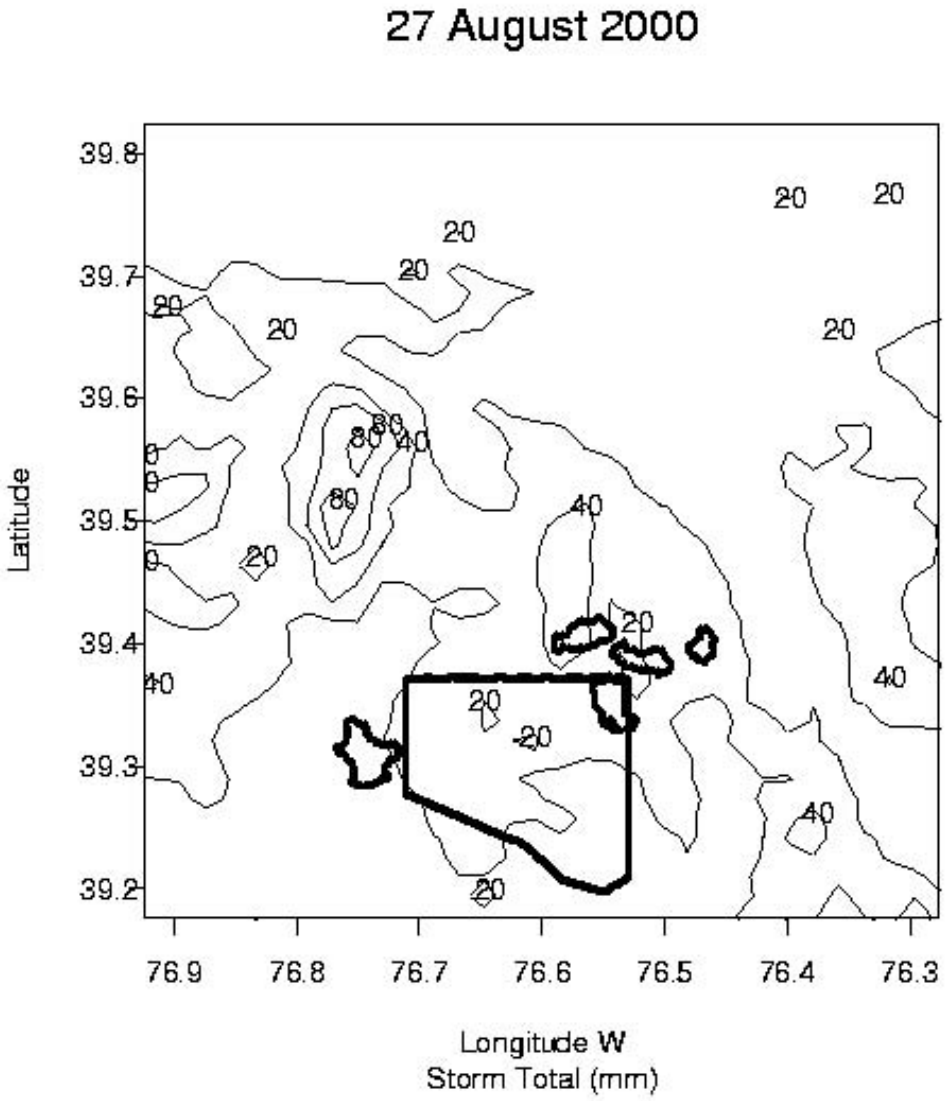

Figure 2.2 k. Storm total rainfall for the 27 August storm.

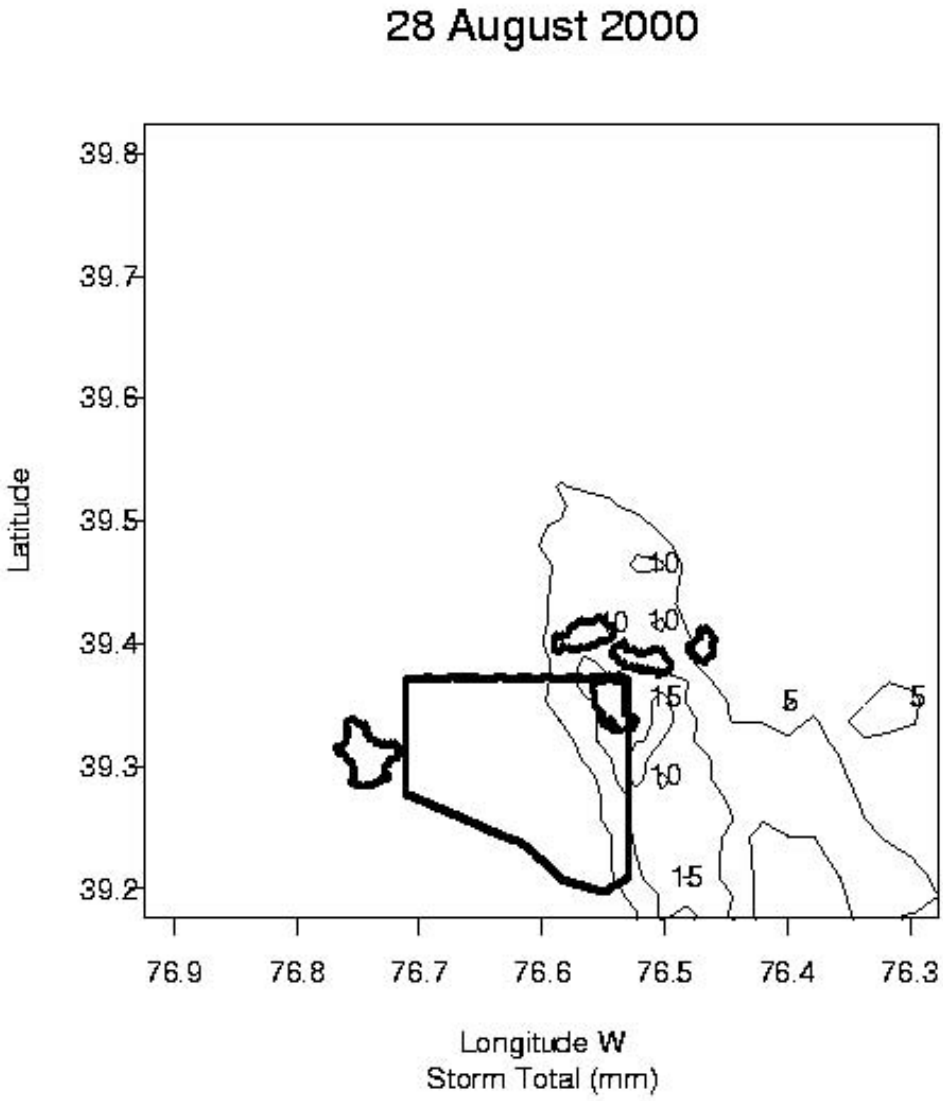

Figure 2.2 l. Storm total rainfall for the 28 August storm.

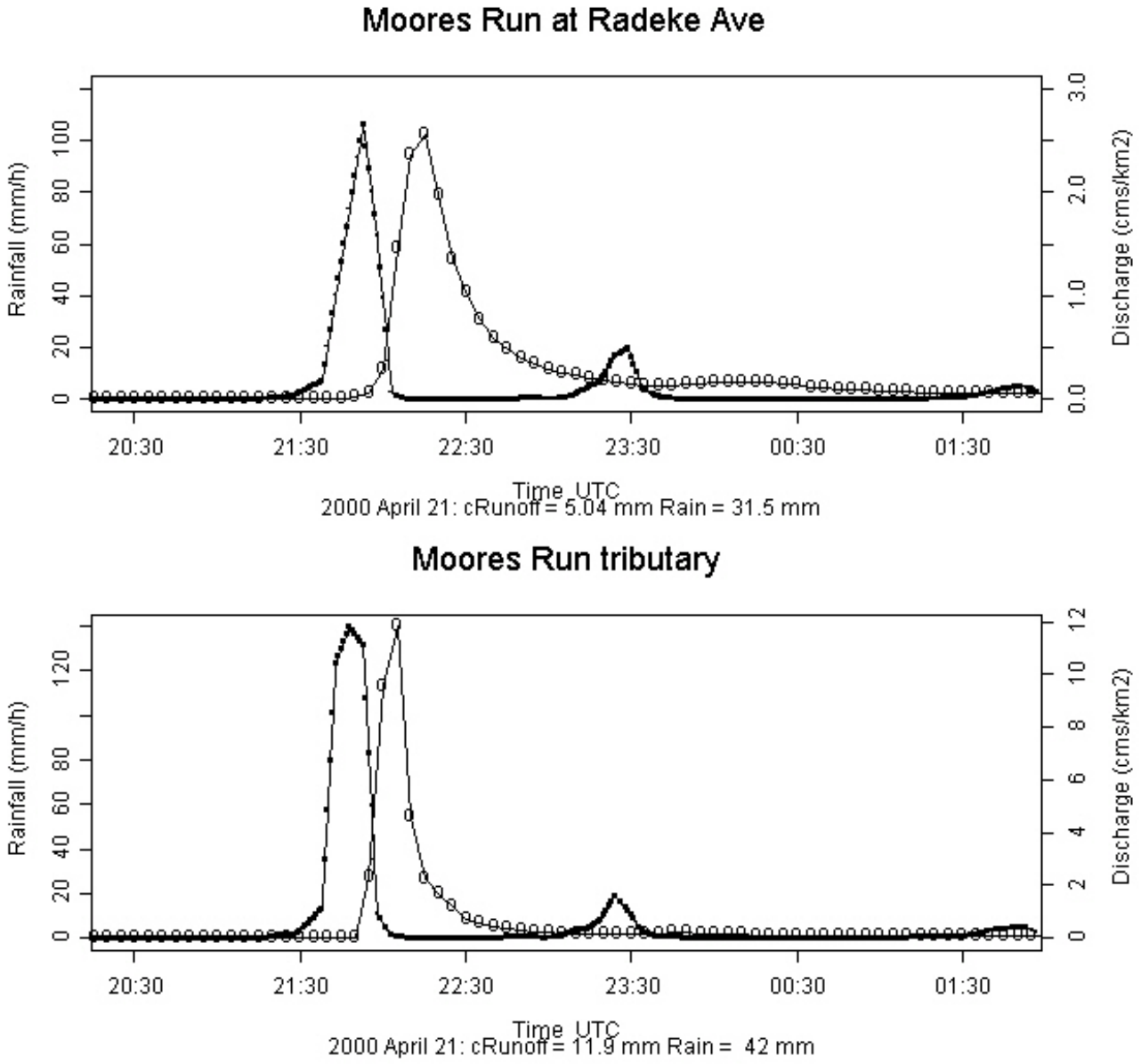

Figure 2.3. Basin-averaged rainfall rate (solid circles) and discharge (open circles) for the 21 April storm and flood event in the two Moores Run drainage basins. Rainfall rate is expressed in mm h^{-1}. Discharge is expressed as a unit discharge in $m^3 s^{-1} km^{-2}$. On the following pages, basin-averaged rainfall and discharge time series are presented for the 12 storm events and selected basins (see Fig. 2.1).

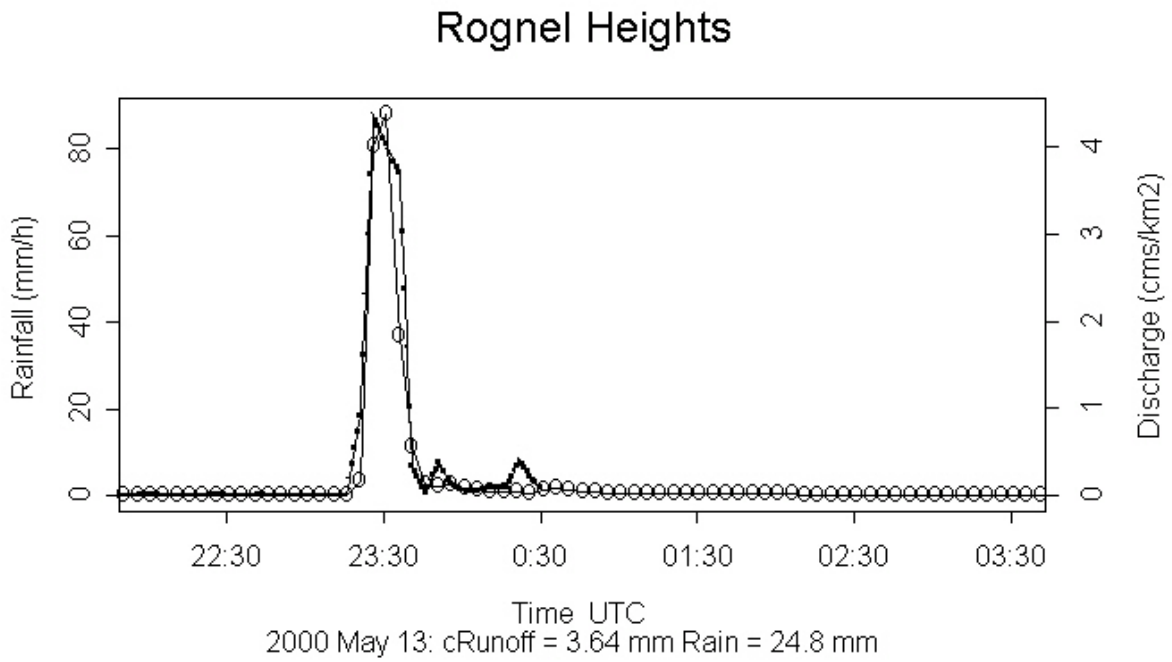
Rognel Heights
Rainfall (mm/h)
0
20
40
60
80
Discharge (cms/km2)
0
1
2
3
4
22:30
23:30
0:30
01:30
02:30
03:30
Time UTC
2000 May 13: cRunoff = 3.64 mm Rain = 24.8 mm

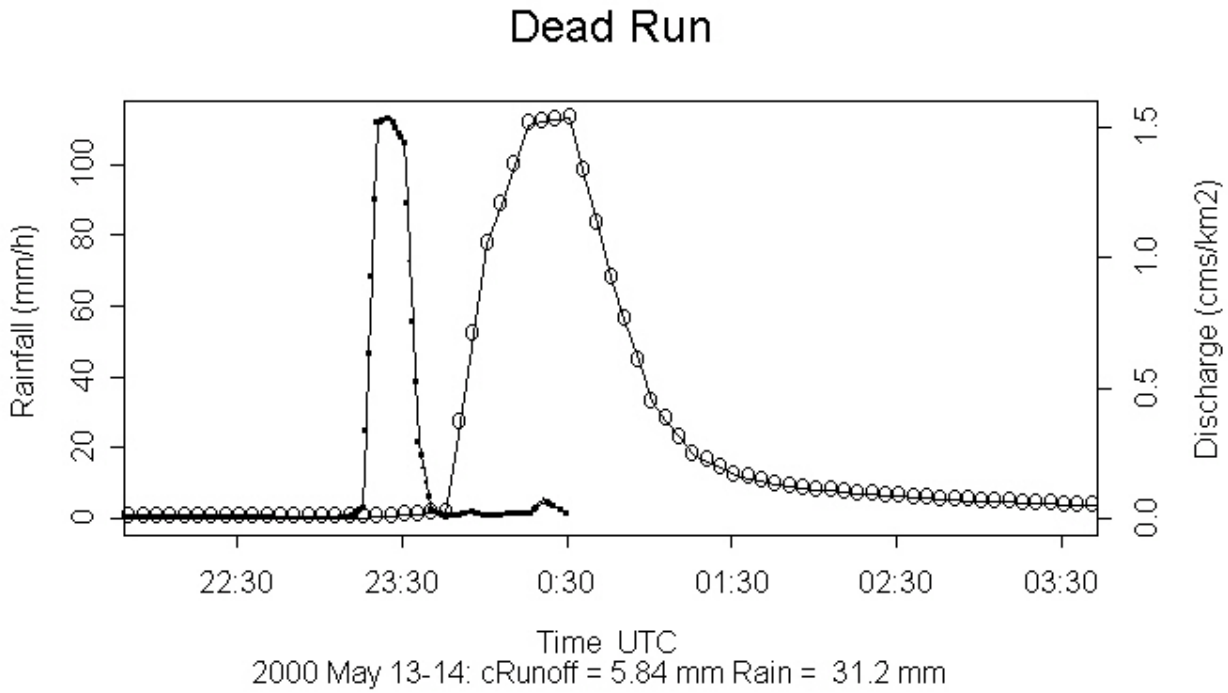
Dead Run
Rainfall (mm/h)
0
20
40
60
80
100
Discharge (cms/km2)
0.0
0.5
1.0
1.5
22:30
23:30
0:30
01:30
02:30
03:30
Time UTC
2000 May 13-14: cRunoff = 5.84 mm Rain = 31.2 mm

Rognel Heights

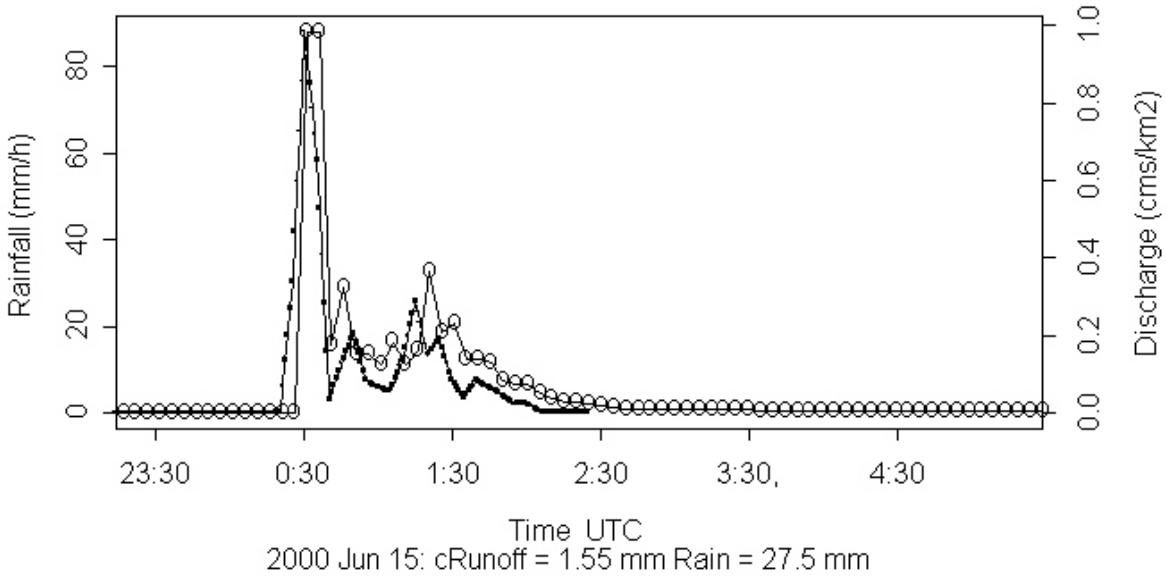

2000 Jun 15: cRunoff = 1.55 mm Rain = 27.5 mm

Minebank

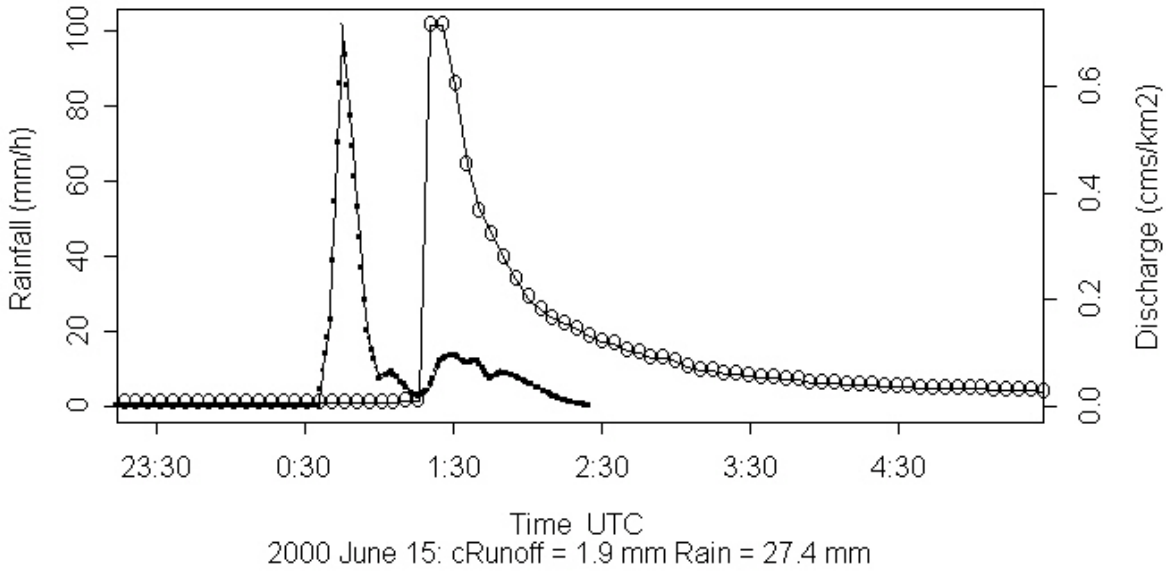

2000 June 15: cRunoff = 1.9 mm Rain = 27.4 mm

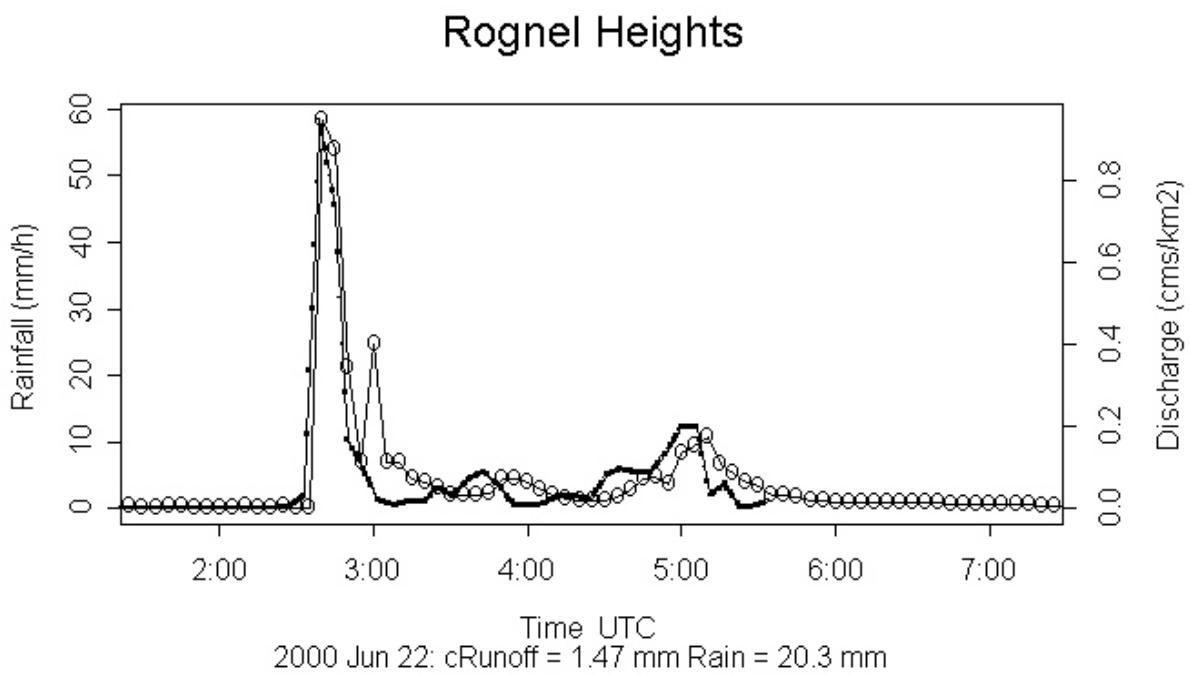
Rognel Heights
Rainfall (mm/h)
0
10
20
30
40
50
60
Discharge (cms/km2)
0.0
0.2
0.4
0.6
0.8
2:00
3:00
4:00
5:00
6:00
7:00
Time UTC
2000 Jun 22: cRunoff = 1.47 mm Rain = 20.3 mm

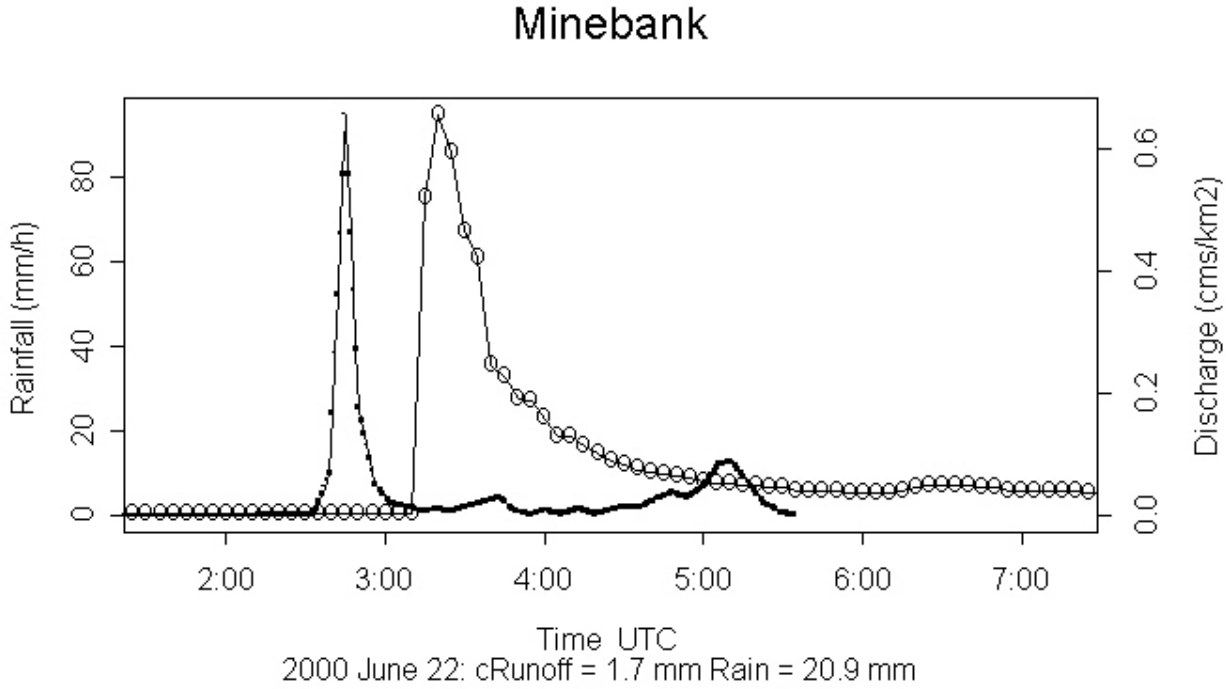
Minebank
Rainfall (mm/h)
0
20
40
60
80
Discharge (cms/km2)
0.0
0.2
0.4
0.6
2:00
3:00
4:00
5:00
6:00
7:00
Time UTC
2000 June 22: cRunoff = 1.7 mm Rain = 20.9 mm

Moores Run at Radeke Ave

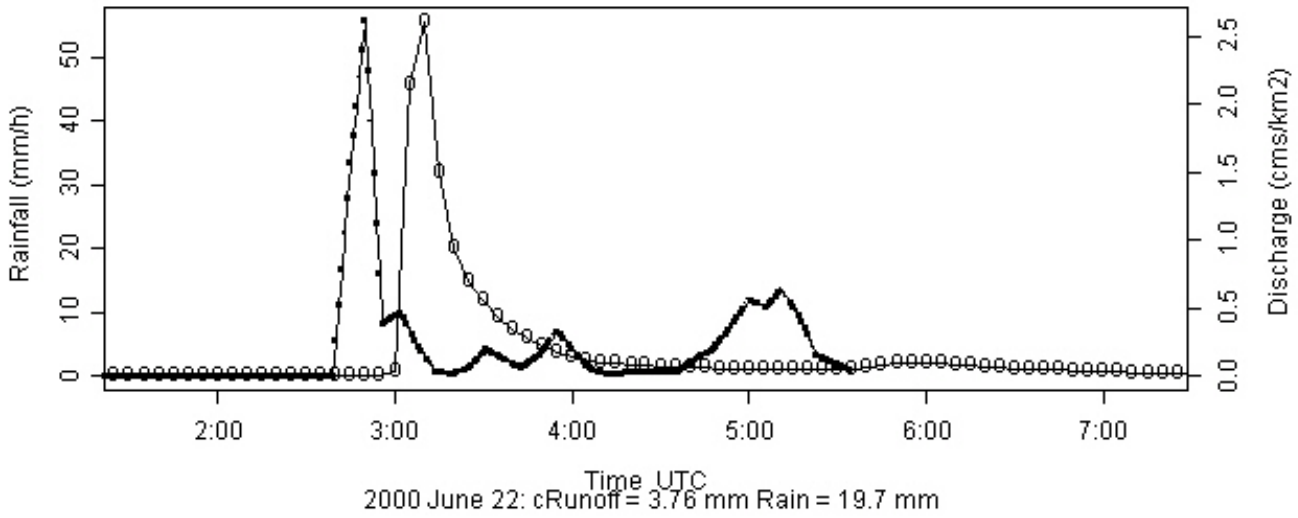

2000 June 22: cRunoff = 3.76 mm Rain = 19.7 mm

Moores Run tributary

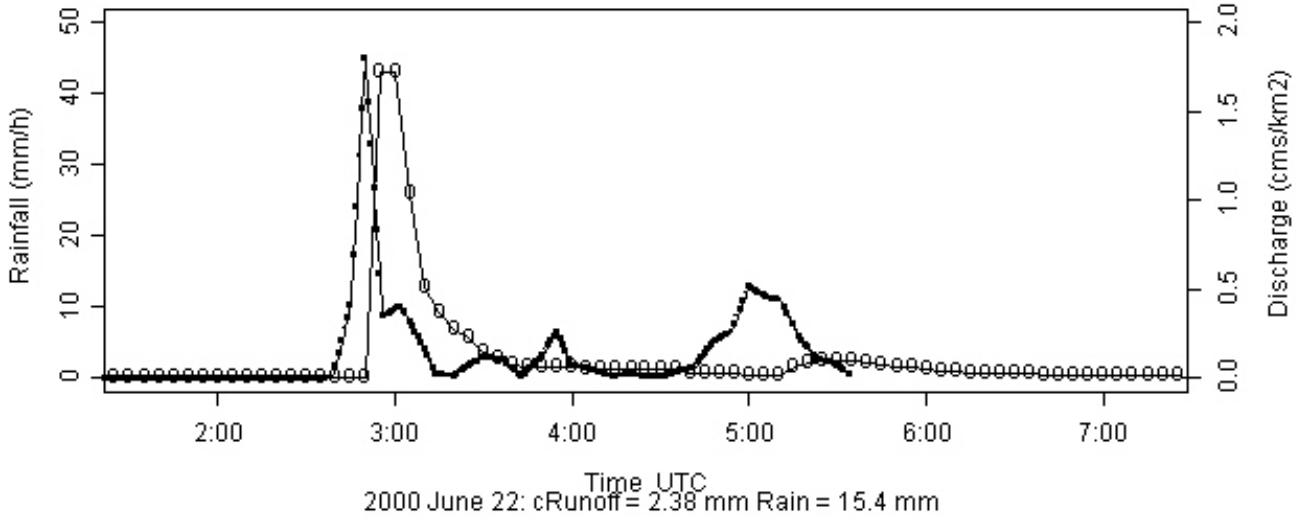

2000 June 22: cRunoff = 2.38 mm Rain = 15.4 mm

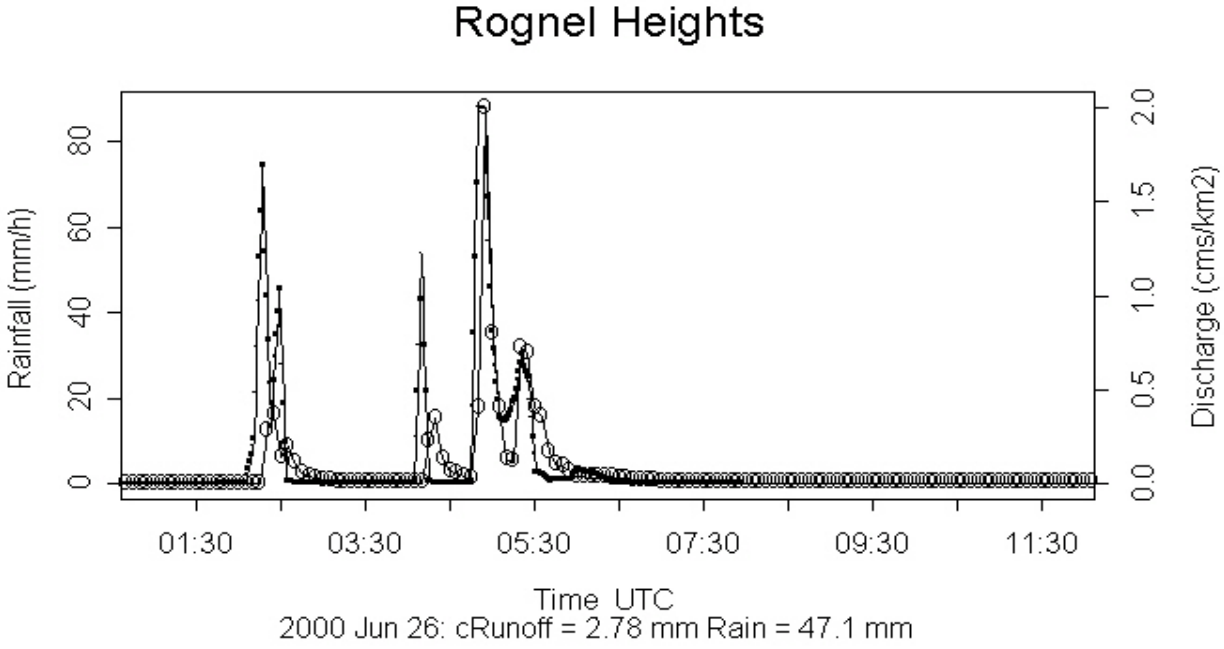
Rognel Heights
Rainfall (mm/h)
0
20
40
60
80
Discharge (cms/km2)
0.0
0.5
1.0
1.5
2.0
01:30
03:30
05:30
07:30
09:30
11:30
Time UTC
2000 Jun 26: cRunoff = 2.78 mm Rain = 47.1 mm

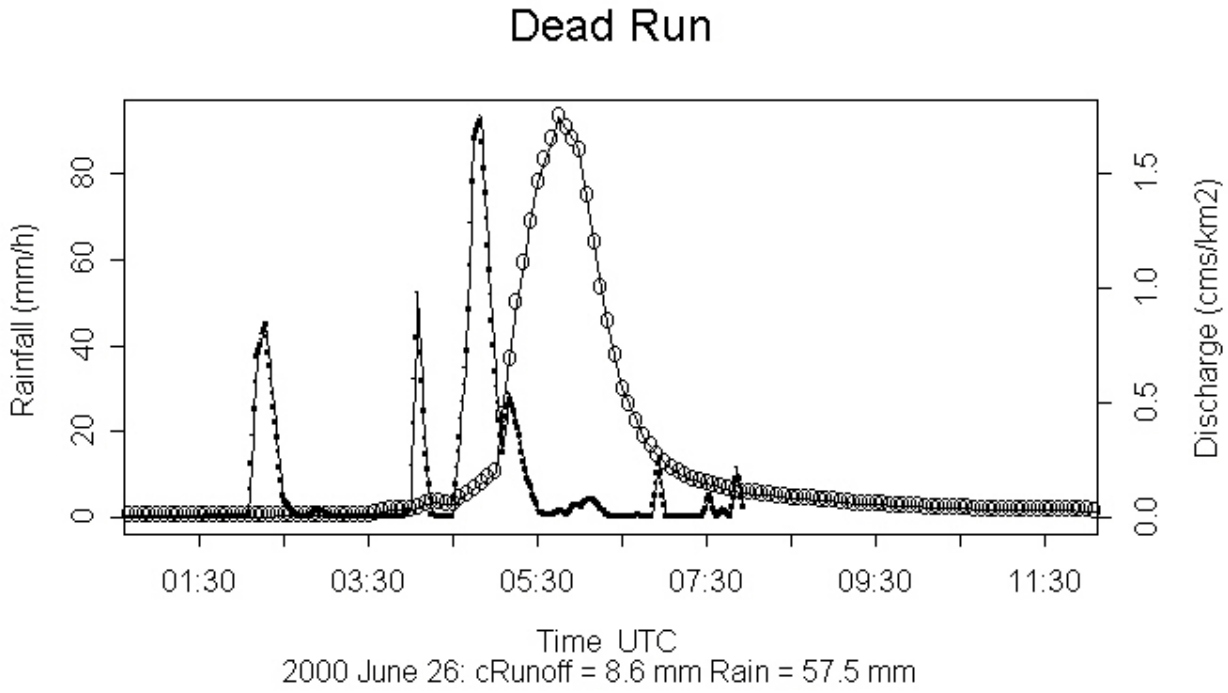
Dead Run
Rainfall (mm/h)
0
20
40
60
80
Discharge (cms/km2)
0.0
0.5
1.0
1.5
01:30
03:30
05:30
07:30
09:30
11:30
Time UTC
2000 June 26: cRunoff = 8.6 mm Rain = 57.5 mm

Moores Run at Radeke Ave

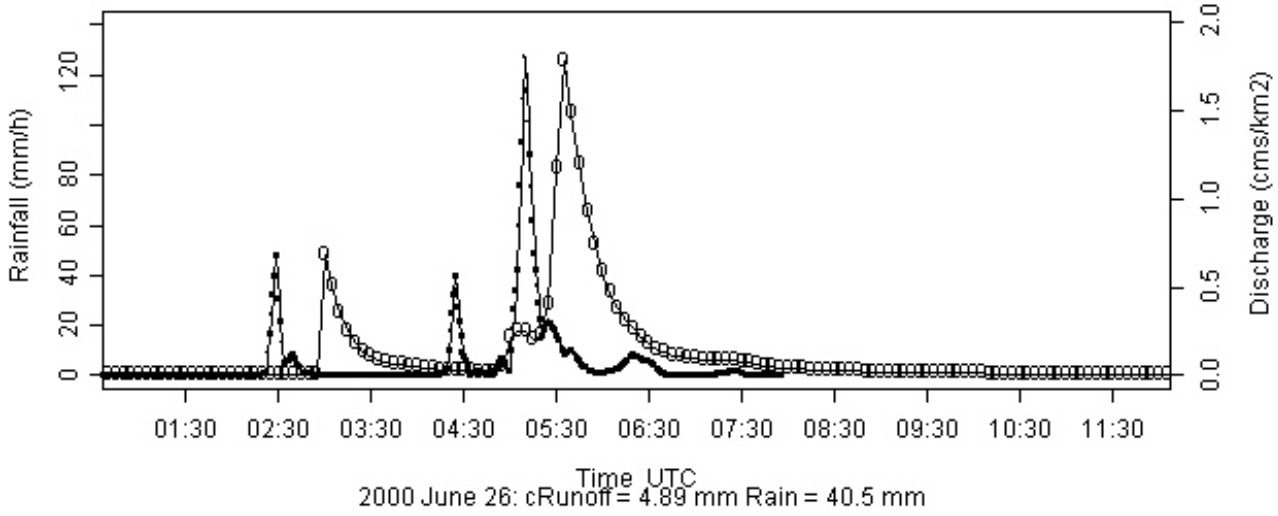

2000 June 26: cRunoff = 4.89 mm Rain = 40.5 mm

Moores Run tributary

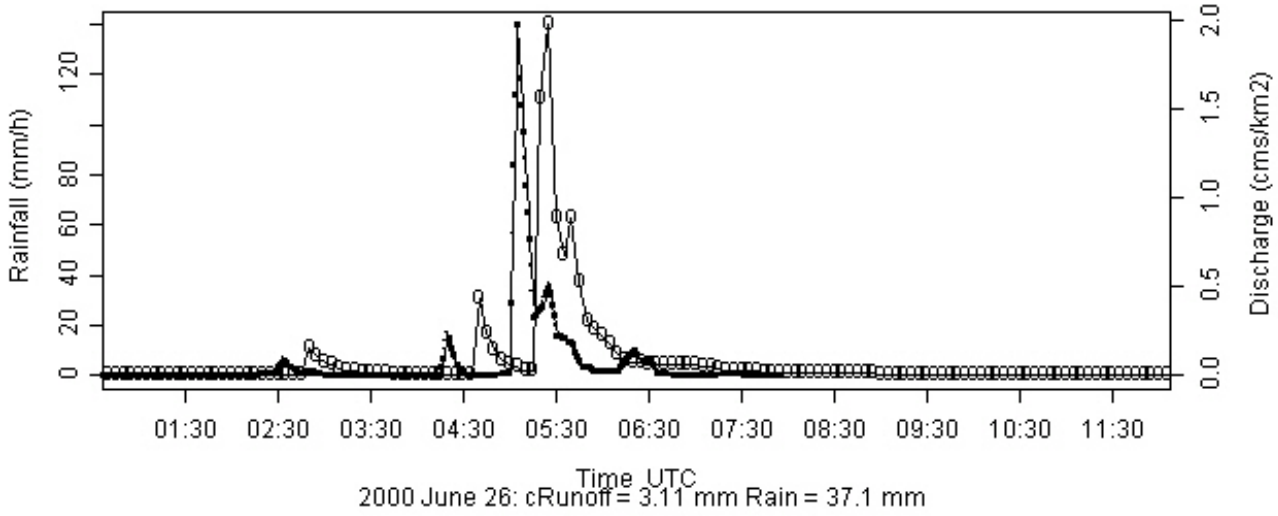

2000 June 26: cRunoff = 3.11 mm Rain = 37.1 mm

White Marsh at Fullerton

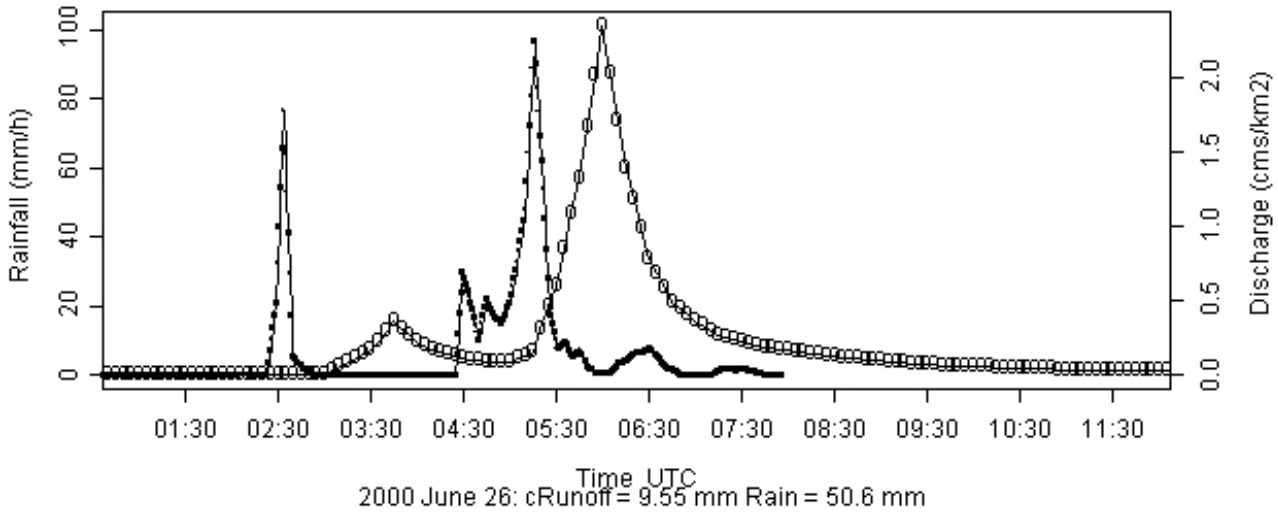

2000 June 26: cRunoff = 9.55 mm Rain = 50.6 mm

North Fork White Marsh

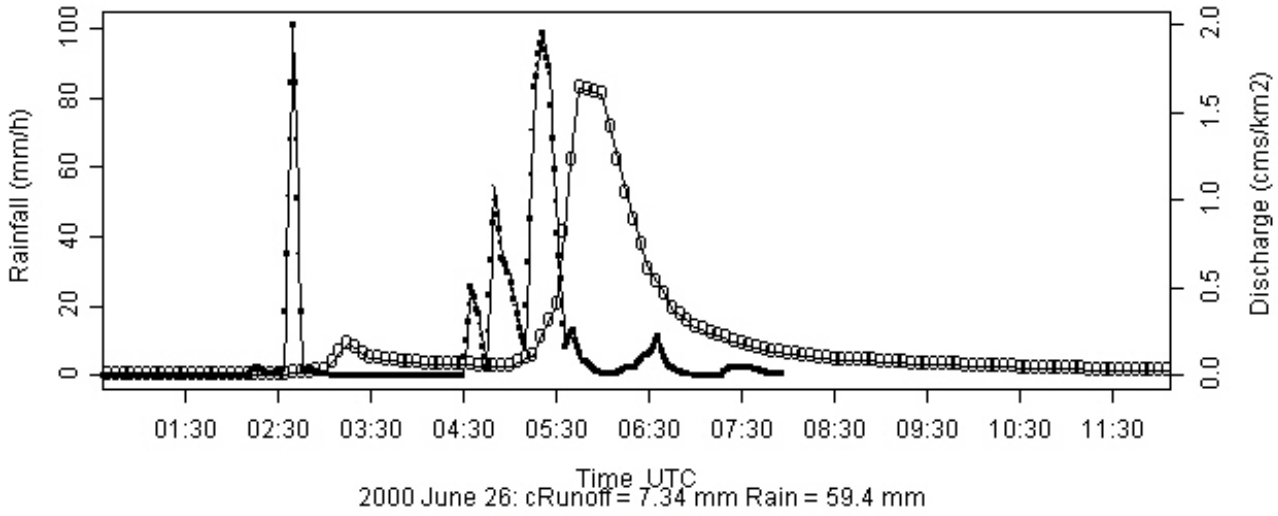

2000 June 26: cRunoff = 7.34 mm Rain = 59.4 mm

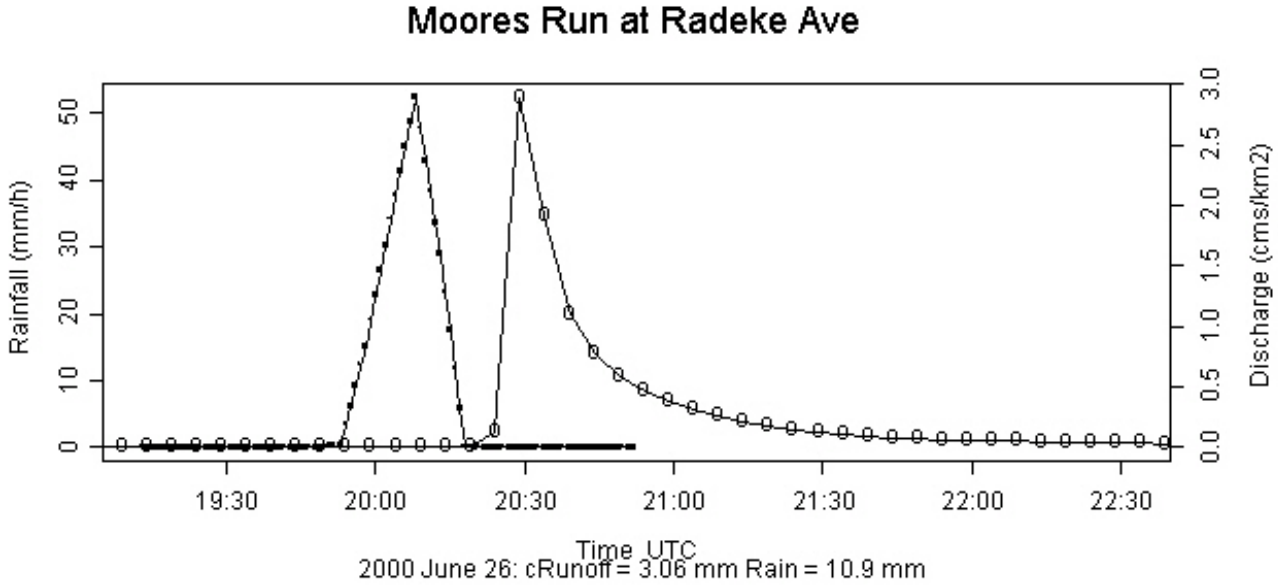
Moores Run at Radeke Ave
Rainfall (mm/h)
0
10
20
30
40
50
Discharge (cms/km2)
0.0
0.5
1.0
1.5
2.0
2.5
3.0
19:30
20:00
20:30
21:00
21:30
22:00
22:30
Time UTC
2000 June 26: cRunoff = 3.06 mm Rain = 10.9 mm

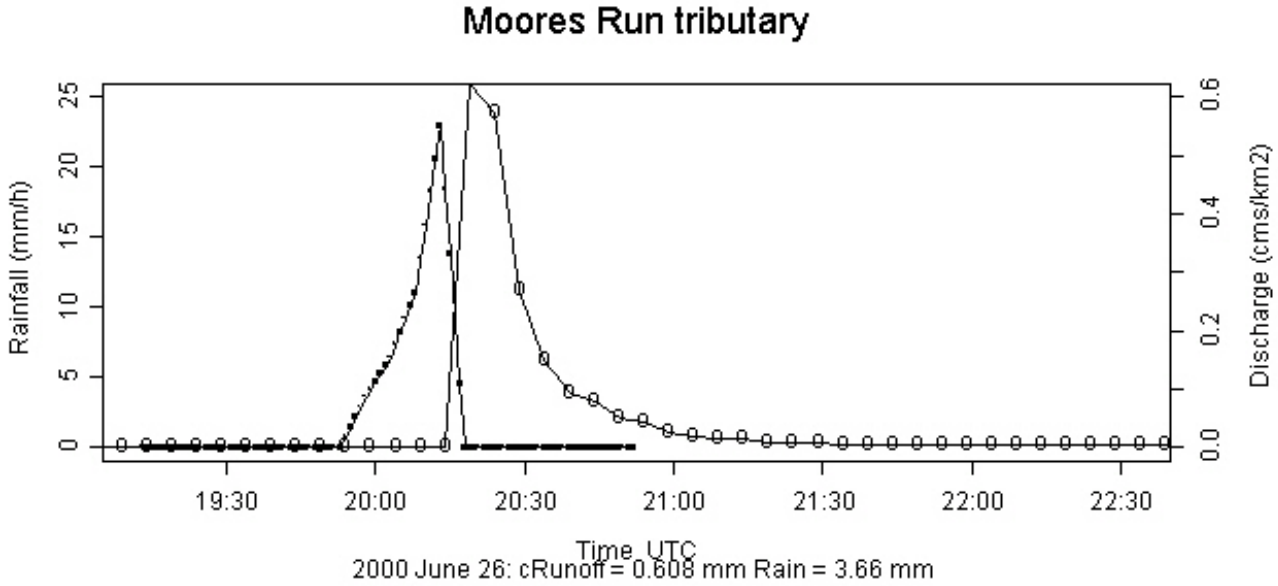
Moores Run tributary
Rainfall (mm/h)
0
5
10
15
20
25
Discharge (cms/km2)
0.0
0.2
0.4
0.6
19:30
20:00
20:30
21:00
21:30
22:00
22:30
Time UTC
2000 June 26: cRunoff = 0.608 mm Rain = 3.66 mm

White Marsh at Fullerton

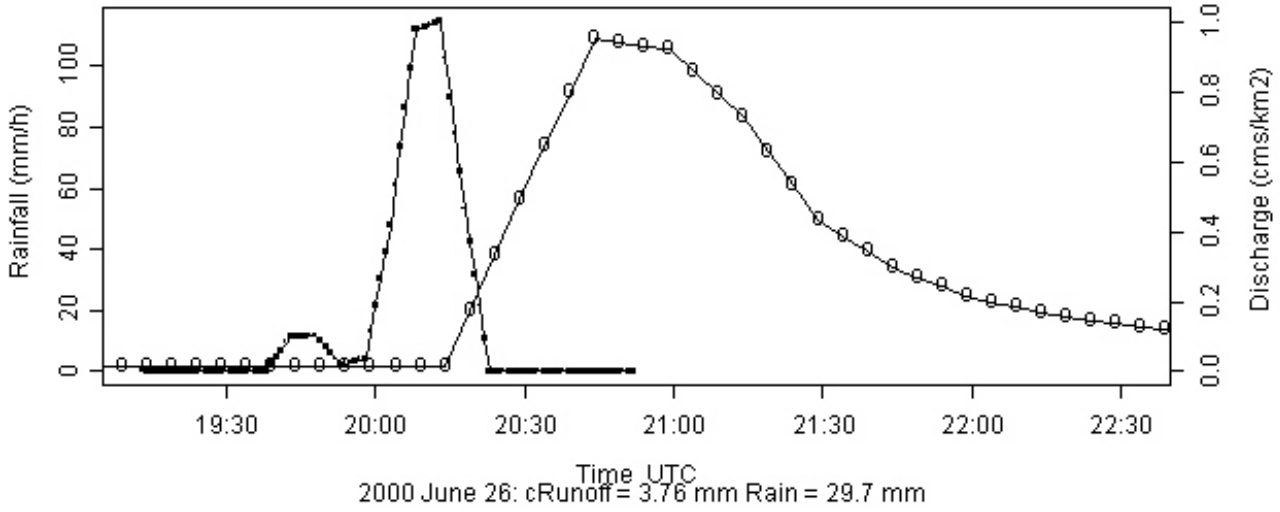

2000 June 26: cRunoff = 3.76 mm Rain = 29.7 mm

North Fork White Marsh

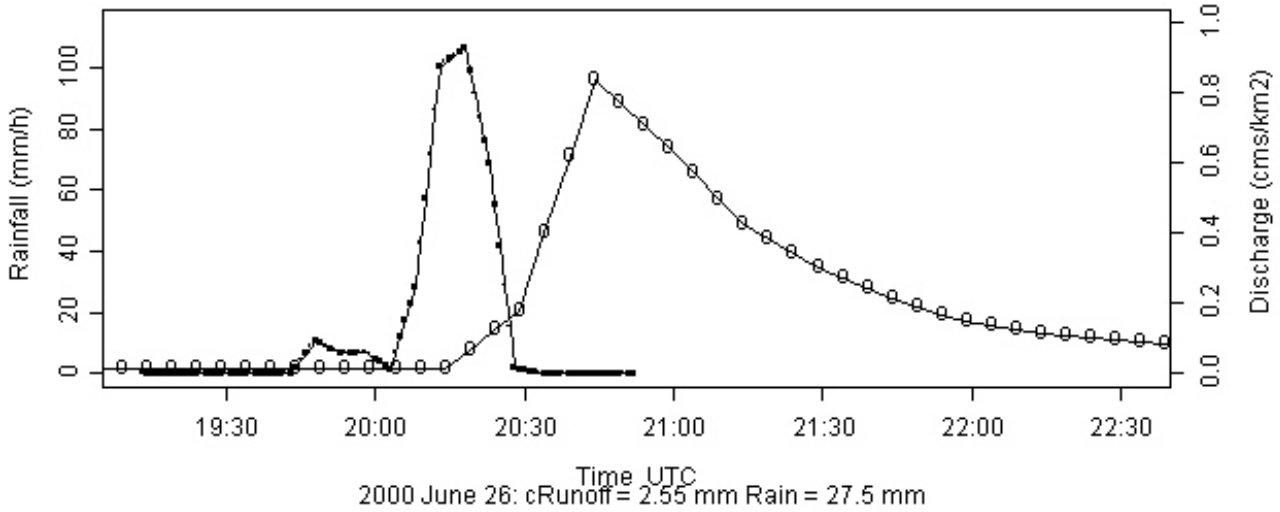

2000 June 26: cRunoff = 2.55 mm Rain = 27.5 mm

White Marsh at Fullerton

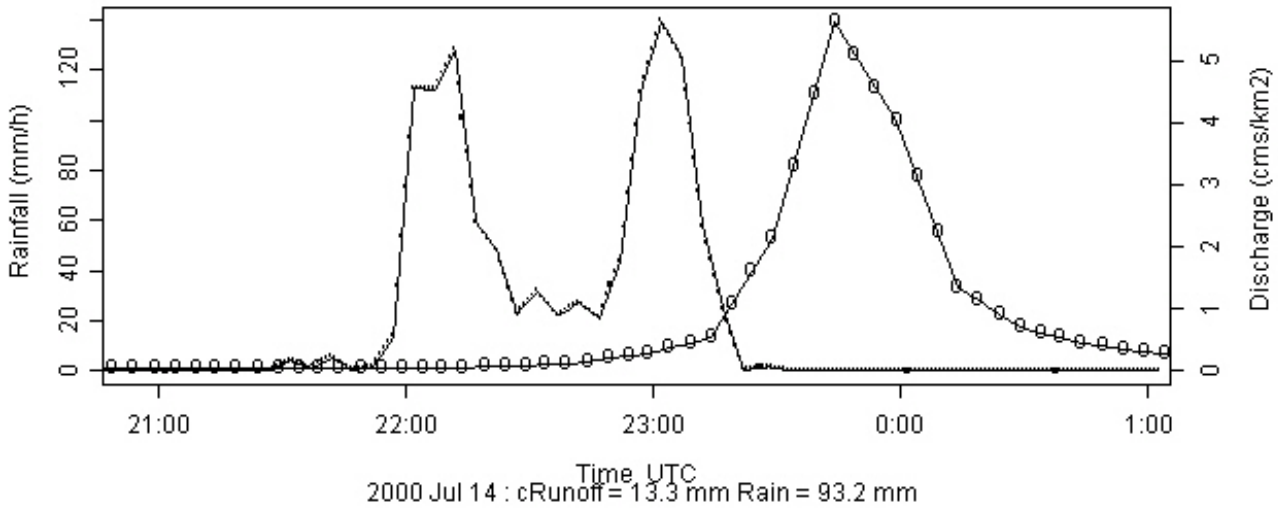

2000 Jul 14 : cRunoff = 13.3 mm Rain = 93.2 mm

North Fork White Marsh

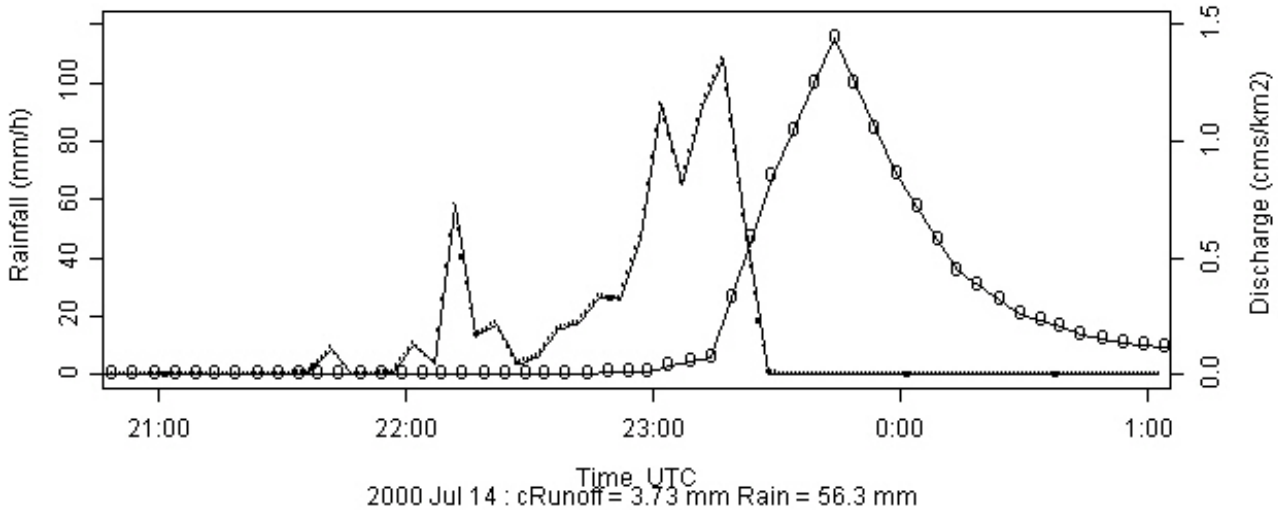

2000 Jul 14 : cRunoff = 3.73 mm Rain = 56.3 mm

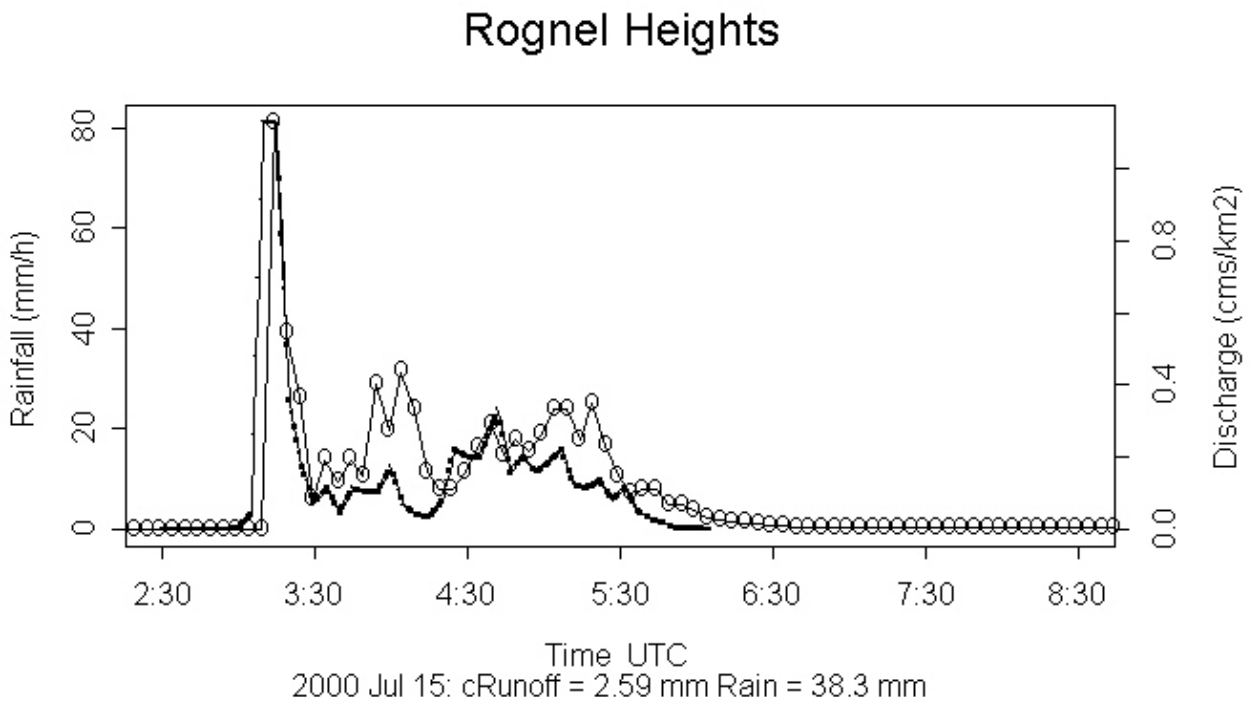
Rognel Heights
Rainfall (mm/h)
0
20
40
60
80
Discharge (cms/km2)
0.0
0.4
0.8
2:30
3:30
4:30
5:30
6:30
7:30
8:30
Time UTC
2000 Jul 15: cRunoff = 2.59 mm Rain = 38.3 mm

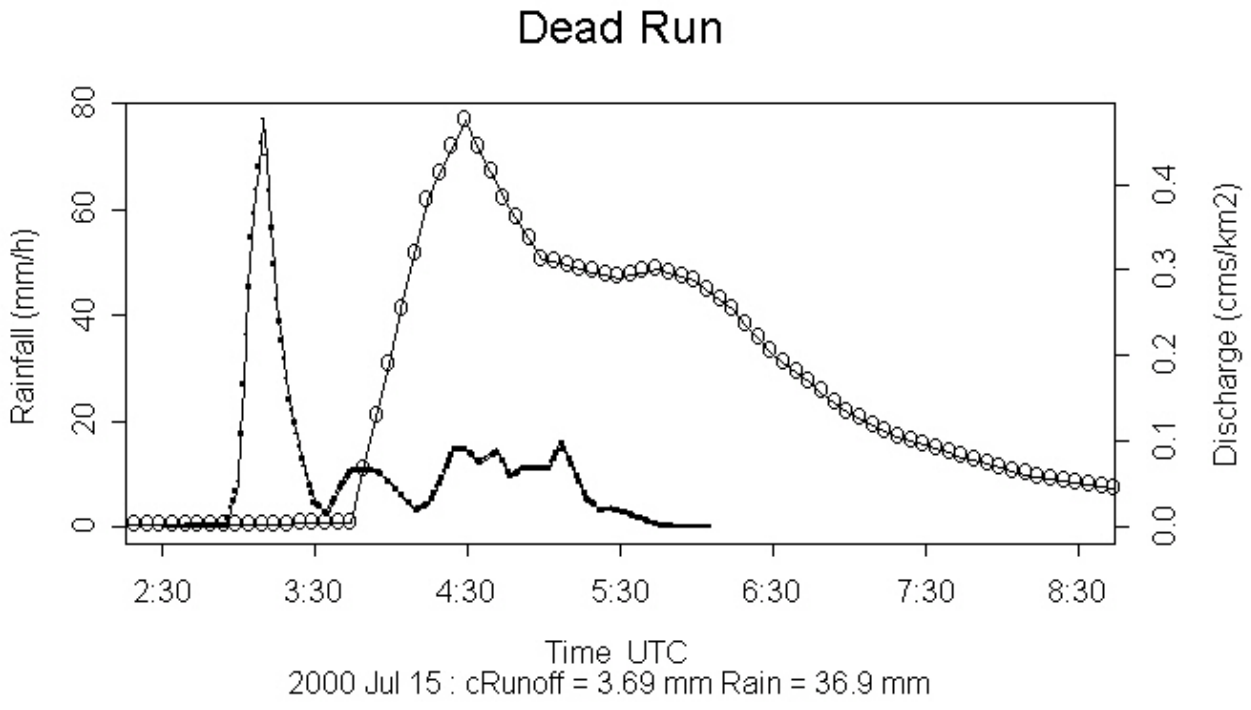
Dead Run
Rainfall (mm/h)
0
20
40
60
80
Discharge (cms/km2)
0.0
0.1
0.2
0.3
0.4
2:30
3:30
4:30
5:30
6:30
7:30
8:30
Time UTC
2000 Jul 15 : cRunoff = 3.69 mm Rain = 36.9 mm

White Marsh at Fullerton

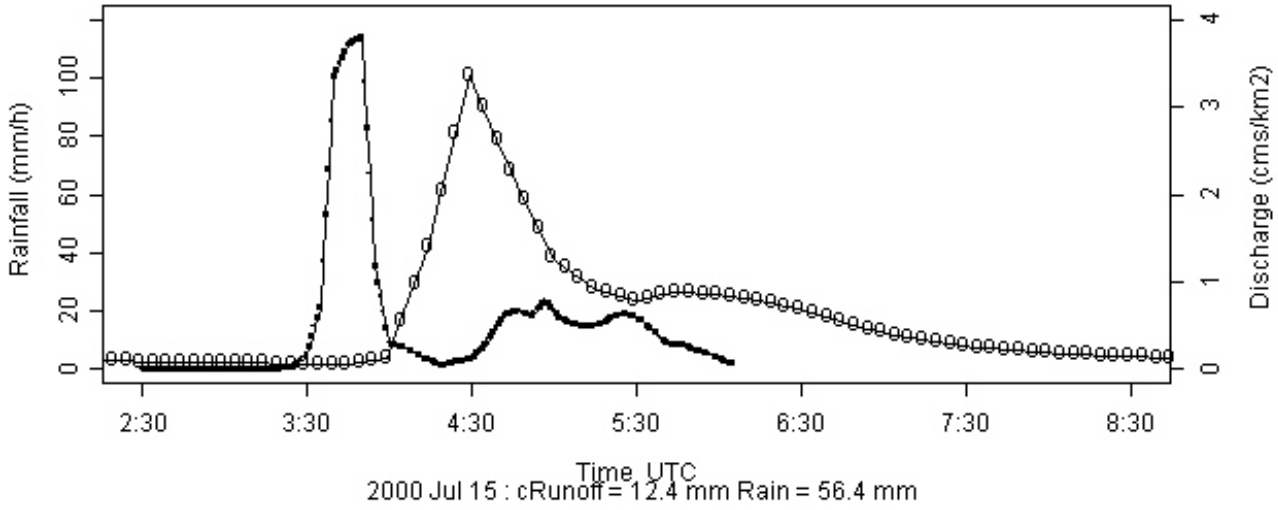

2000 Jul 15 : cRunoff = 12.4 mm Rain = 56.4 mm

North Fork White Marsh

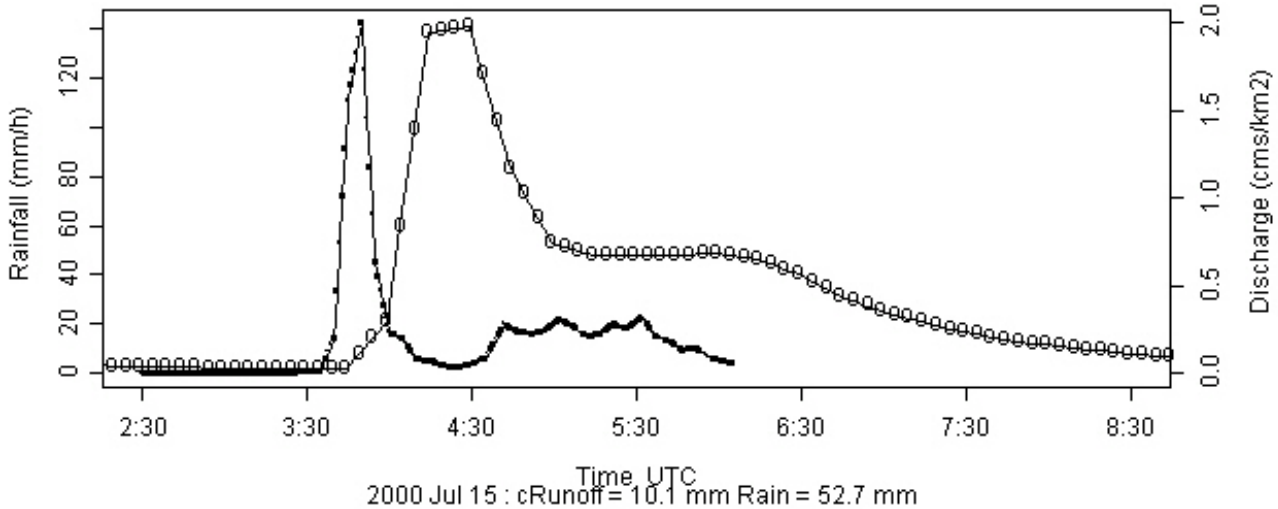

2000 Jul 15 : cRunoff = 10.1 mm Rain = 52.7 mm

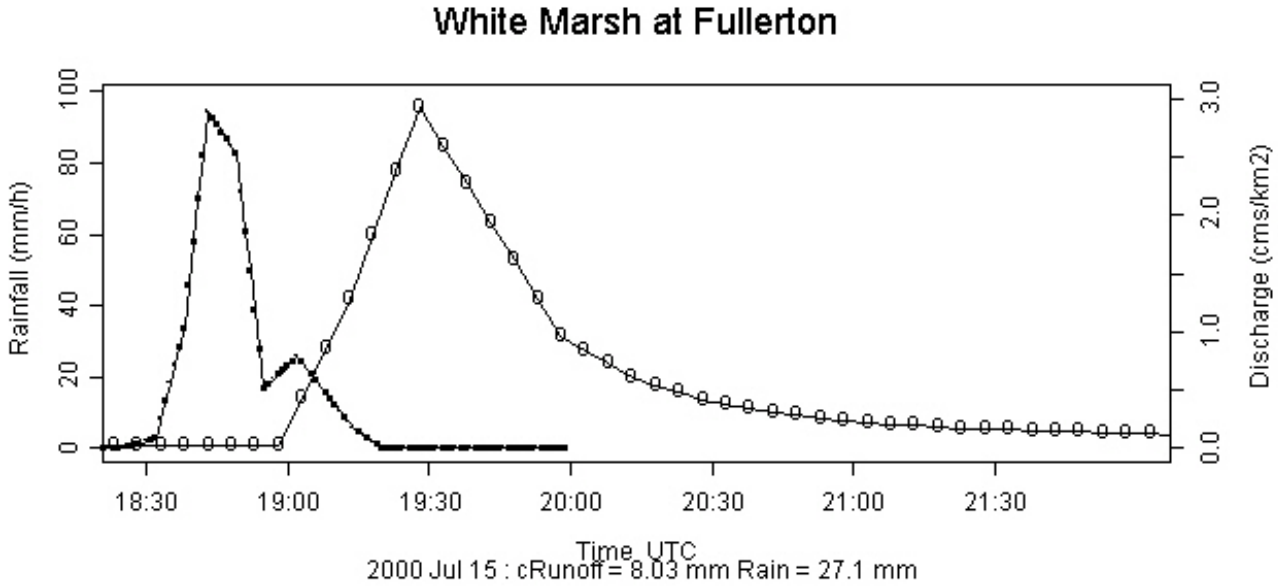
White Marsh at Fullerton
Rainfall (mm/h)
0
20
40
60
80
100
Discharge (cms/km2)
0.0
1.0
2.0
3.0
18:30
19:00
19:30
20:00
20:30
21:00
21:30
Time UTC
2000 Jul 15 : cRunoff = 8.03 mm Rain = 27.1 mm

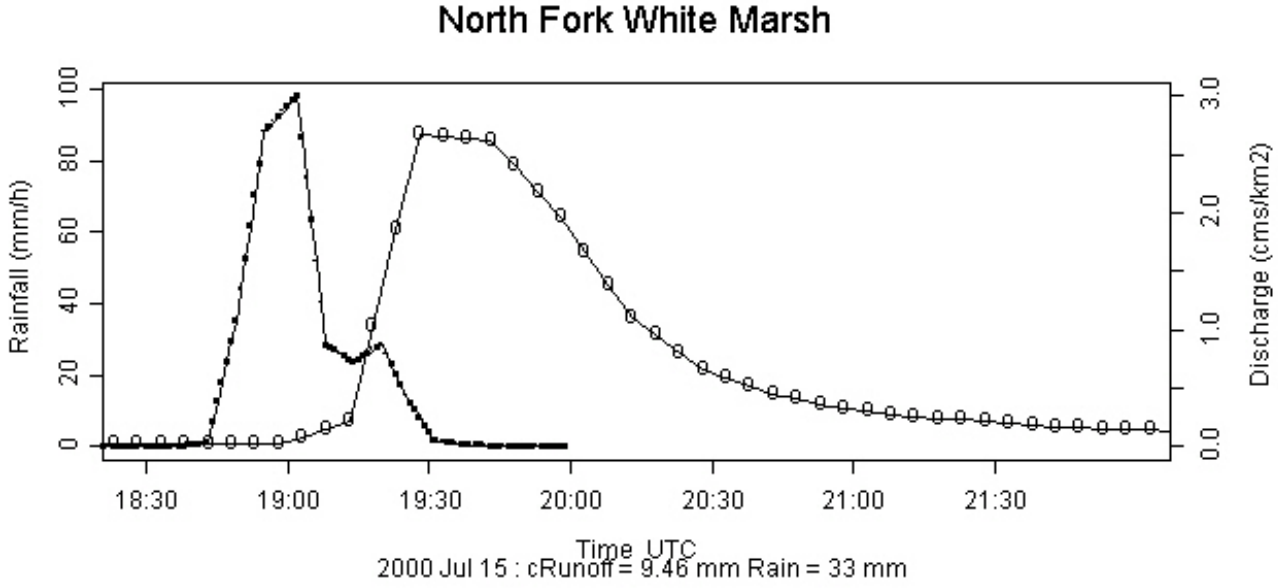
North Fork White Marsh
Rainfall (mm/h)
0
20
40
60
80
100
Discharge (cms/km2)
0.0
1.0
2.0
3.0
18:30
19:00
19:30
20:00
20:30
21:00
21:30
Time UTC
2000 Jul 15 : cRunoff = 9.46 mm Rain = 33 mm

White Marsh at Fullerton

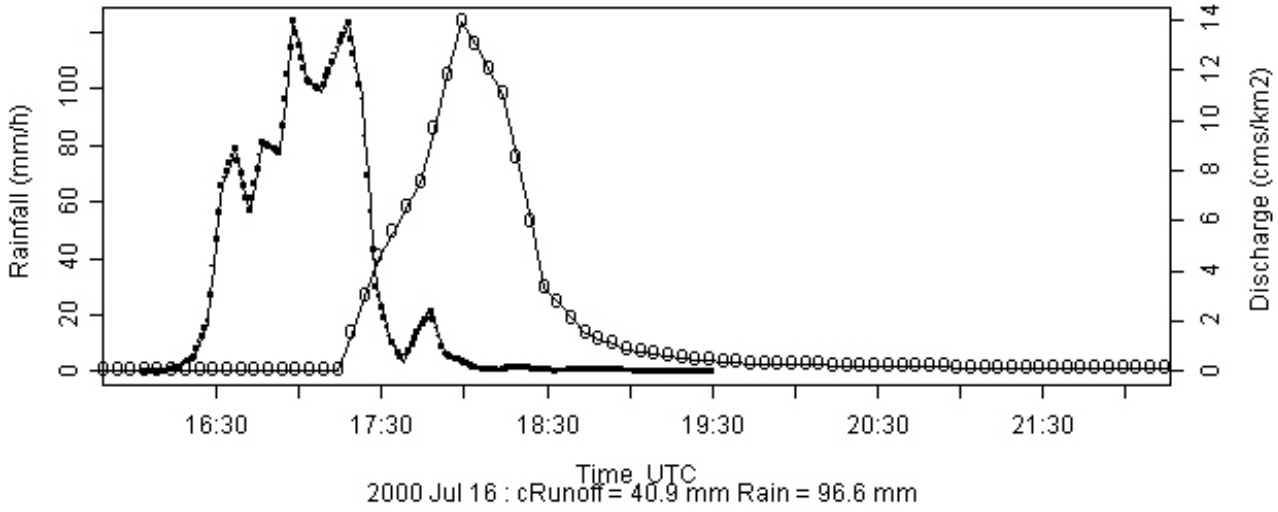

2000 Jul 16 : cRunoff = 40.9 mm Rain = 96.6 mm

North Fork White Marsh

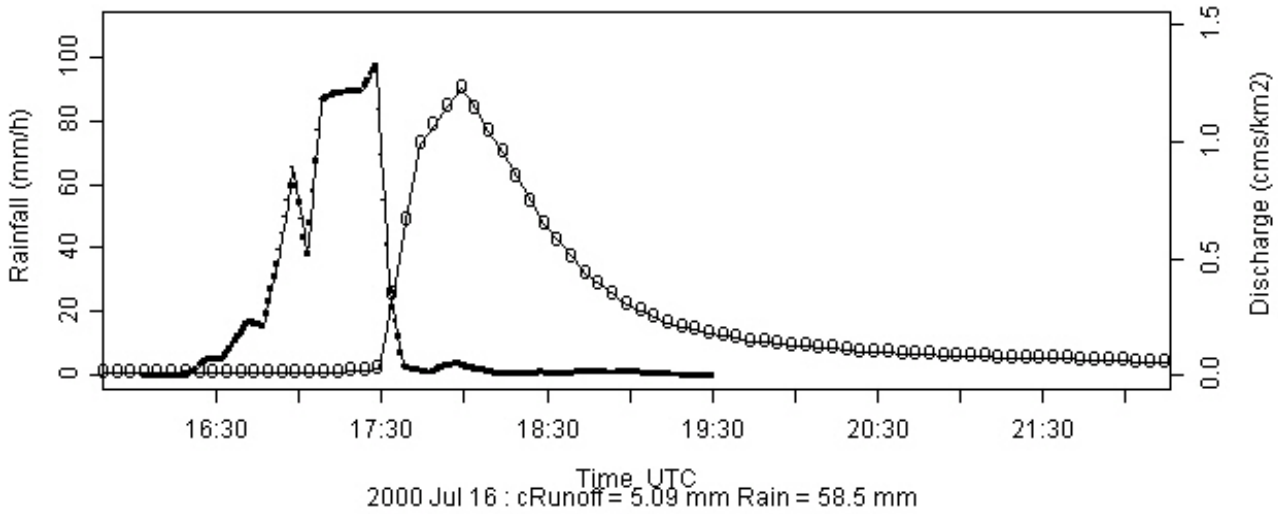

2000 Jul 16 : cRunoff = 5.09 mm Rain = 58.5 mm

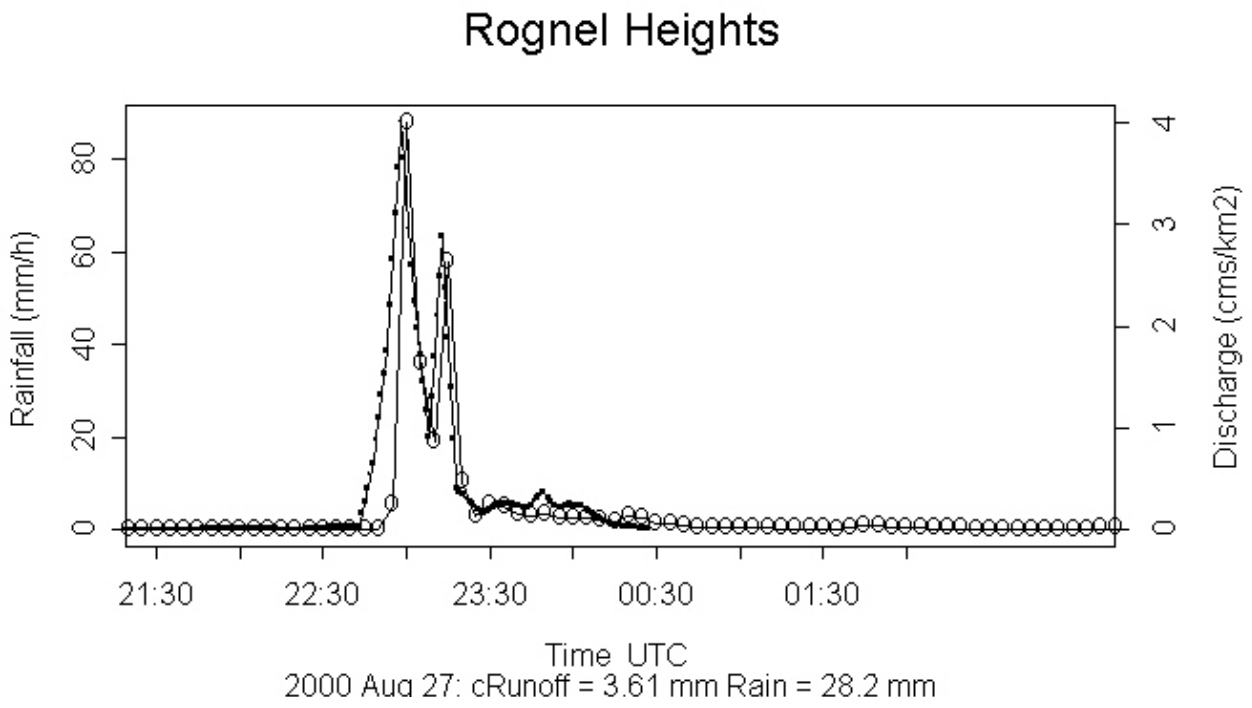
Rognel Heights
Rainfall (mm/h)
0
20
40
60
80
Discharge (cms/km2)
0
1
2
3
4
21:30
22:30
23:30
00:30
01:30
Time UTC
2000 Aug 27: cRunoff = 3.61 mm Rain = 28.2 mm

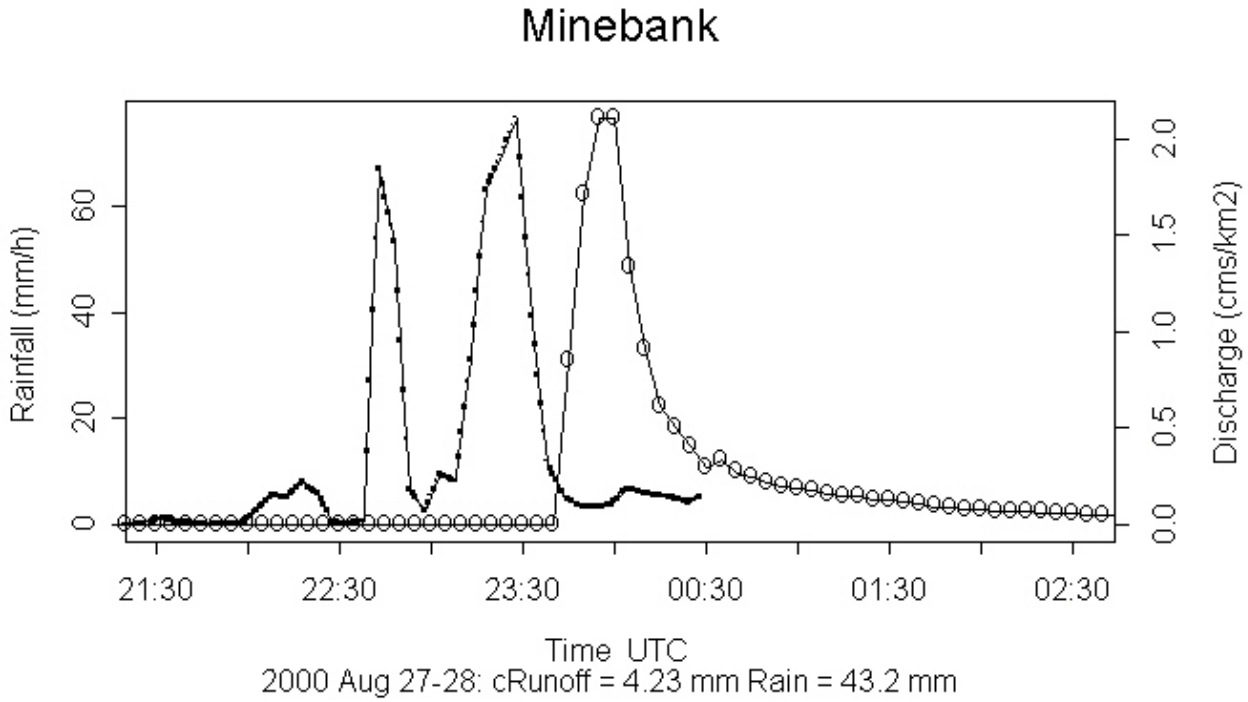
Minebank
Rainfall (mm/h)
0
20
40
60
Discharge (cms/km2)
0.0
0.5
1.0
1.5
2.0
21:30
22:30
23:30
00:30
01:30
02:30
Time UTC
2000 Aug 27-28: cRunoff = 4.23 mm Rain = 43.2 mm

Moores Run at Radeke Ave

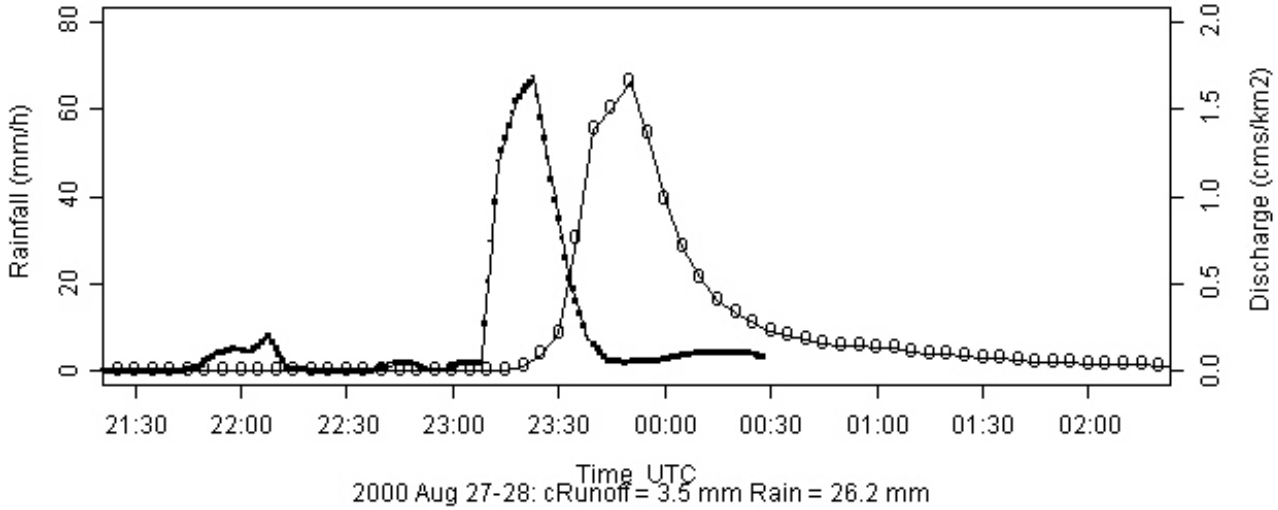

2000 Aug 27-28: cRunoff = 3.5 mm Rain = 26.2 mm

Moores Run tributary

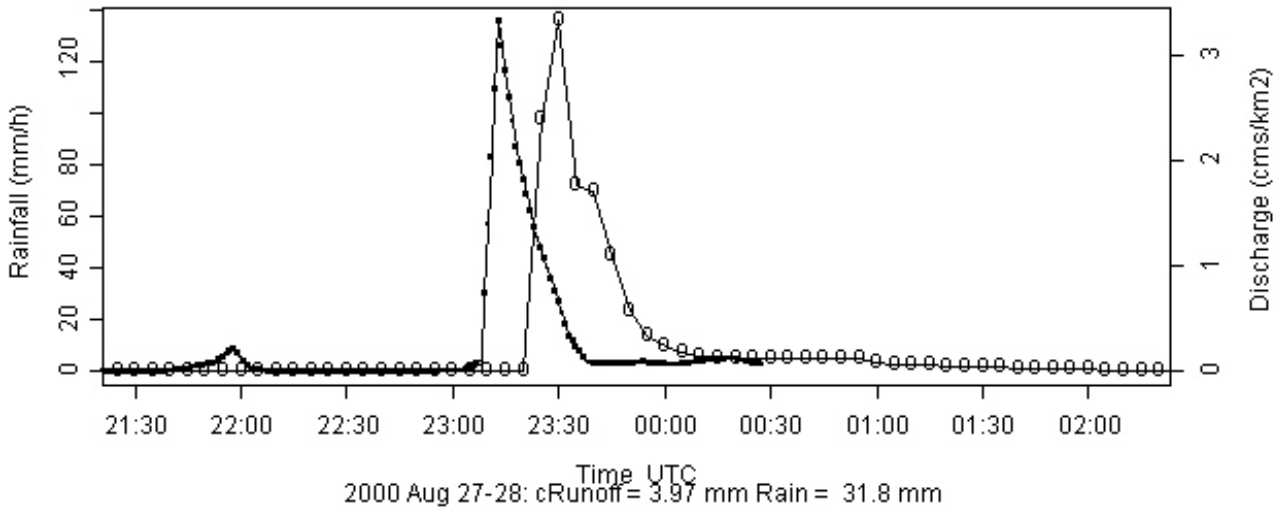

2000 Aug 27-28: cRunoff = 3.97 mm Rain = 31.8 mm

White Marsh at Fullerton

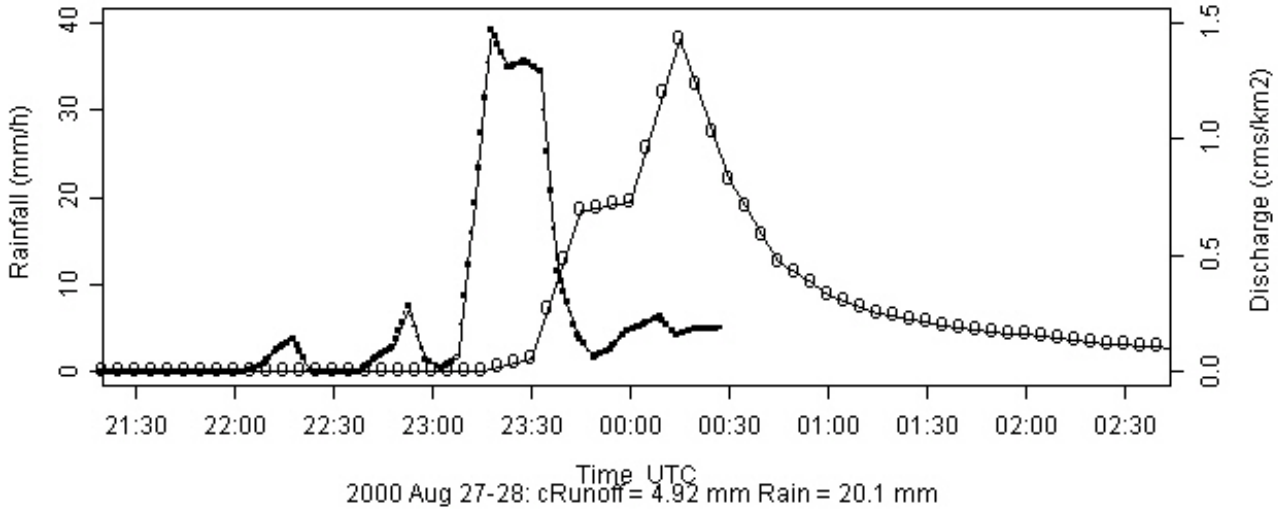

2000 Aug 27-28: cRunoff = 4.92 mm Rain = 20.1 mm

North Fork White Marsh

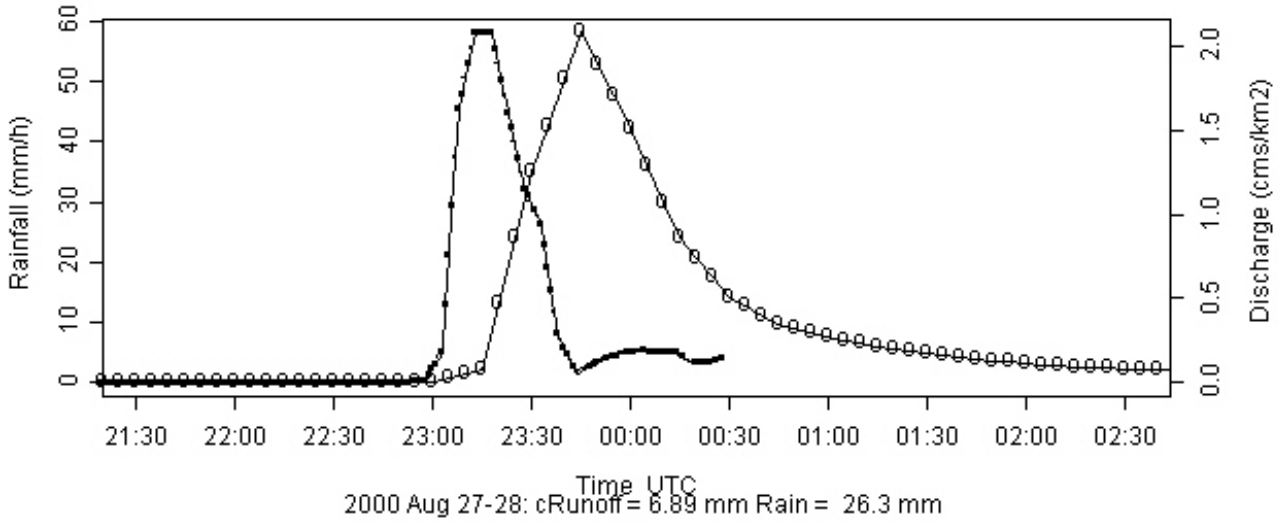

2000 Aug 27-28: cRunoff = 6.89 mm Rain = 26.3 mm

Moores Run at Radeke Ave

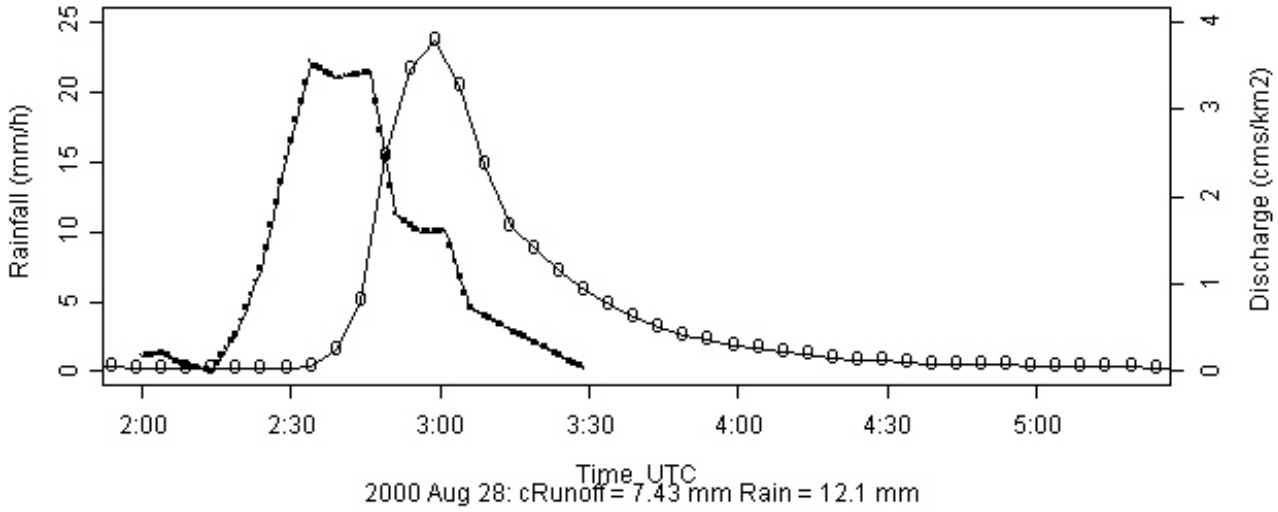

2000 Aug 28: cRunoff = 7.43 mm Rain = 12.1 mm

Moores Run tributary

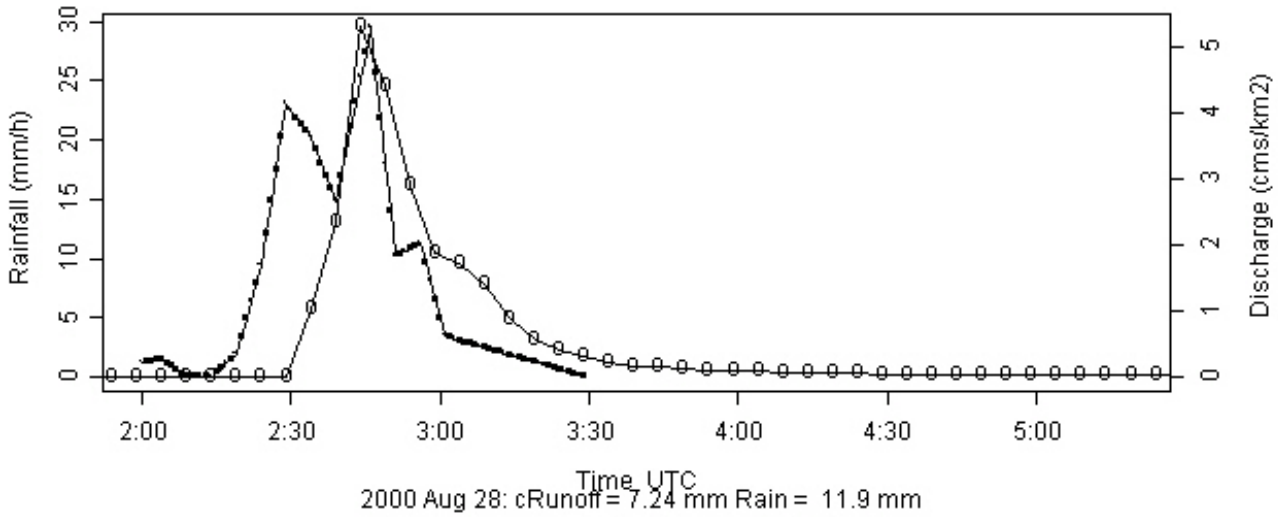

2000 Aug 28: cRunoff = 7.24 mm Rain = 11.9 mm

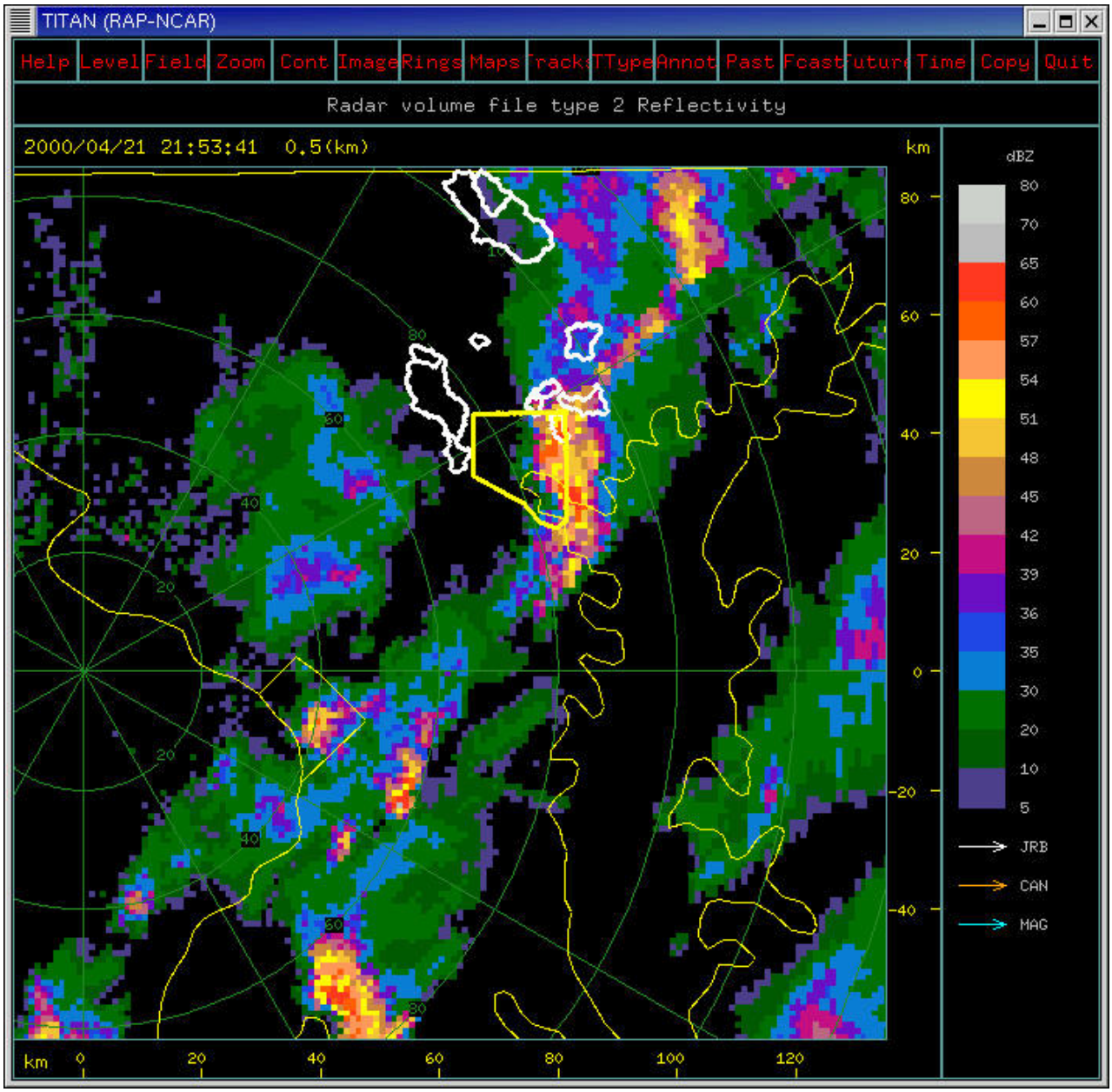

Figure 2.4. Refllectivity image (1.5 km CAPPI) at 2153 UTC on 21 April. The Baltimore City boundary is outlined in yellow. Dead Run, Moores Run, Minebank Run and Whitemarsh Run basin boundaries are outlined in white.

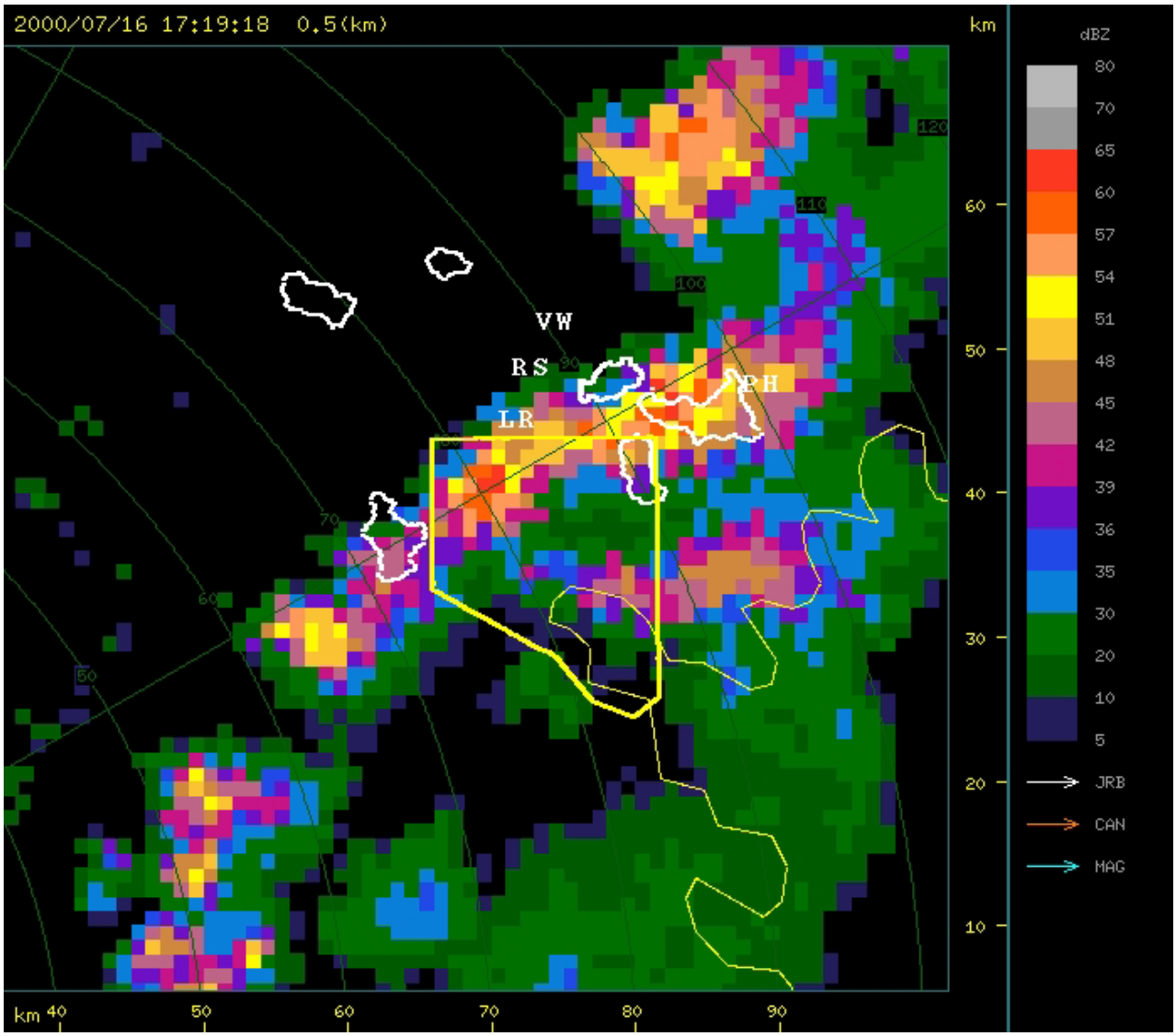

Figure 2.5. Reflectivity image at 1918 UTC on 16 July (as in Fig. 2.4).

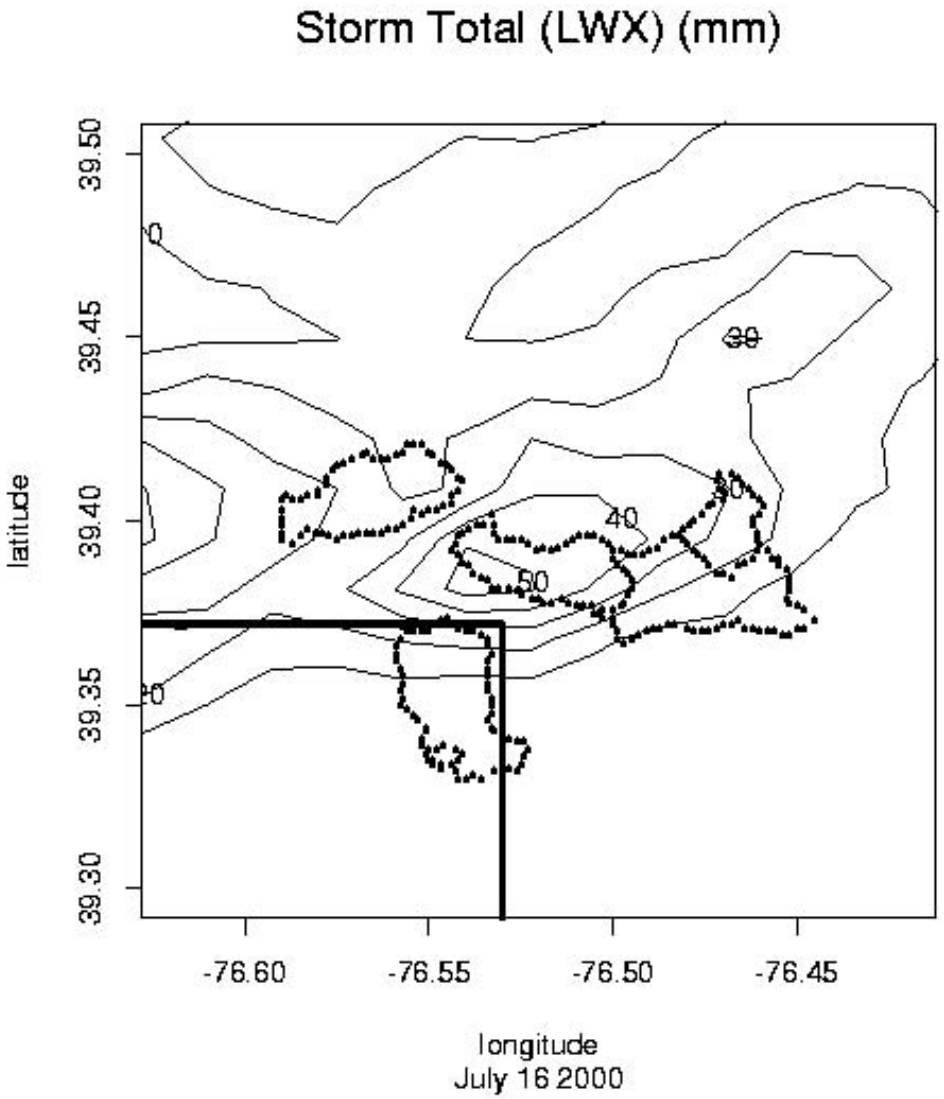

Figure 2.6. Storm total rainfall map for the 16 July storm (closeup).

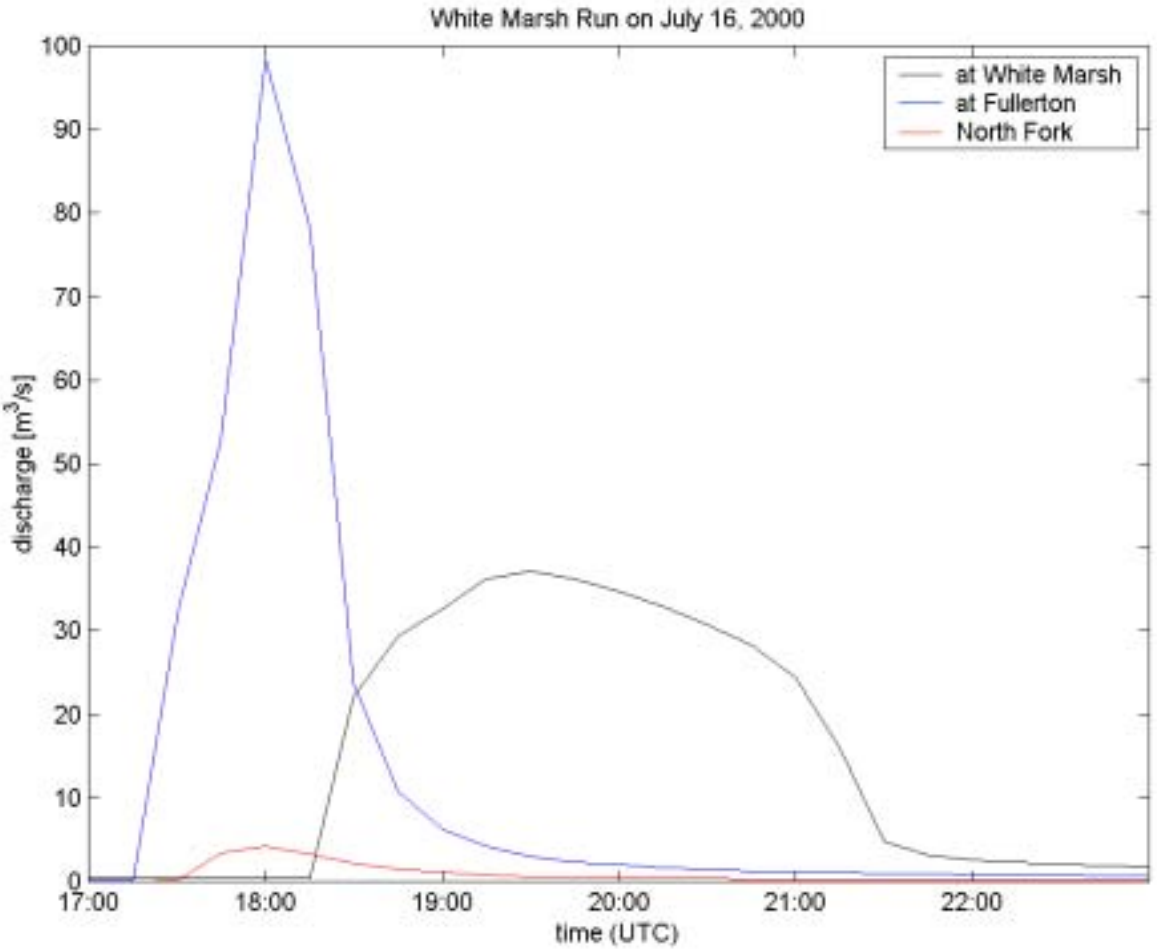

Figure 2.7. Time series of discharge ($m^3 s^{-1}$) for Whitemarsh Run at Fullerton (blue), North Fork Whitemarsh Run (red) and Whitemarsh Run at Whitemarsh.

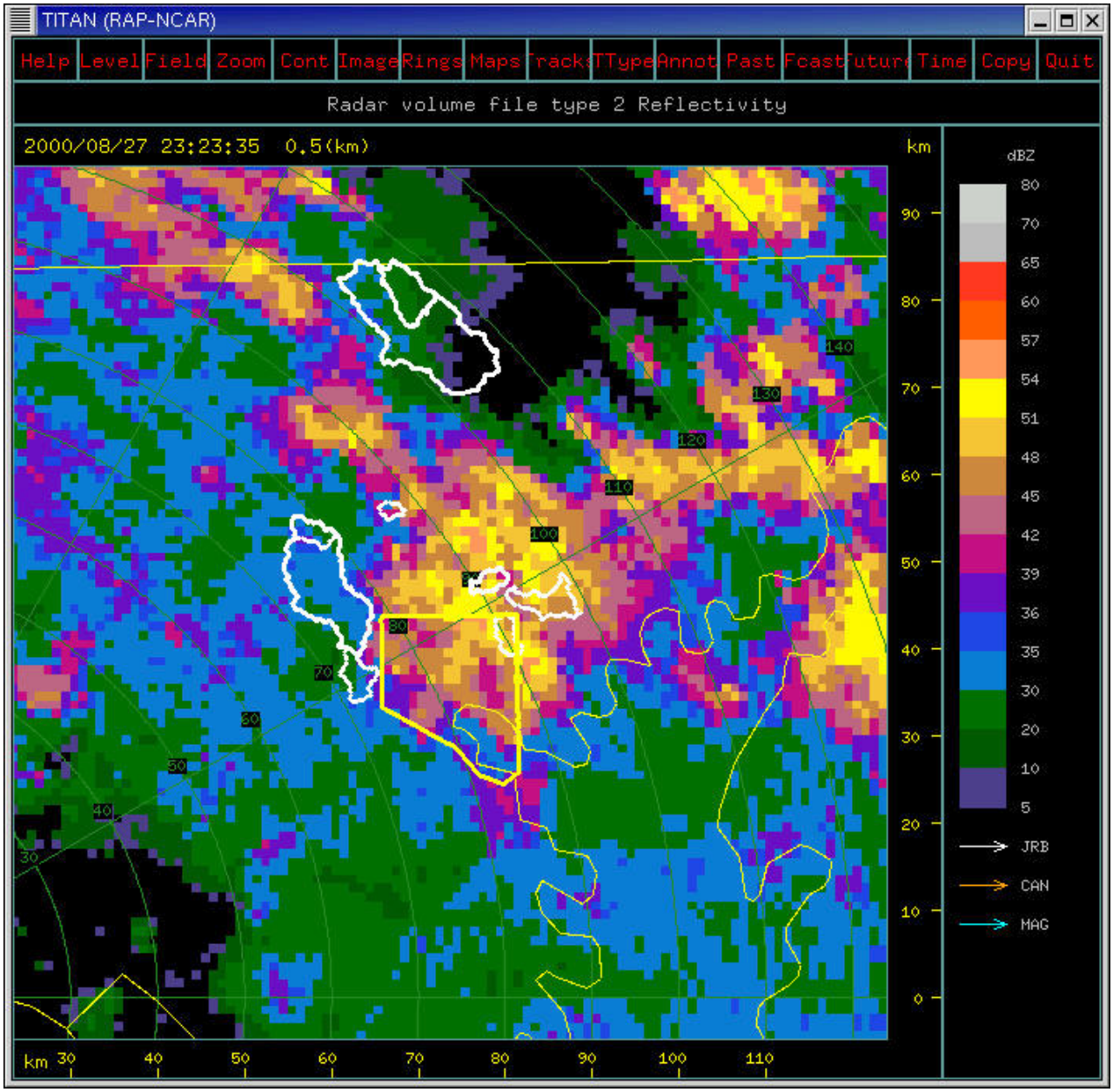

Figure 2.8. Reflectivity image (as in Fig. 2.5) at 2323 UTC on 27 August.

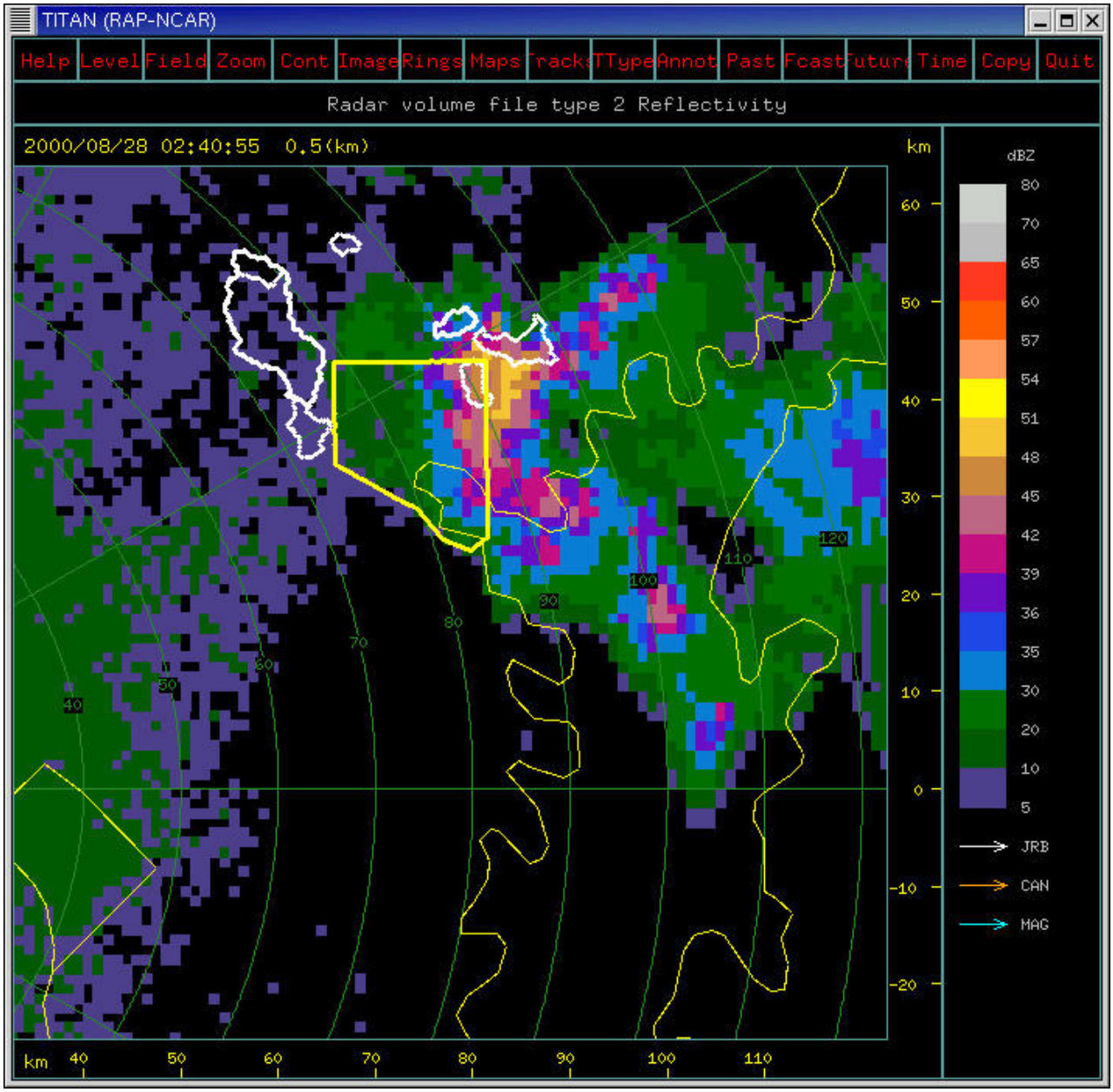

Figure 2.9. Reflectivity image at 0240 UTC on 28 August (as in Fig. 2.5).

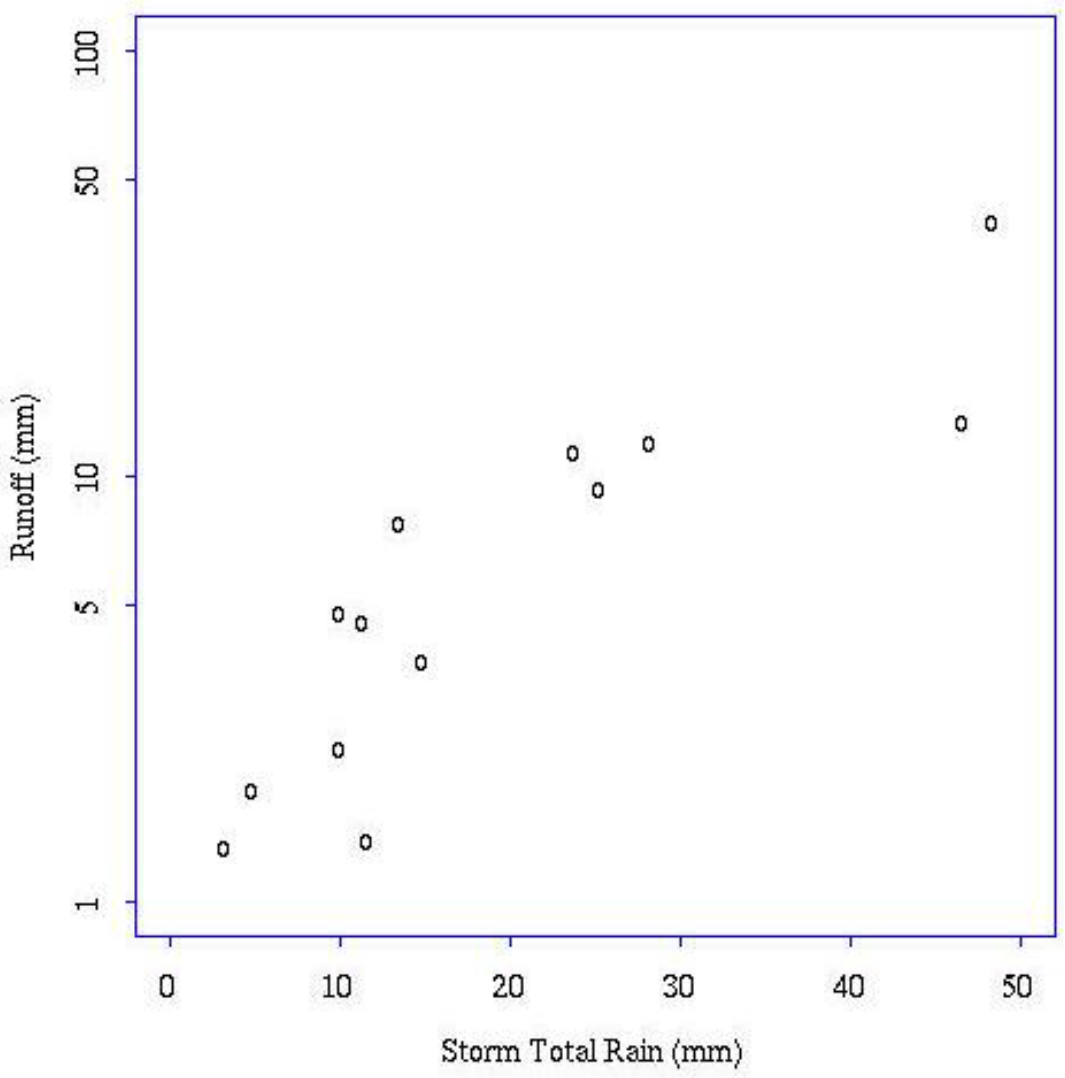

Figure 2.10 Storm total rainfall and runoff in Whitemarsh Run for warm season events in 2000.

3. The 23 July 1997 Storm and Flood in the Charlotte, North Carolina Metropolitan Area

Rainfall accumulations of more than 250 mm were recorded in Mecklenburg County, North Carolina during an 18 hour period on 23 July 1997, more than doubling the record 24 hour accumulation from a 100 year rain gage record in Charlotte. Heavy rainfall was distributed throughout the Charlotte metropolitan region, with record flooding in the urban core of the city. In this study, we use observations from an urban rain gage mesonet, two WSR-88D (Weather Surveillance Radar – 1988 Doppler) weather radars, and a dense network of stream gages to examine rainfall estimation for extreme, flash flood producing storms in an urban environment.

The Charlotte, North Carolina metropolitan area (Figure 3.1) has experienced extensive urban and suburban growth during the last 40 years (Smith et al. [2002]). The urban core of the region is drained by Little Sugar Creek (Fig. 3.1), which has seen a sharply increasing trend in flood magnitude punctuated by a series of extreme floods during the late 1990s (Smith et. al. [2002]). The four largest flood peaks, and five of the largest seven flood peaks, in the 76-year discharge record have occurred since August 1995. This study focuses on the most heavily urbanized portion of the Little Sugar Creek basin, which is located above the U.S. Geological Survey (USGS) stream gage at Medical Center Drive.

The 23 July 1997 storm produced two peaks of 150 $m^3 s^{-1}$ in Little Sugar Creek (at a drainage area of 32 km^2; see Fig. 3.2) from two periods of rainfall with very different rain rate distributions. Runoff of 86 mm for the first period of rainfall was produced by 134 mm of rainfall. The second period of rainfall produced 60 mm of runoff from 60 mm of rainfall. Storage processes clearly played a central role in the contrasting response of Little Sugar Creek to the two periods of rainfall on 23 July 1997.

Rainfall estimates were derived for the 23 July 1997 storm at 1 km^2 grid scale and 5-minute time scale from WSR-88D observations at Greer, South Carolina (KGSP) and Columbia, South Carolina (KCAE). The USGS rain gage network in Mecklenburg County (see Hazell and Bales [1997] and Robinson et. al. [1998]) consists of 46 tipping bucket rain gages, of which nine are located in or adjacent to the Little Sugar Creek basin

above the Medical Center gage (Figure 3.2). The dense network of rain gages is used to examine the radar rainfall estimates for the 23 July 1997 event.

Radar rainfall estimates from the Columbia and Greer radars were computed using a standard Z-R conversion and bias correction (Baeck and Smith [1998], Fulton et al. [1998] and Seo et al. [1999]). The bias was estimated as the ratio between the gage and radar measurements of storm total rainfall, for radar bins containing rain gages (see Smith and Krajewski [1993]). The bias estimate for the 23 July 1997 storm was 1.54 for the Greer radar and 1.64 for the Columbia radar. The distance from each radar to the Charlotte region is approximately 100 km. The differences in bias between the two radars may reflect a modest calibration difference between the two radars (Smith et al. [1996]). The magnitude of the bias is within the range associated with low-echo centroid storms (see additional discussion below and in Krajewski and Smith [2002], Smith et al. [1996b] and [2001]).

For the 23 July 1997 event, the root mean square error (RMSE) between gage measurements and radar observation from Greer and Columbia was computed at 5, 15, and 60-minute time scale and for the storm total accumulation (Table 3.1). The average rainfall rate for a gage is computed from periods of non-zero rainfall rates. For the 5-minute time step the RMSE (16.2 mm h^{-1}) was 80% of the mean rain rate for both the Greer and Columbia radars. For the 15-minute time step the RMSE was 66% and 70% of the mean rain rate, for 1-hour time step 42% and 49%, and for the storm total 8% and 12%, respectively. The relatively large ratios of RMSE to rainfall rate highlight the difficulty of comparing measurements with different spatial scales and sampling methods (see Ciach and Krajewski [1999]). Bias correction is an important element of rainfall estimation for the 23 July storm. For storm total rainfall estimates, it is a dominant element.

Comparison of rainfall rates between the two radars yields an additional measure of the variability of rain rate estimates (Table 3.1). The ratio of RMSE to measured rainfall for the 5-minute time step was 52%, for the 15-minute time step 52%, for the 1-hour time-step 43%, and for the storm total 11%.

Record rainfall accumulations from the 23 July storm resulted from convective elements repeatedly forming west of Mecklenburg County along an east-west oriented

frontal boundary and tracking to the east over the Charlotte metropolitan area (Figure 3.3). In this sense, the 23 July storm is similar to storms studied by Chappel [1989] and termed "quasistationary convective systems". The elements of the 23 July event were small multi-cellular storms, resulting in large spatial gradients in rainfall rate. The storm total rainfall distribution (Figure 3.2) strongly reflects storm structure, motion, and evolution of individual convective elements of the storm system. Even for the storm total rainfall field, which represents accumulations during a time period greater than 12 hours, the dense Mecklenburg County rain gage network is inadequate for representing the detailed spatial distribution of rainfall.

A comparison of time series for rain gage and radar measurements from six locations within and surrounding the Little Sugar Creek basin further highlights the spatial and temporal variability in rain rates and the ability of radar observations to capture this variability (Figure 3.4 a-f). The Little Sugar Creek basin received the largest rainfall rates and accumulations during the first pulse of rainfall from 5 – 7 UTC (Fig. 3.4). For locations just south of the Medical Center stream gage rainfall accumulations for the second pulse (11-15 UTC) are comparable to or larger than the first pulse. Based on the gage-radar comparison, radar observations are able to accurately resolve the rainfall field at a high spatial and temporal resolution.

The 23 July 1997 storm was an organized thunderstorm system with modest cloud-to-ground (CG) lightning strikes. The maximum storm total CG strike density (figure not shown) of 1 CG strike km^{-2} was located approximately 5 km north of Little Sugar Creek and was produced largely during the first period of heavy rainfall. CG strike densities over much of the region were less than 0.5 CG strike km^{-2}. Echo tops for the storms were markedly lower than those produced by typical severe thunderstorms. Lightning and vertical structure analyses suggest that the 23 July storm bears similarities to "low echo centroid" storms in which high rainfall rates are linked with efficient cloud microphysical processes. These storms are often associated with large bias values in WSR-88D rainfall estimates based on the default Z-R relationship. The tropical Z-R relationship (Fig. 3.5) results in storm total rainfall estimates that are systematically larger than those from the default Z-R relationship (although the relative errors in storm

total accumulation are somewhat smaller). Bias correction would be required for the tropical Z-R relationship.

Basin-averaged rainfall time series were developed for seven drainage basins adjacent to or near Little Sugar Creek. These time series (at 5 minute time interval) were compared with 15 minute discharge observations (Figure 3.6). The six drainage basins in addition to Little Sugar Creek are: 1) Irwin Creek (immediately west of Little Sugar Creek), 2) Briar Creek (immediately east of Little Sugar Creek), 3) Little Hope Creek (immediately south of Little Sugar Creek), 4) McMullen Creek (immediately east of Briar Creek), Long Creek (northwest of Irwin Creek) and Mallard Creek (northeast of Little Sugar Creek). As with the Baltimore analyses, the rainfall – discharge analyses demonstrate the capability of WSR-88D rainfall estimates to resolve flash-flood producing rainfall in urban settings.

CONCLUSIONS:

Radar rainfall estimates for the 23 July 1997 event capture the timing, spatial variability of rainfall, and magnitude of short-duration rainfall rates. The RMSE of storm total rainfall, relative to rain gage observations, is within the range of measurement error for the rain gage observations. Increasing RMSE for shorter time durations principally reflects the temporal and spatial sampling differences of the two sensor systems. The spatial resolution of the "dense" Mecklenburg County rain gage network is inadequate to resolve spatial variability of flash flood-producing storms like the July 23, 1997 event. The bias of radar rainfall estimates for the default Z-R relationship is approximately 1.5 (with evidence of a modest calibration difference between Greer and Columbia). The tropical Z-R relationship results in overestimation of storm total rainfall. Bias-corrected rainfall estimates for the 23 July 1997 storm provide exceptional observations for forecasting the flash flood response in urban and urbanizing drainage basins in the Charlotte metropolitan region. In this respect, the analyses augment the conclusions drawn from the Baltimore analyses in Section 2.

Table 3.1.

	5 – minute	15 - minute	1-hour	Storm Total
Average Rainfall Rate				
Gage (mm h^{-1})	20.3	15.2	11.3	10.9
Ratio of RMSE to Average Rainfall Rate at Gage				
Gage v. Greer	0.80	0.66	0.42	0.08
Gage v. CAE	0.80	0.70	0.49	0.12
Ratio of RMSE to Average Rainfall Rate at Gage				
CAE v. Greer	0.52	0.52	0.43	0.11

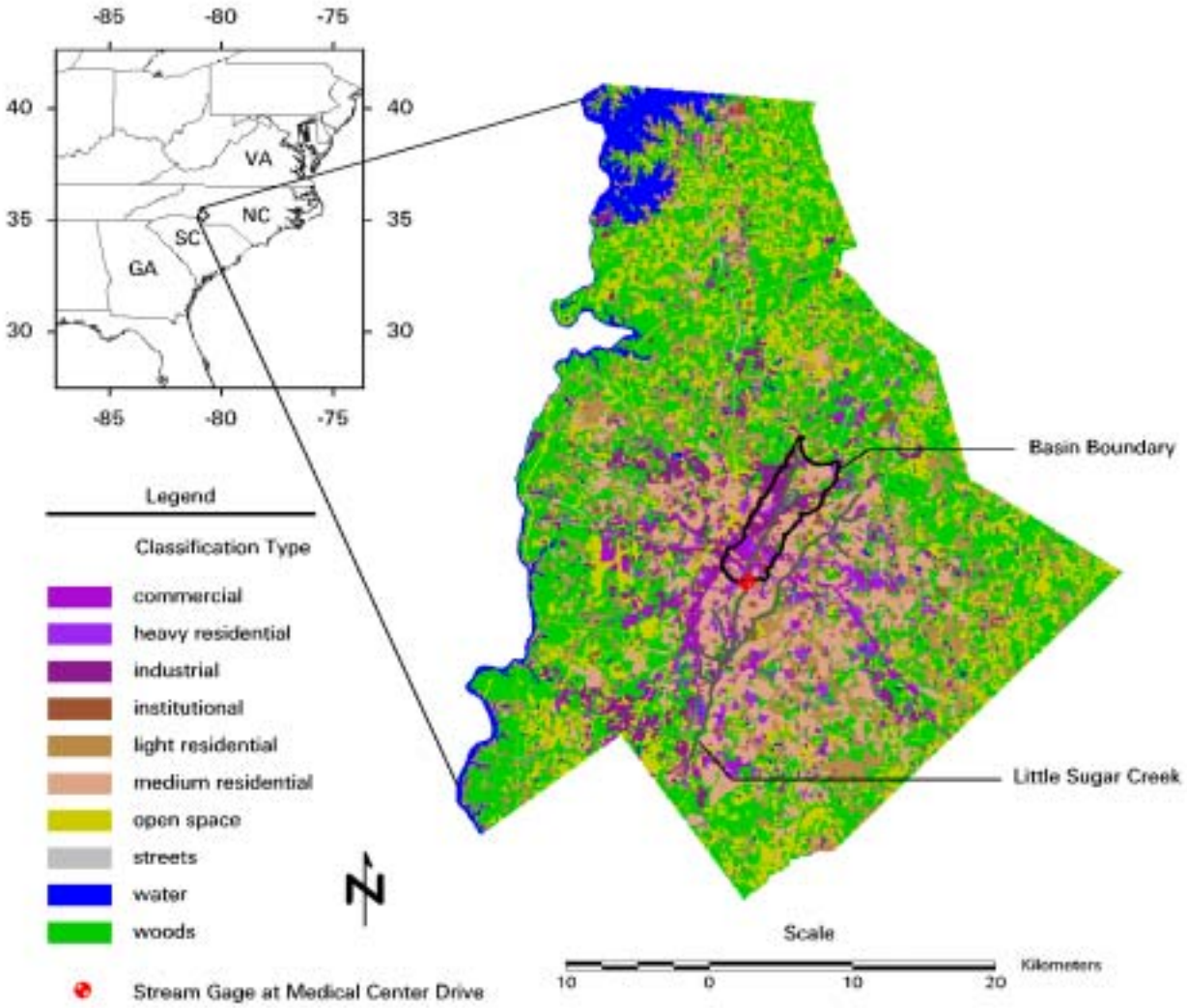

Figure 3.1 Location map for the Charlotte NC study region. The Little Sugar Creek basin boundary (above Medical Center stream gage) is outlined in black.

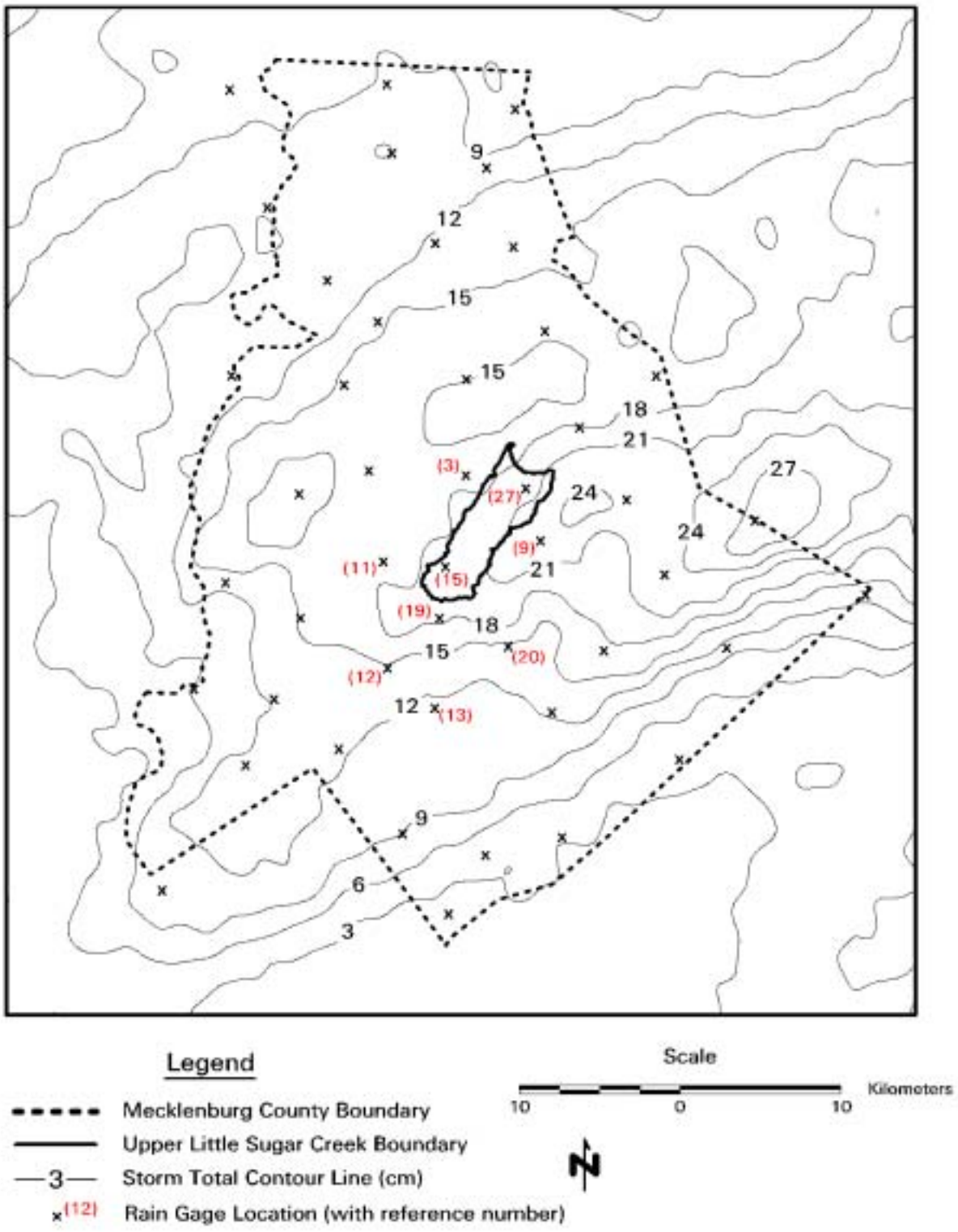

Figure 3.2 Storm total rainfall map for the 23 July 1997 storm (see Fig. 3.1 for location map).

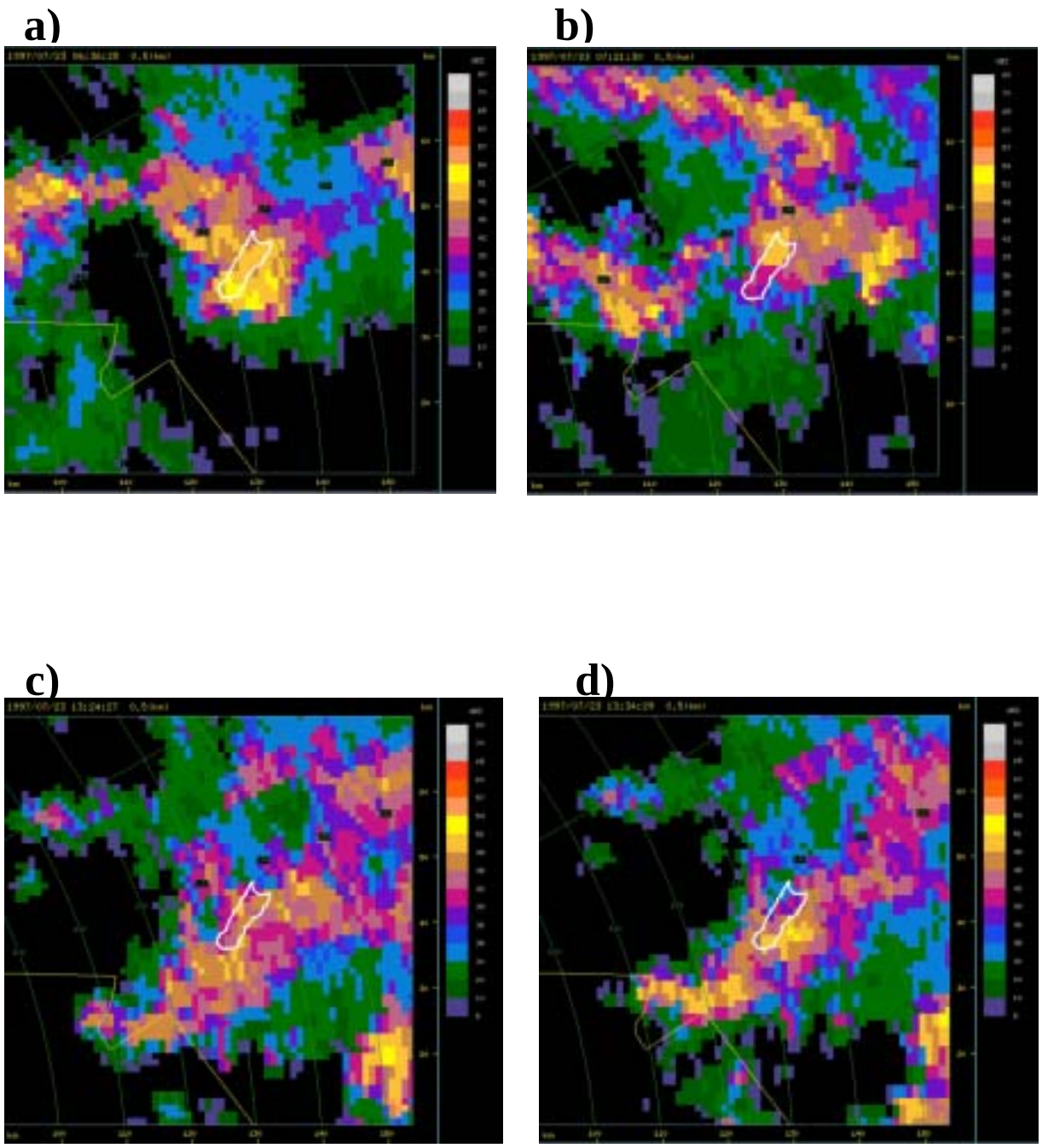

Figure 3.3. Reflectivity images from the Greer WSR-88D for the periods of heaviest rainfall over the Charlotte region on 23 July 1997: a) 0636 UTC, b) 0721 UTC, c) 1324 UTC, and d) 1334 UTC .

Gage 11

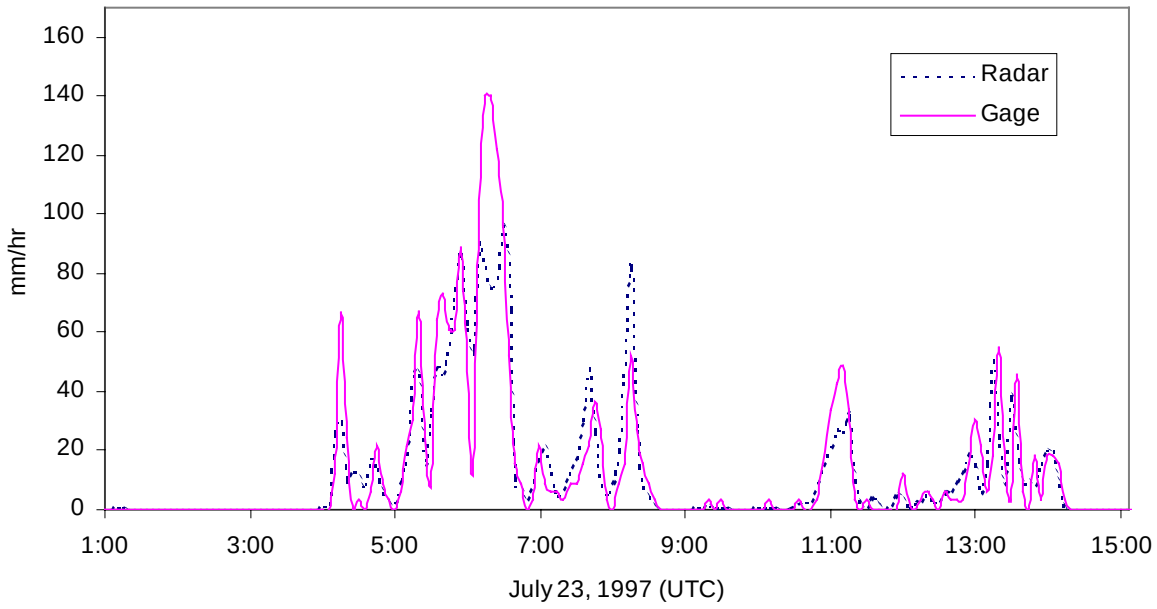

Figure 3.4a

Gage 15

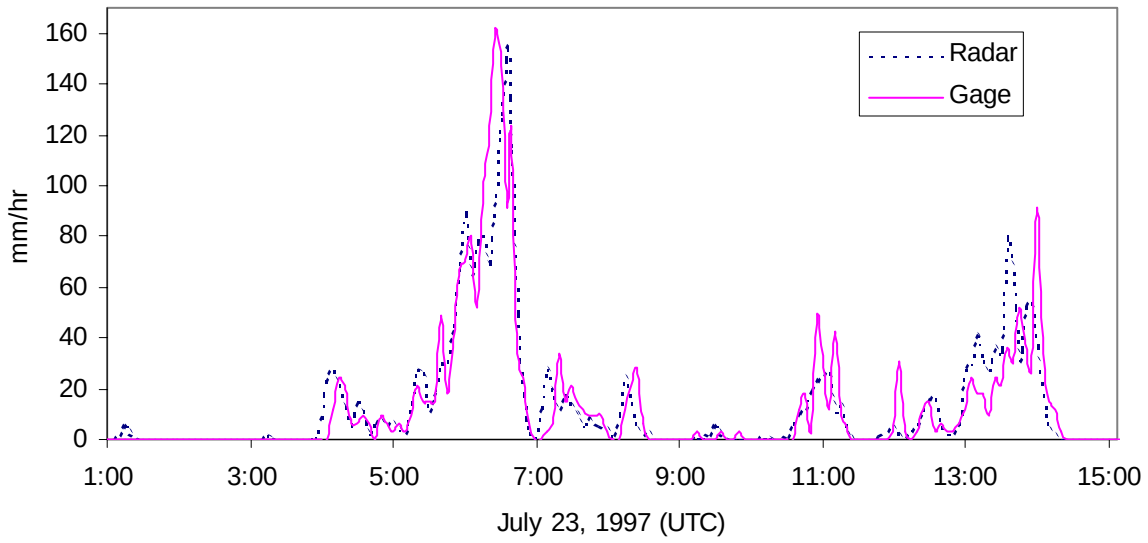

Figure 3.4b

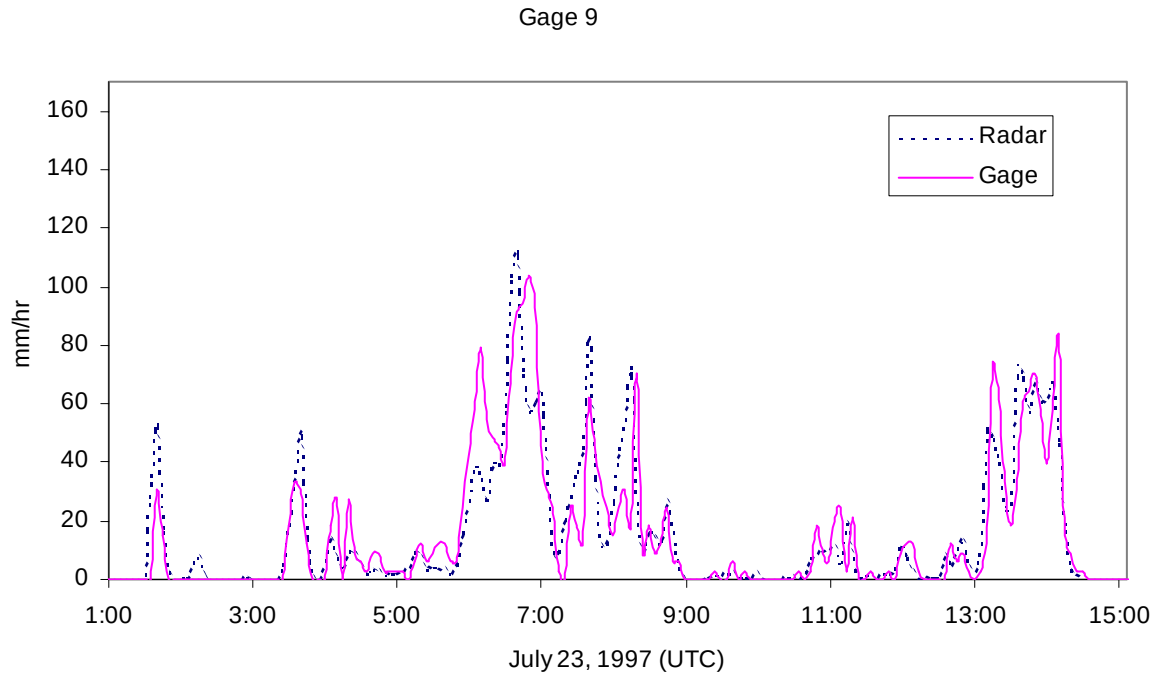

Figure 3.4c

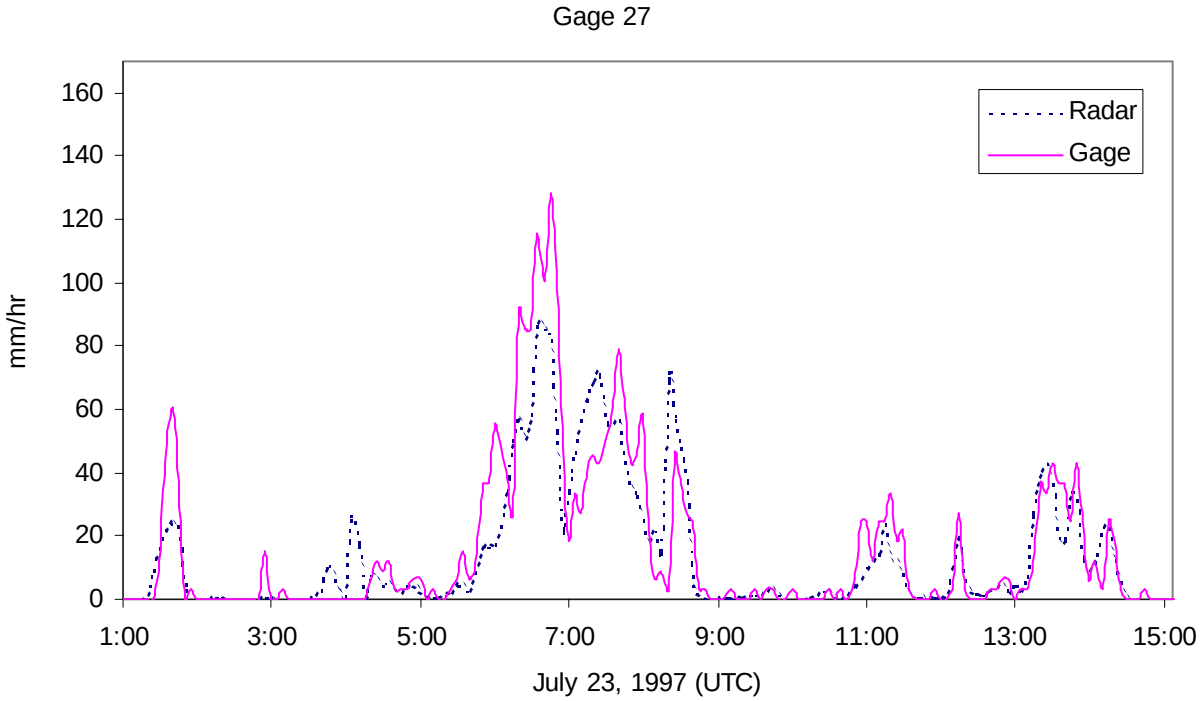

Figure 3.4d

Gage 19

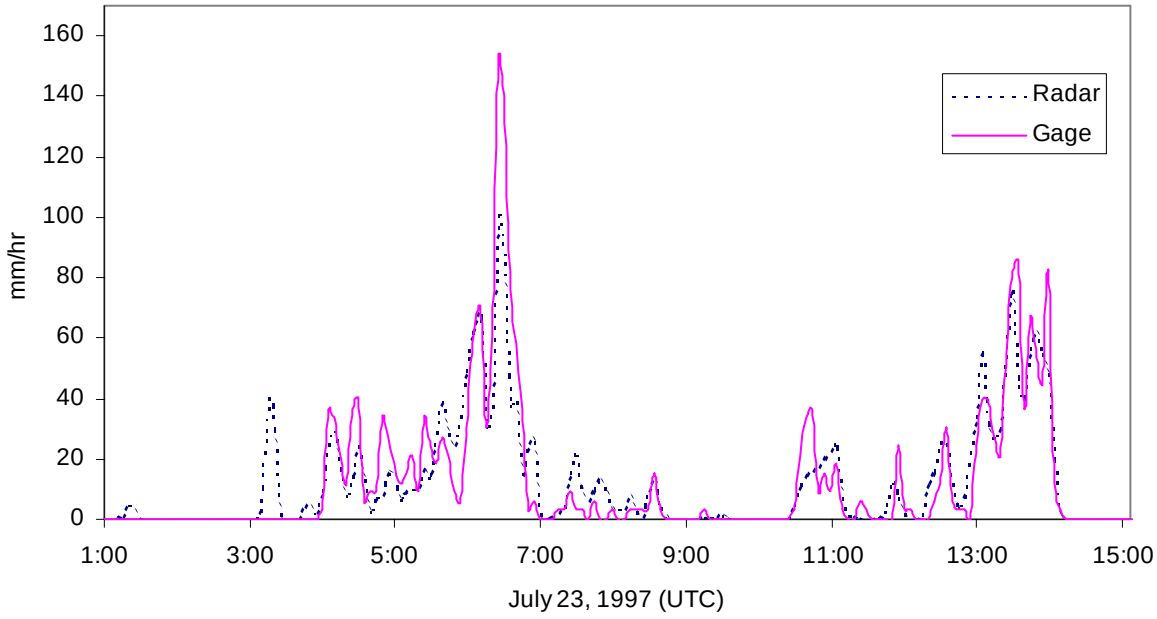

Figure 3.4e

Gage 12

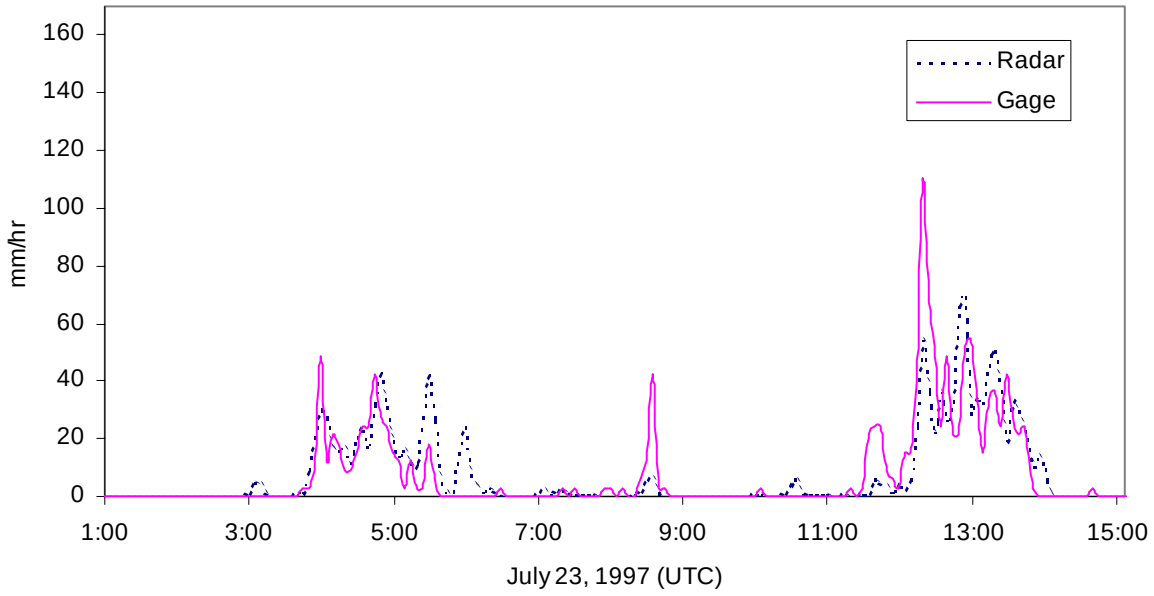

Figure 3.4f

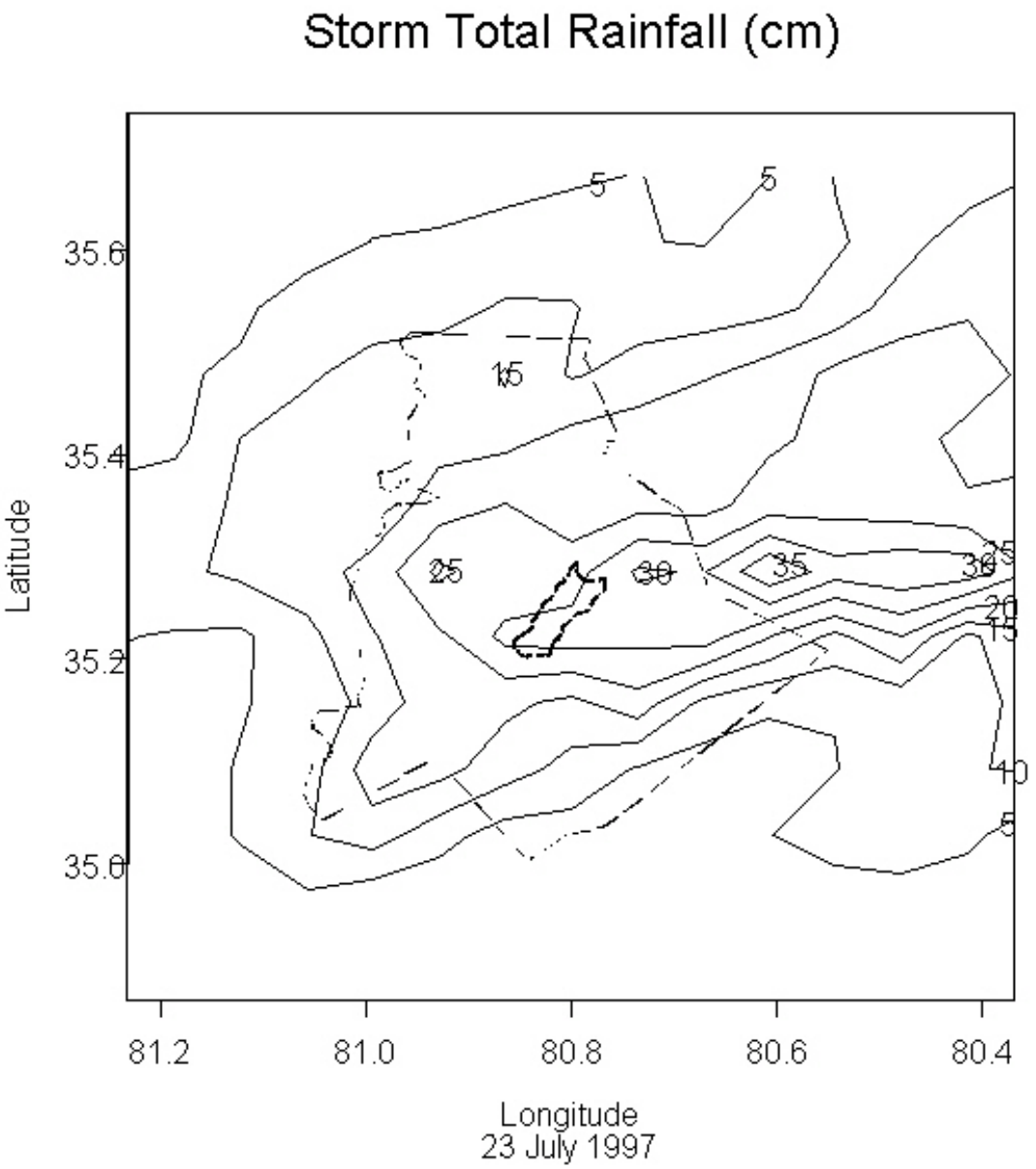

Figure 3.5. Storm total rainfall accumulation for the 23 July storm using the tropical Z-R relationship.

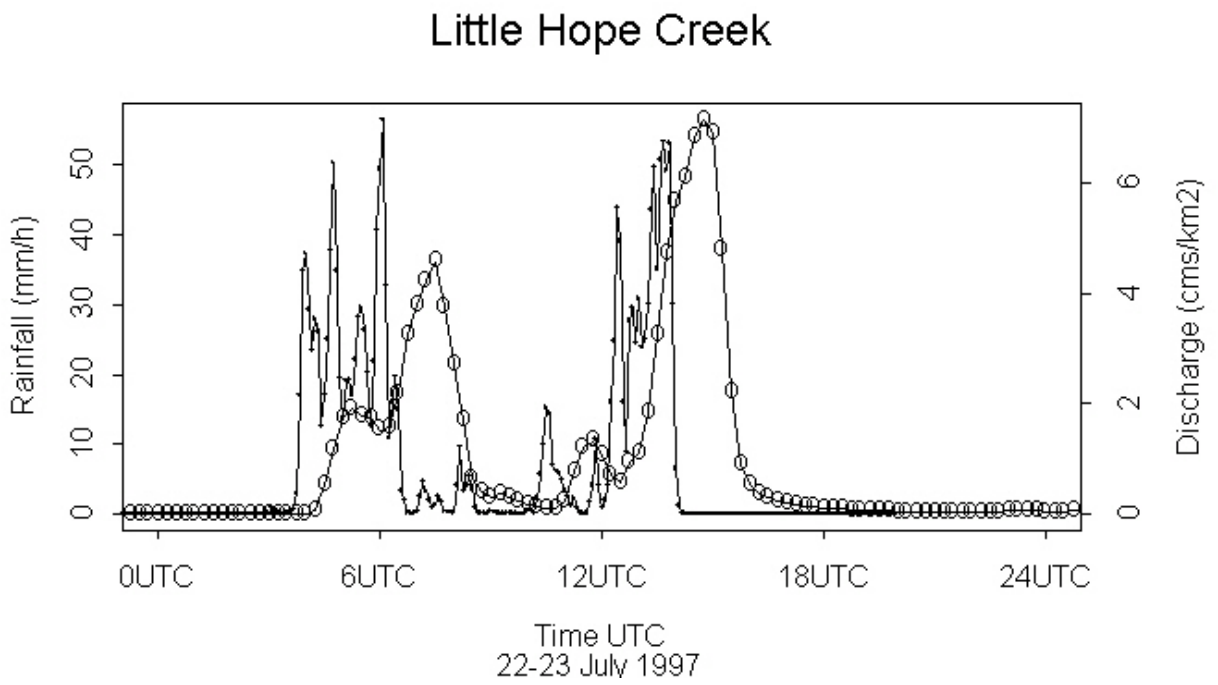

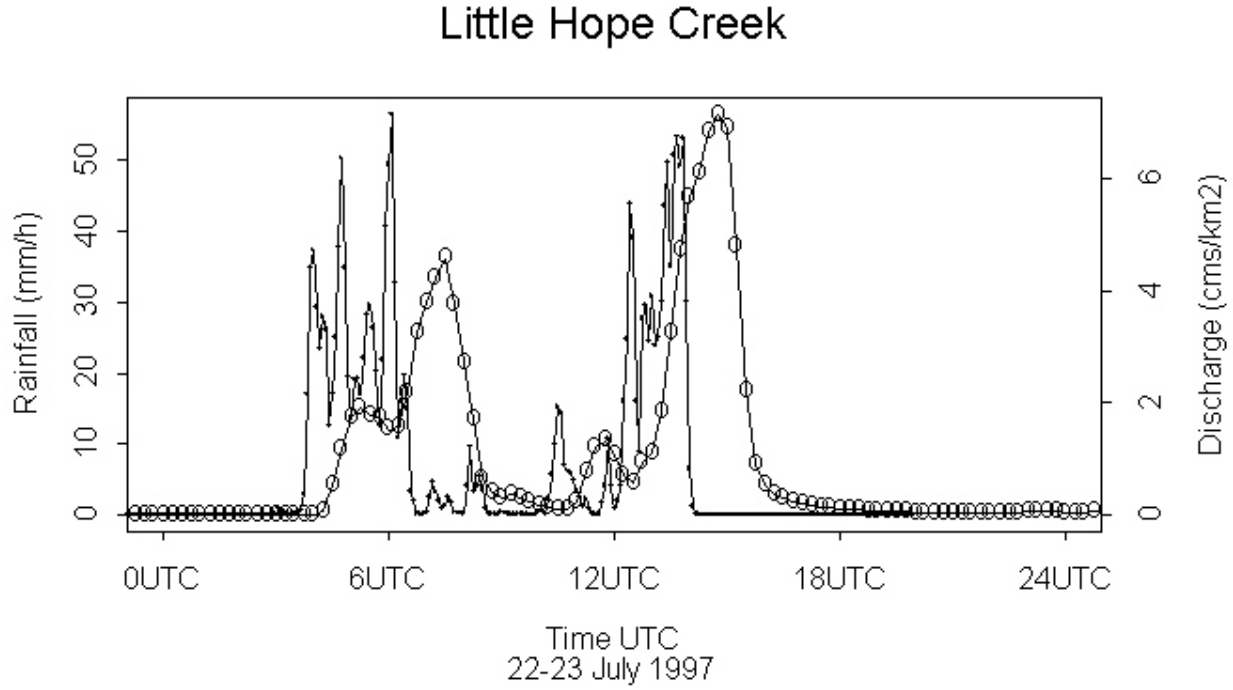

Figure 3.6 Basin-averaged rainfall rate and discharge for Little Sugar Creek, Little Hope Creek, Irwin Creek, Briar Creek, McMullen Creek, Long Creek and Mallard Creek (see following pages).

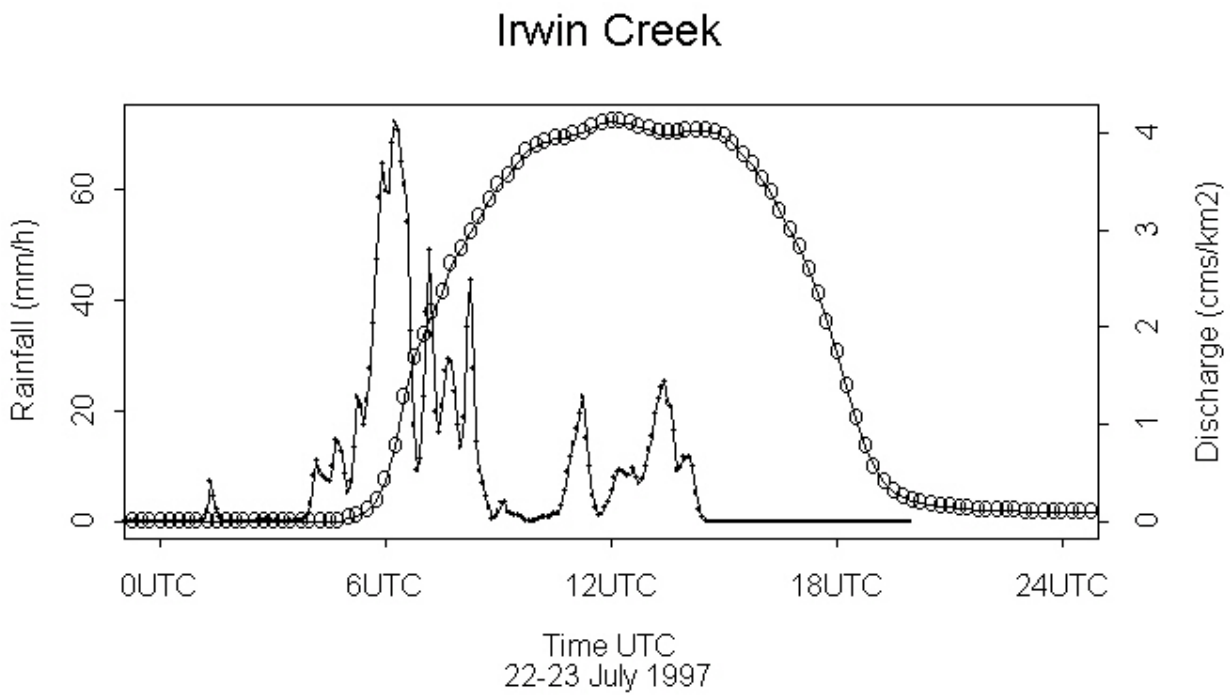
Irwin Creek
Rainfall (mm/h)
0
20
40
60
Discharge (cms/km2)
0
1
2
3
4
0UTC
6UTC
12UTC
18UTC
24UTC
Time UTC
22-23 July 1997

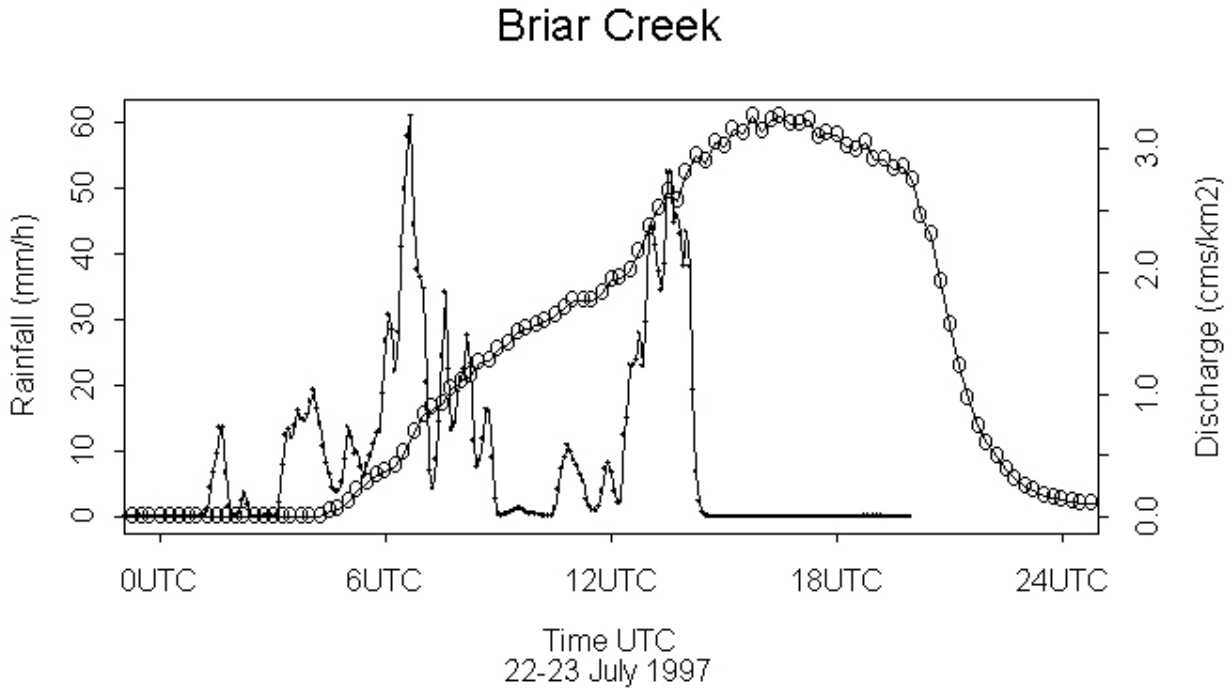
Briar Creek
Rainfall (mm/h)
0
10
20
30
40
50
60
Discharge (cms/km2)
0.0
1.0
2.0
3.0
0UTC
6UTC
12UTC
18UTC
24UTC
Time UTC
22-23 July 1997

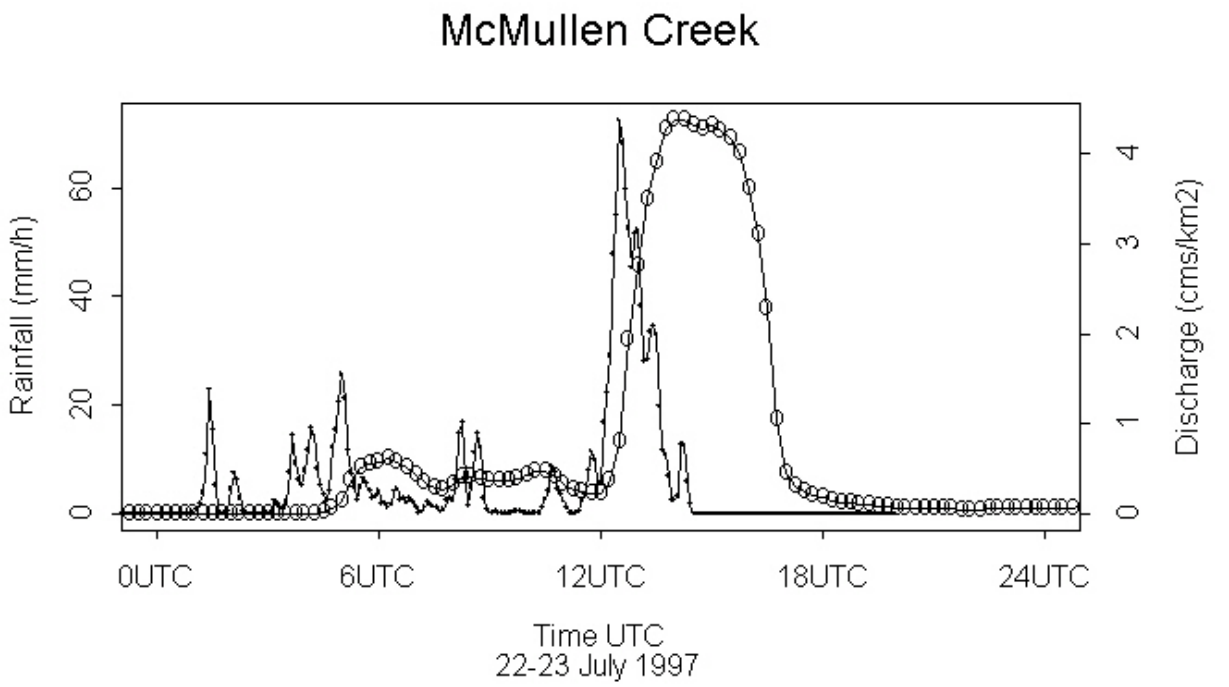
McMullen Creek
Rainfall (mm/h)
0
20
40
60
Discharge (cms/km2)
0
1
2
3
4
0UTC
6UTC
12UTC
18UTC
24UTC
Time UTC
22-23 July 1997

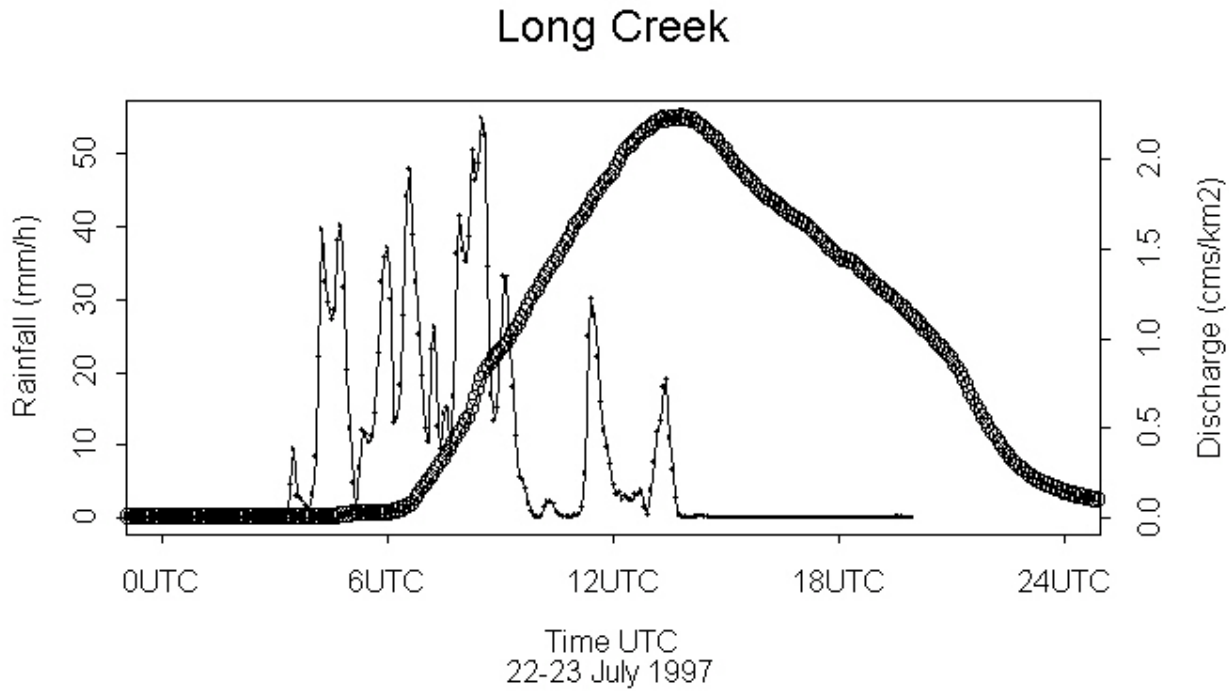
Long Creek
Rainfall (mm/h)
0
10
20
30
40
50
Discharge (cms/km2)
0.0
0.5
1.0
1.5
2.0
0UTC
6UTC
12UTC
18UTC
24UTC
Time UTC
22-23 July 1997

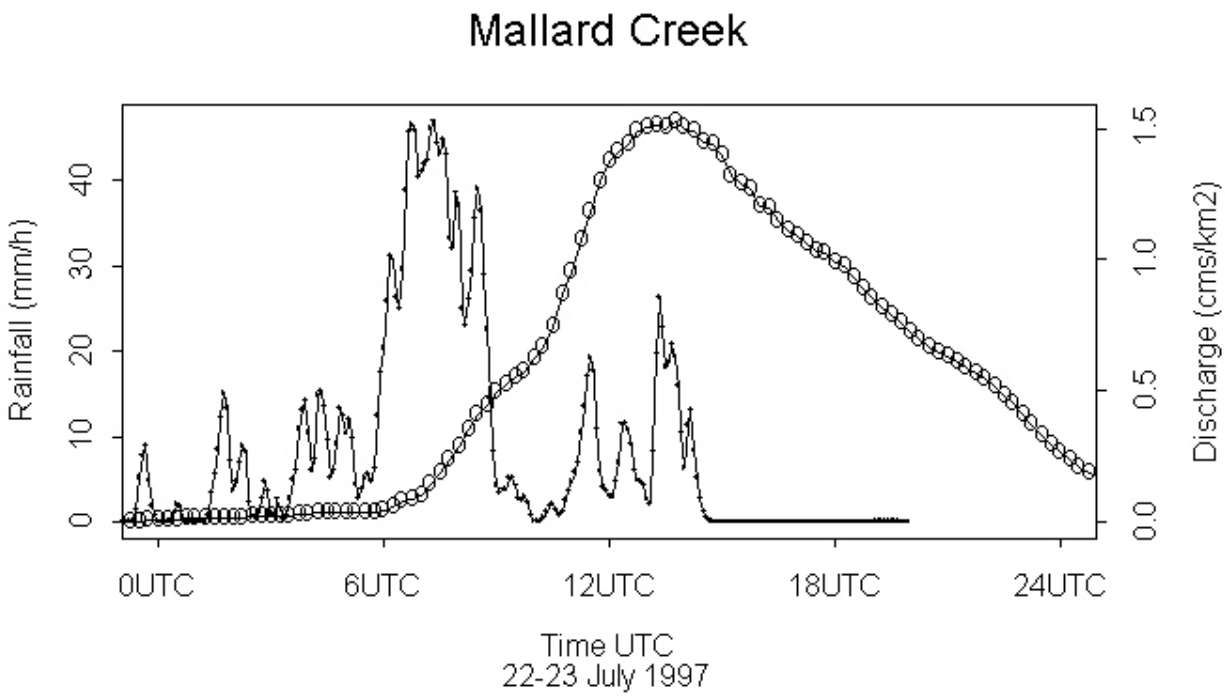
Mallard Creek
Rainfall (mm/h)
0
10
20
30
40
Discharge (cms/km2)
0.0
0.5
1.0
1.5
0UTC
6UTC
12UTC
18UTC
24UTC
Time UTC
22-23 July 1997

4. Extreme Rainfall Estimation for Hurricane Georges in Puerto Rico, 21-22 September 1998

The principal topic of this section is the estimation of extreme rainfall from tropical storms in the complex terrain of Puerto Rico. In particular we examine WSR-88D rainfall estimates and the associated flood hydrology of Puerto Rico catchments (see Fig. 4.1 for location map) for Hurricane Georges, which passed over the island 21-22 September 1998. The flood hydrology of Puerto Rico is of special interest because of the high frequency of extreme "unit discharge" flood peaks relative to other locations in the United States. As in previous sections, USGS discharge observations provide important "validation" data for radar rainfall estimates.

Tropical storms play a central role in the hydrology of extreme floods in Puerto Rico. Hurricane Georges and Hortense (10 September 1996) are responsible for the record peak discharge at most active USGS gaging stations in Puerto Rico. Hurricane Donna (6 September 1960) is prominently represented in the flood record of gaging stations with records extending to 1960. Tropical storms are, however, rare events (especially those like Georges) and Puerto Rico is a high rainfall environment even in the absence of tropical storms. Annual rainfall ranges from 3000 mm along the central mountain range to 2000 mm along coastal regions.

Orographic amplification of rainfall played a central role in flood response to Hurricane Georges. Analyses of radar, rain gage and discharge observations for Hurricane Georges are used to examine the problems that arise in estimating extreme rainfall in complex terrain with pronounced orographic enhancement of rainfall. Measurement of rainfall and discharge for extreme flood events is, in general, a major challenge. Peak discharge measurements for extreme flood events are subject to numerous errors. Rain gages are often inadequate for characterizing flood-producing rainfall, even in the absence of hurricane-force winds. We examine WSR-88D estimation

of extreme rainfall in the context of observing system uncertainties for radar, rain gage and discharge observations.

The rainfall analyses utilize 15 minute rain gage observations from a network maintained by the U. S. Geological Survey (USGS) and radar reflectivity observations from the San Juan WSR-88D radar. "Unit values" discharge observations (at 15 minute time scale) from USGS stream gaging stations play a central role in hydrometeorological analyses.

Analyses of radar, rain gage and discharge observations (Figs. 4.2 – Figs. 4.5) focus on estimation of rainfall in complex terrain and on the contrasting rainfall properties of the island of Puerto Rico. The "east-to-west" structure of analyses is incorporated into gage-radar intercomparison (Figs. 4.3), storm total rainfall analyses (Figs. 4.4) and rainfall – discharge analyses (Figs. 4.5). For the rainfall – discharge analyses we utilize 5 pairs of drainage basins (either adjacent or nested) and examine the capability of resolving timing and magnitude of flood response based on WSR-88D rainfall estimates.

Hurricane Georges moved from east to west over Puerto Rico at a speed of approximately 21 km h^{-1} (Figs. 4.2 a – e). The 190 km path over the island took 9 hours (2120 UTC on September 21 to 0620 UTC on 22 September) and the period of significant rainfall over the island was approximately 24 hours (1930 UTC on 2100 September to 2000 UTC on 22 September). Storm speed did not vary markedly as the system passed over Puerto Rico. The eye of the storm passed directly over the island and storm motion oscillated slightly from northwest (as it reached the island) to west-southwest (as it exited the western end of the island). The low-reflectivity region of the eye was more than 1000 km^2 in size both on entering the island (Fig. 4.2b) and after exiting the island (Fig. 4.2g).

Flood-producing rainfall from the storm resulted from both eyewall convection and rain bands. There were pronounced asymmetries in the structure of both eyewall convection and rain bands. Rain bands developed in the southeastern sector of the storm and passed from south to north over the island, often with a south-north orientation of the

band. Eyewall convection interacted with terrain during passage of the storm over Puerto Rico, resulting in intensification of eyewall convection on the south side of the eye.

The center of the eye of Hurricane Georges was less than 50 km from the coastline at 1923 UTC (Fig. 4.2a) on 21 September. The eye is apparent as a low reflectivity region with an area of approximately 1000 km^2. The reflectivity structure of the storm exhibited a pronounced asymmetry with more extensive development in the southern and eastern sectors of the storm. As a consequence, the onset of rainfall on the eastern portion of the island did not begin until approximately 1930 UTC. This asymmetry persisted throughout the life cycle of the storm. Extensive flood-producing rainfall affected the central and western end of the island for many hours after the eye had passed over the island.

The eye of Georges reached the eastern end of the island at 2117 UTC (Fig. 4.2b). The eye region was still structured as a near-circular, low-reflectivity region. A thin rain band extended from north-to-south over the island, passing through the San Juan WSR-88D radar location. This band was responsible for the first significant pulse of high rainfall rates in the eastern and central portions of the island (see Figs. 4.3 and 4.5).

Eyewall convection intensified markedly as the eye passed over the eastern margin of the island, resulting in a high-reflectivity region along the southeastern and eastern portion of the island at 2353 UTC (Fig. 4.2c). Peak flooding in the eastern catchments of Puerto Rico (Fig. 4.5a and b) was associated with this element of the storm. This element of the storm produced the highest short-term (5 – 15 minutes) rain gage measurements of rainfall rate (as discussed below) and the peak discharge for the Rio Grande de Loiza (Fig. 4.4b and 4.5b), which exceeded the United States flood peak envelope curve.

The largest rainfall accumulations from the storm occurred in the central mountains of the island and the largest rainfall rates contributing to peak accumulations were associated with eyewall convection (Figs. 4.2 d and e). During the period of peak rainfall rates over the central mountains (Figs. 4.2 d and e at 0141 and 0300 UTC), eyewall convection developed over ocean south of the island and wrapped cyclonically up to the mountain barrier. Interaction of eyewall convection with terrain played a central role in extreme flood response, as discussed in greater detail below.

The eyewall exited Puerto Rico at 0600 UTC (Fig. 4.2f). At this time, north-south oriented rain bands were producing heavy rainfall (rain rates greater than 25 mm h^{-1}) over the island. During the next 12 hours, embedded rain band convection developed in the southeastern sector of the storm and intensified over Puerto Rico in north-south oriented regions of embedded convection (Figs. 4.2 g and h). Flooding over the western end of the island was dominated by embedded rain band convection.

A closer look at the paired gage and radar rainfall estimates (Figs.4.3) at 15 minute time scale and five rain gage locations (the radar rainfall estimate is a time-aggregated estimate for the 1 km bin containing the rain gage) illustrates the time history of flood-producing rainfall over the island. Radar rainfall estimates were computed using the "tropical" Z-R equation, $Z = 250R^{1.2}$.

Peak rainfall rates at Rio Humacao (USGS ID 50081000; the easternmost rain gage in Fig. 4.1) near the eastern end of Puerto Rico reached 160 mm h^{-1} at 15 minute time scale (Fig. 4.3a). Large rainfall rates on the eastern portion of the island, as represented by the Rio Humacao observations, were associated with explosive growth of eyewall convection (Fig. 4.2c). Storm total rainfall at Rio Humacao of 232 mm was largely associated with extreme rainfall rates from eyewall convection during a 1-hour period centered at 0000 UTC on September 22. The tropical Z-R relationship underestimates peak rainfall rates but slightly overestimates subsequent rainfall with a storm total of 266 mm.

The Rio Gurabo (USGS ID 50057000; located northwest of Rio Humacao as shown in Fig. 4.1) observations (Fig. 4.3.b) show somewhat lower peak rainfall rates (but still exceeding 100 mm h^{-1}) than for the eastern portion of the island, but larger contributions to storm total accumulation from subsequent rain bands. The storm total accumulation of 307 mm was produced by eyewall convection centered at 0015 UTC on September 22 (Fig. 4.2 c), a five hour period (0130 to 0630) of 20 – 40 mm h^{-1} rain rates from rain bands (Figs. 4.2 c - g) and a final period of rain band rainfall centered at 1200 UTC . The Rio Gurabo observations represent heavy rainfall in low elevation regions of the Rio Grande de Loiza basin. Rain gage observations are not available at high elevation regions of the basin with largest storm total accumulations from radar (as discussed below). These regions were responsible for the record peak discharge from the

Rio Grande de Loiza (Fig. 4.5b). Radar rainfall estimates are biased low both for the period of eyewall convection and the subsequent period of rain band rainfall from 0130 to 0630 UTC. The final period of heavy rainfall around 1200 UTC is overestimated by the tropical Z-R equation. The storm total accumulation from radar (254 mm) is almost 20% lower than the rain gage accumulation.

The Rio Orocovis rain gage is collocated with the Rio Orocovis stream gage (see Fig. 4.1). Peak rainfall rates at this gage reach only 65 mm h^{-1} (Fig. 4.3c). The rain gage storm total accumulation of 401 mm is approximately 20 % less than the storm total rainfall accumulation from radar. Flood peaks at Rio Orocovis and the downstream Rio Grande de Manati gage (Fig. 4.5 c) were produced by a second round of intense eyewall convection, which formed over ocean south of the island and wrapped up to the central highlands. Lower rainfall accumulations and flood peaks in the region between Loiza and Manati were due to diminished rainfall accumulations from eyewall convection. The Orocovis gage – radar analyses (Fig. 4.3c) illustrate the continuing east to west pattern of rainfall with diminishing eyewall rain rates and increasing contribution from rain bands. As with eastern stations, there is severe overestimation for the later period of rain band convection (1300 – 1600 UTC).

The rain gage collocated with the Rio Saliente stream gage (USGS ID 50025155; see also Fig 4.1) recorded 532 mm of rainfall. There is excellent agreement in temporal pattern of rain rates between gage and radar (Fig. 4.3d). Storm total rainfall from radar rainfall estimates using the tropical Z-R relationship was 617 mm. Peak 15 minute rainfall rates from gage of 80 mm h^{-1} were recorded. The overestimation of storm total rainfall at Rio Saliente is tied in part to overestimation of rainfall for the embedded rain band convection that passed over the region from 13 – 18 UTC. As noted above, this feature is characteristic of many of the gage – radar intercomparisons.

The peak in Arecibo rainfall rates (USGS ID 50021700; westernmost gage location shown in Fig.4. 1) was at 0800 UTC (see Fig. 4.3e) and was produced by rain bands not eyewall convection. Rio Tanama and Rio Grande de Arecibo have sharp flood peaks associated with the period of rain band rainfall centered at 0800 UTC (Fig. 4.5e). Western island peaks resulted not from eyewall convection but from either rain bands or a combination of eyewall convection and rain bands. The tropical Z-R rainfall estimates

seriously underestimate storm total rainfall over much of the western portion of the island.

Storm total accumulation maps were developed from WSR-88D reflectivity observations for five regions, each of 900 km^2 size. The five regions contain the five paired watersheds used for hydrologic analyses in the following section. In each case, the rainfall maps were developed using the tropical Z-R equation with a 52 dBZ reflectivity threshold (rainfall estimates were not overly sensitive to the reflectivity threshold, based on analyses using thresholds ranging from 50 – 55 dBZ).

For the Rio Saliente, Manati and Arecibo basins, analyses utilized the second tilt (1.5 degrees) due to extensive regions of ground returns at the lowest elevation angle. For the Loiza and Canovanas analyses the lowest tilt was used. Ground returns were encountered at high elevation regions. To eliminate this problem, 41 of 900 bins were removed from the Rio Canovanas analyses and 55 of 900 bins from the Loiza analyses. For these bins, rainfall rates were interpolated from the nearest "good bins".

The San Juan radar is located immediately southwest of the Loiza and Turabo basins. The "cone of silence" for the 0.5 degree tilt does not extend into the Loiza or Turabo basins (higher elevation angles could not be used; even for the 1.5 degree tilt, the cone of silence extends well into the Loiza and Turabo basins). In presenting the storm total rainfall analyses we proceed from the highest elevation region of the central mountains, which have the largest rainfall accumulations.

Rio Saliente storm total rainfall estimates (Fig. 4.4d) are based on the 1.5 degree elevation angle reflectivity observations. The storm total rainfall maximum of 730 mm is centered on the southern portion of the Rio Saliente basin. This rainfall maximum corresponds with the 900 – 1000 mm rainfall maximum in the USGS rain gage analysis (figure not shown).

The contours of maximum rainfall from the radar rainfall analyses are oriented from southwest to northeast over the Rio Saliente basin, following the contours of the high elevation maxima of the region (Fig.4.1). The gradients in rainfall accumulation from the center of the Rio Saliente basin are much sharper to the north, with storm total rainfall decreasing from a maximum of 720 mm to a minimum of 400 mm at the basin outlet. An elevated region of storm total rainfall estimates exceeding 500 mm extends

southward from the Rio Saliente basin. Analyses indicate a rainfall maximum extending southward from the highest elevation region of the island, with a sharp dropoff to the north of the mountain barrier.

The pattern of storm total accumulation is more complex for the Manati basin and its surroundings (Fig. 4.4c). There is a general decrease in rainfall accumulation to the north from the rainfall maximum at the southern boundary of the basin. There is also a sharp contrast in rainfall accumulations on the eastern and western margins of the basin. To the west lies the rainfall peaks over the Saliente basin. To the east lies the rainfall minima associated with the cycles of eyewall convection and rain band development.

Storm total rainfall estimates for the Loiza basin and surroundings (Fig.4.4b) are developed from the 0.5 degree elevation angle and range from 800 mm immediately southwest of the basin to 200 mm in the northern portion of the region. There is a sharp gradient in rainfall accumulation over the Loiza basin, but relatively low gradients over much of the area north and east of the Loiza basin. Storm total accumulations range from 700 mm at the southern boundary of the basin to 300 mm at the basin outlet. The local maximum in rainfall accumulation over the southern boundary of Loiza and Turabo are not reflected in the rain gage analyses. They do suggest, however, that flood peaks should be most extreme in these regions, which was the case (see discussion below).

Storm total rainfall estimates for the Canovanas basin and surroundings (Fig. 4.4a) exhibit the striking controls of orographic precipitation mechanisms. The axis of rainfall accumulations exceeding 400 mm contains the line of highest elevation in the Luquillo (note three peaks in Fig. 4.1). Rainfall accumulations contours from 200 – 400 mm northwest of the rainfall maximum are oriented southwest to northeast, roughly following the elevation contours. The 200 mm contour in the southwestern portion of the 900 km^2 region is contained within the low-elevation valley between Canovanas and Loiza. The local accumulation maximum of 350 mm (see also Loiza analyses in Fig. 4.4b) coincides with a local topographic maximum in the valley. As noted above, ground returns do not contribute to rainfall analyses

The Arecibo rainfall analyses (Fig. 4.4e) exhibit a complex spatial pattern, including the western end of the Saliente rainfall maximum (to the east of Arecibo), a southwestern rainfall maximum in Arecibo, and decreasing accumulation from south to

north, with relatively low accumulations over Rio Tanama. The Arecibo rainfall analyses differ from those in basins to the east in that eyewall convection played a relatively smaller role in rainfall distribution in comparison with rain band rainfall.

The preceding analyses of rainfall have focused on orographic amplification of rainfall and the east to west contrasts in rainfall distribution. We conclude this section with an examination of discharge for 5 sets of paired basins. Discharge observations highlight the capability of WSR-88D rainfall estimates to capture the essential elements of rainfall distribution and flood response. Paired watersheds are: 1) Rio Canovanas (50061800) and Rio Grande near El Verde (50064200), 2) Rio Grande de Louiza (50050900) and Rio Turabo (50053025), 3) Rio Orocovis (50030460) and Rio Grande de Manati near Morovis (50031200), 4) Rio Saliente (50025155) and Rio Caonnillas (50026025) and 5) Rio Grande de Arecibo below Utuado (50024950) and Rio Tanama near Utuado (50028000). Time series plots of basin-averaged rainfall rate (aggregated to 15 minute time interval) derived from WSR-88D observations as described above and discharge (at 15 minute time interval) are presented in Figure 4.5.

The sharp peak in gage rainfall estimates for the two eastern rain gages (Fig 4.3 a and b) is reflected in the sharp, early peaks in discharge for the Rio Canovanas and Rio Grande el Verde stream gaging stations (Fig. 4.5a). The Rio Grande gaging station has a larger peak discharge, near 30 $m^3 s^{-1} km^{-2}$ as compared with 17 $m^3 s^{-1} km^{-2}$ for Rio Canovanas, but a lower storm total runoff (285 mm versus 360 mm for Rio Canovanas).

The Rio Grande de Loiza peak (Fig. 4.5b) discharge of 80 $m^3 s^{-1} km^{-2}$ is the largest unit discharge flood peak in the US for comparable drainage areas. The peak unit discharge of 80 $m^3 s^{-1} km^{-2}$ can also be expressed as a discharge rate of 300 mm h^{-1}. For both the Loiza and Rio Turabo discharge observations, there are a sequence of peaks associated with rain bands from Hurricane Georges. The peak discharge from both stations was produced by the explosive period of eyewall convection early in the storm. The peak discharge of the Rio Turabo was ¼ the magnitude of the Loiza peak. The storm total runoff from the Loiza discharge observations of 1450 mm is significantly larger than the storm total rainfall estimates. It is also much larger than the Rio Turabo runoff of 285 mm. Although there is clearly pronounced orographic amplification of rainfall in the upper Loiza basin, there is not additional evidence to support the extreme magnitudes of

the Loiza peak and runoff total. In particular, there is no direct evidence of accumulations approaching 1.5 meters or rainfall rates approaching 300 mm h^{-1}. Because the Loiza peak is a US record, additional examination of these observations is warranted. The WSR-88D rainfall estimates provide the only direct evidence of amplification of rainfall in the upper Loiza basin.

Peak discharges for the Rio Orocovis and Rio Grande de Manati stream gages are also associated with eyewall convection and occur early in the flood period. There are a series of subsequent peaks produced by the series of rain bands passing over the basin. An important point to note in these analyses, as in the Loiza/Turabo analyses is that the flood response, as reflected in the discharge, is relatively smaller for the final period of intense rainfall between 1400 and 1600 UTC than for the earlier eyewall convection. Estimated basin-averaged rainfall rates are higher for the 1400 – 1600 UTC period, than for the 0000 – 0400 UTC period, but the flood peaks are lower. These observations support the conclusion that radar-based rainfall estimates for the late periods of rain band convection are biased high, relative to the earlier rainfall periods.

Rainfall and discharge analyses clearly point to time-varying bias as an important element of WSR-88D rainfall estimation. Overestimates of rainfall in later periods of the storm (after soil moisture storage has presumably been depleted) would result in significant potential for overestimates of flood peaks.

The Rio Saliente stream gage only operated through the first peak in response to eyewall convection. The discharge record for the downstream gage at Rio Caonillas exhibited 5 peaks in discharge, with the first peak at 0430 UTC the largest (note again the lower response to the final period of rain band rainfall). These peaks correspond to peaks in the 15 minute rainfall rate time series. Storm total runoff from the Rio Caonillas gage was 388 mm. Storm total runoff for the Rio Salinete up until the gage ceased reporting was 175 mm. For a corresponding time period, the runoff from Rio Caonillas was 95 mm, suggesting that the storm total runoff from the high-elevation region above Rio Saliente exceeded 700 mm. These runoff values are consistent with the spatial pattern of storm total rainfall (Fig. 4.4d).

For the final pair of stream gages, the Rio Tanama and Rio Grande de Arecibo, the flood peaks were produced not by eyewall convection but by a period of intense rain

band rainfall between 0600 and 0800 UTC. The Tanama and Arecibo analyses are representative of flood response on the western portion of the island, where peak response is dominated by rain bands instead of eyewall convection. Runoff accumulations of 263 mm for Arecibo and 191 mm for Tanama are consistent with the spatial distribution of rainfall.

CONCLUSIONS:

The interior mountain region of Puerto Rico produces some of the largest unit discharge flood peaks in the United States. These floods are largely the product of rainfall from tropical storms. Orographic amplification of rainfall in Puerto Rico plays a fundamental role in extreme flood hydrology. Beam blockage, partial beam blockage and low-level growth of precipitation are problems that make estimation of rainfall from the WSR-88D difficult in Puerto Rico. Analyses of rainfall and discharge observations from Hurricane Georges, however, demonstrate that exceptional rainfall estimates can be developed for flood forecasting applications. The quality of the Hurricane Georges rainfall analyses was strongly dependent on eliminating the influence of beam blockage and partial beam blockage. For the eastern basins, the lowest elevation angle was used and the relatively small area of ground returns was removed from analyses. Radar and rain gage analyses indicate large gradients over the Rio Grande de Loiza basin, but do not provide direct evidence for rainfall accumulations approaching 1.5 m or rainfall rates approaching 300 mm h^{-1} .

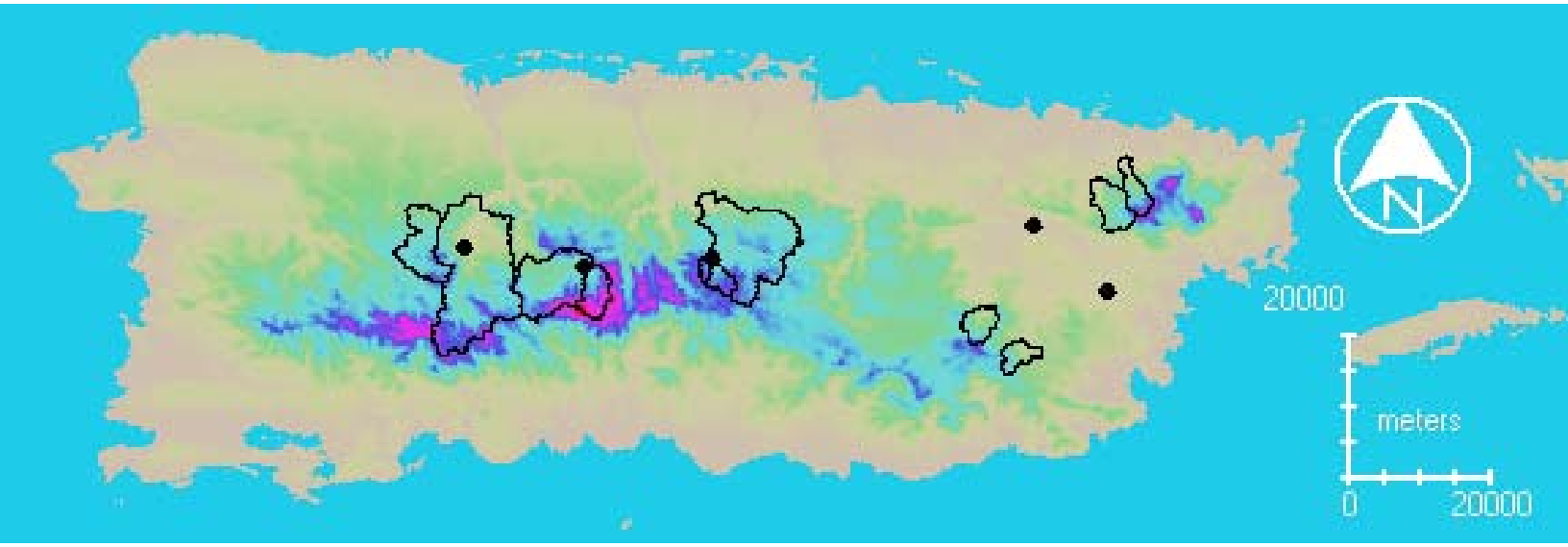

Figure 4.1. Location map for Puerto Rico. Paired drainage basins are, from east to west, Rio Canovanas and Rio Grande el Verde, Rio Grande de Loiza and Rio Turabo, Rio Orocovis and Rio Grande de Manati, Rio Saliente and Rio Caonillas, Rio Grande de Arecibo and Rio Tanama. Rain gages (solid dots) are, from east to west, Rio Humacao, Rio Gurabo, Rio Orocovis, Rio Saliente, and Rio Grande de Arecibo. Elevation ranges from sea leval to more than 1500 m (purple).

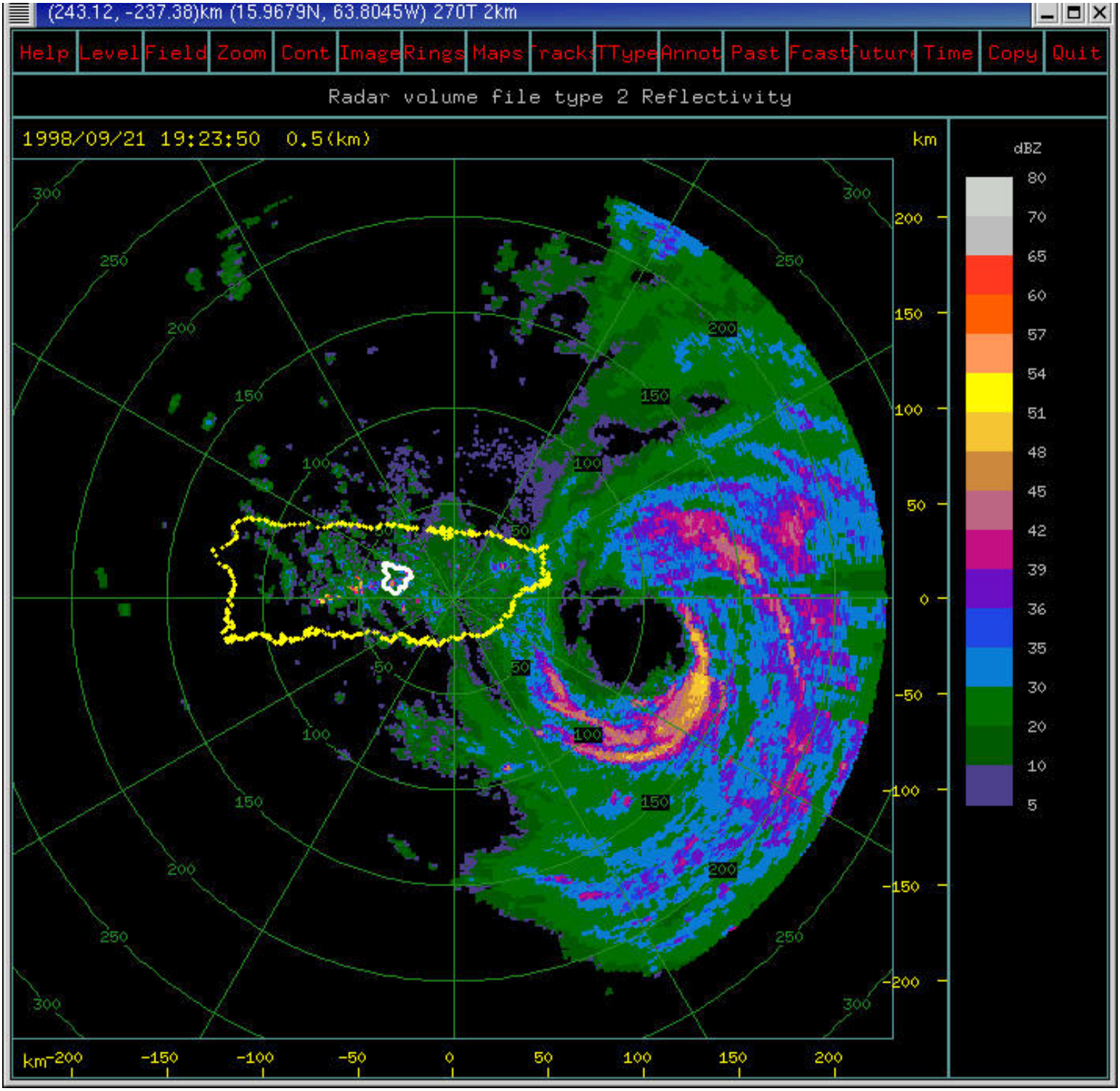

Figure 4.2a Reflectivity image from lowest elevation at 1923 UTC on 21 September 1998. Puerto Rico is outlined in yellow and the Rio Grande de Manati basin boundary is outlined in white.

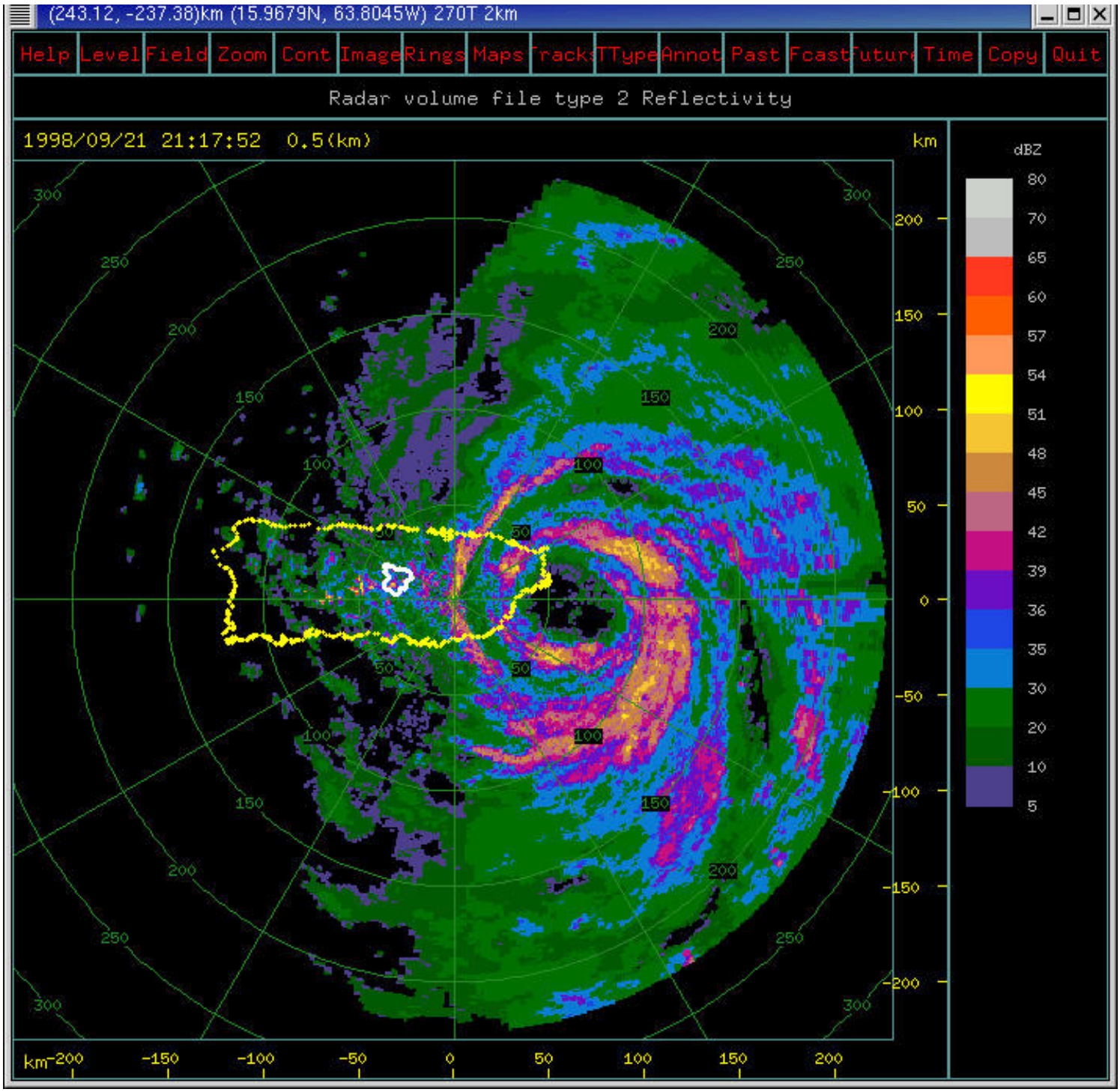

Figure 4.2b. Same as in 2a, but 2117 UTC.

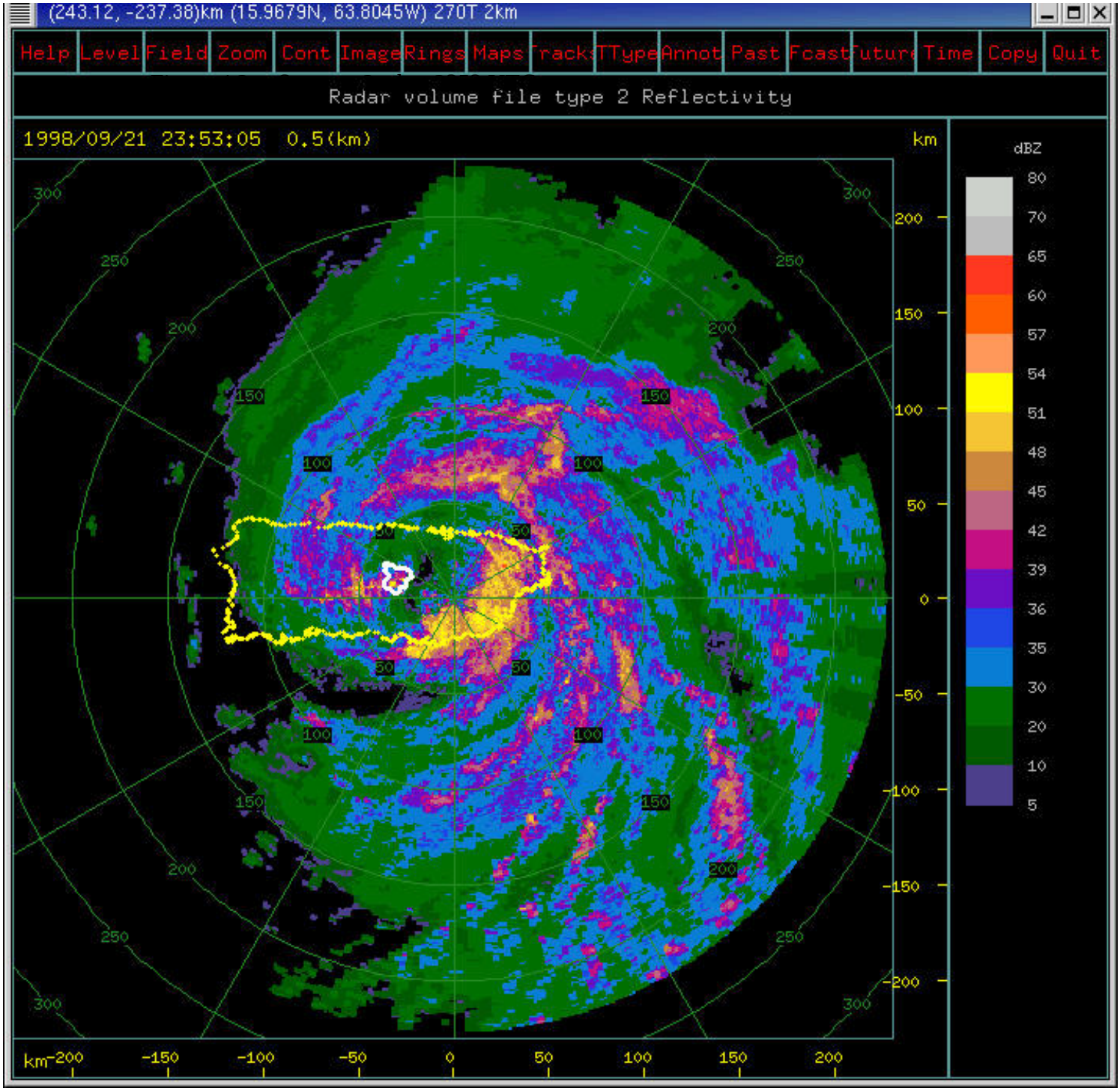

Figure 4.3c. Same as in 2a, but 2353 UTC.

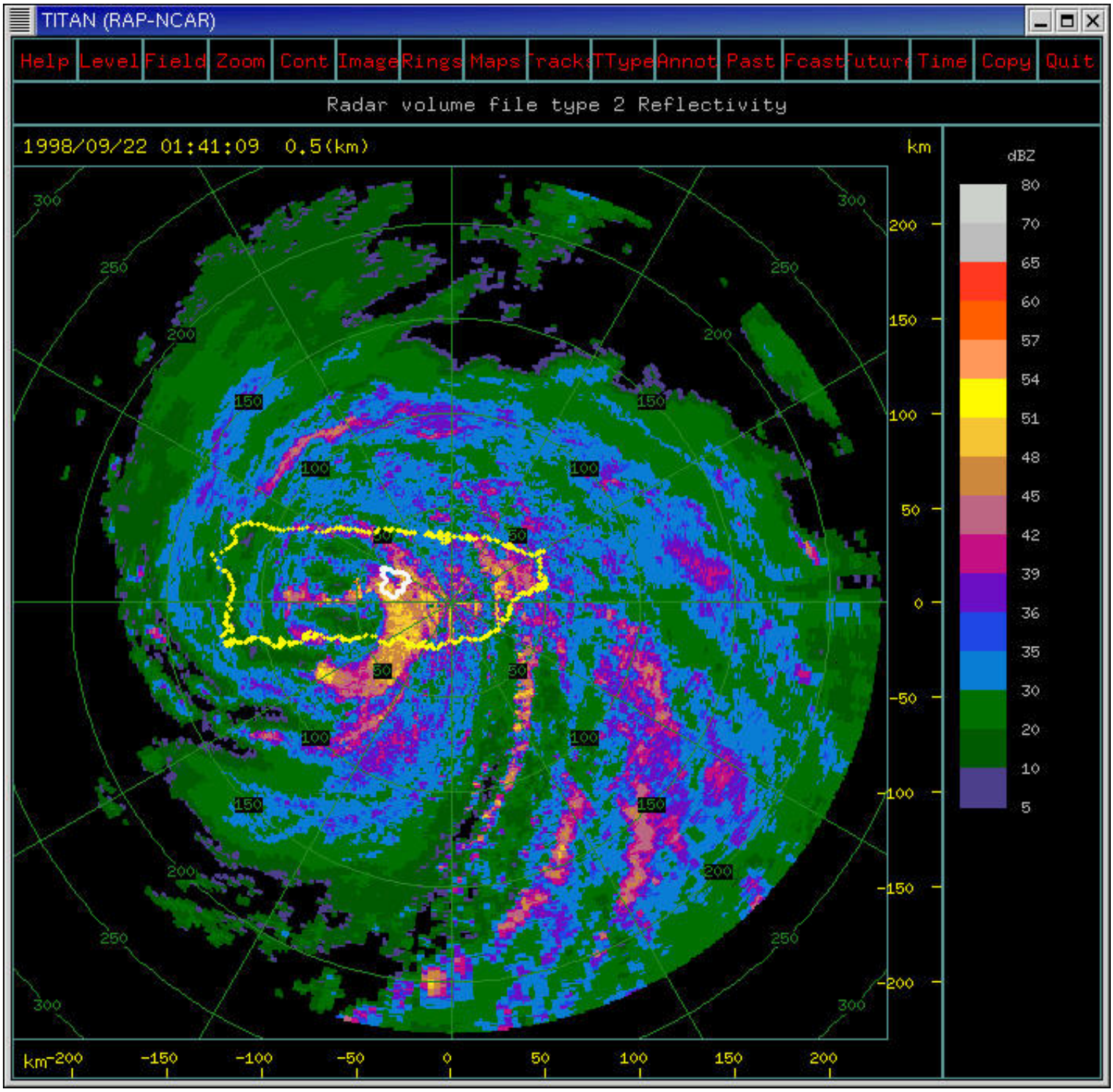

Figure 4.2d. Same as 2a, but 0141 on 22 September.

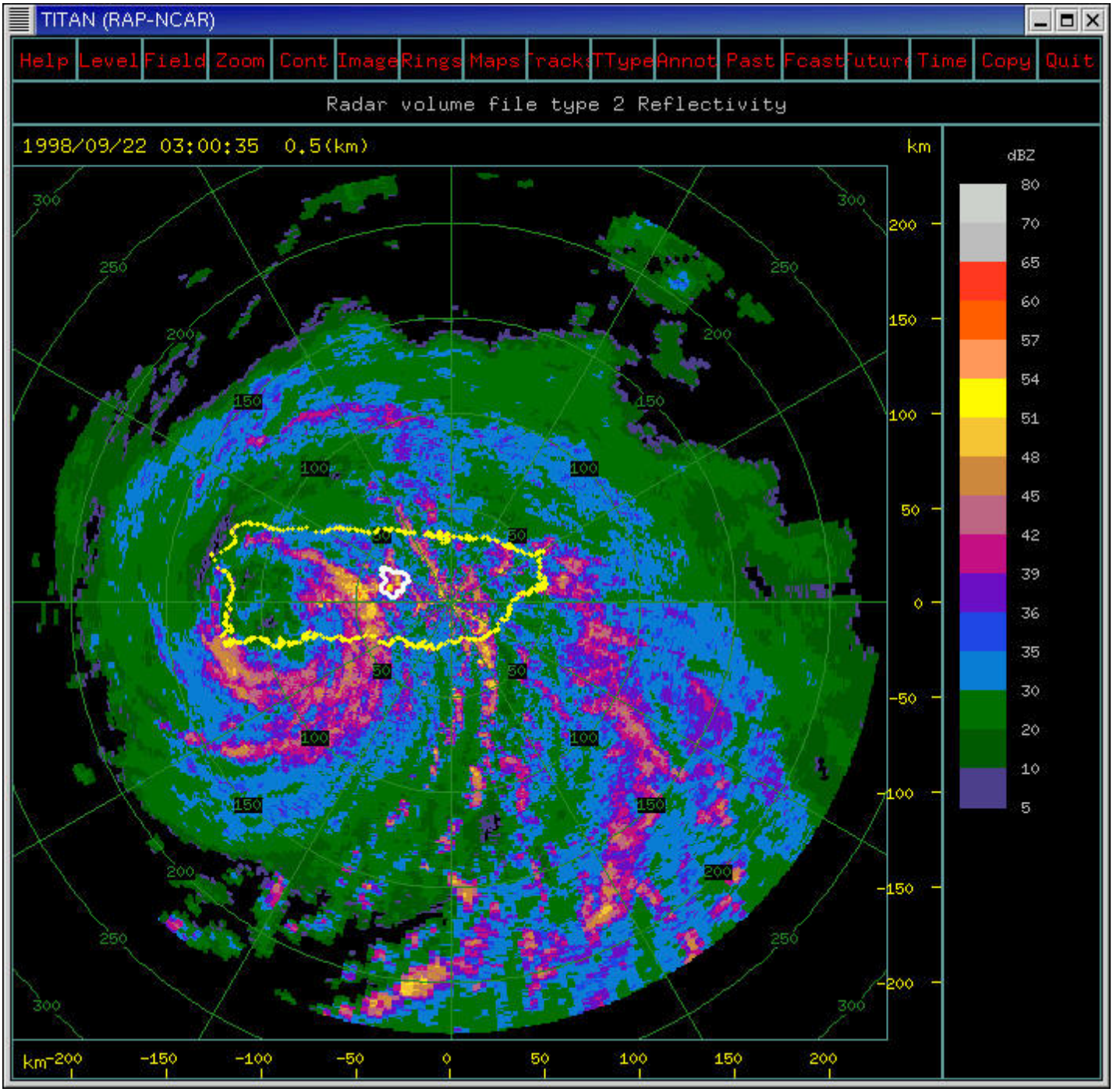

Figure 4.2e. Same as 2a, but 0300 UTC on 22 September.

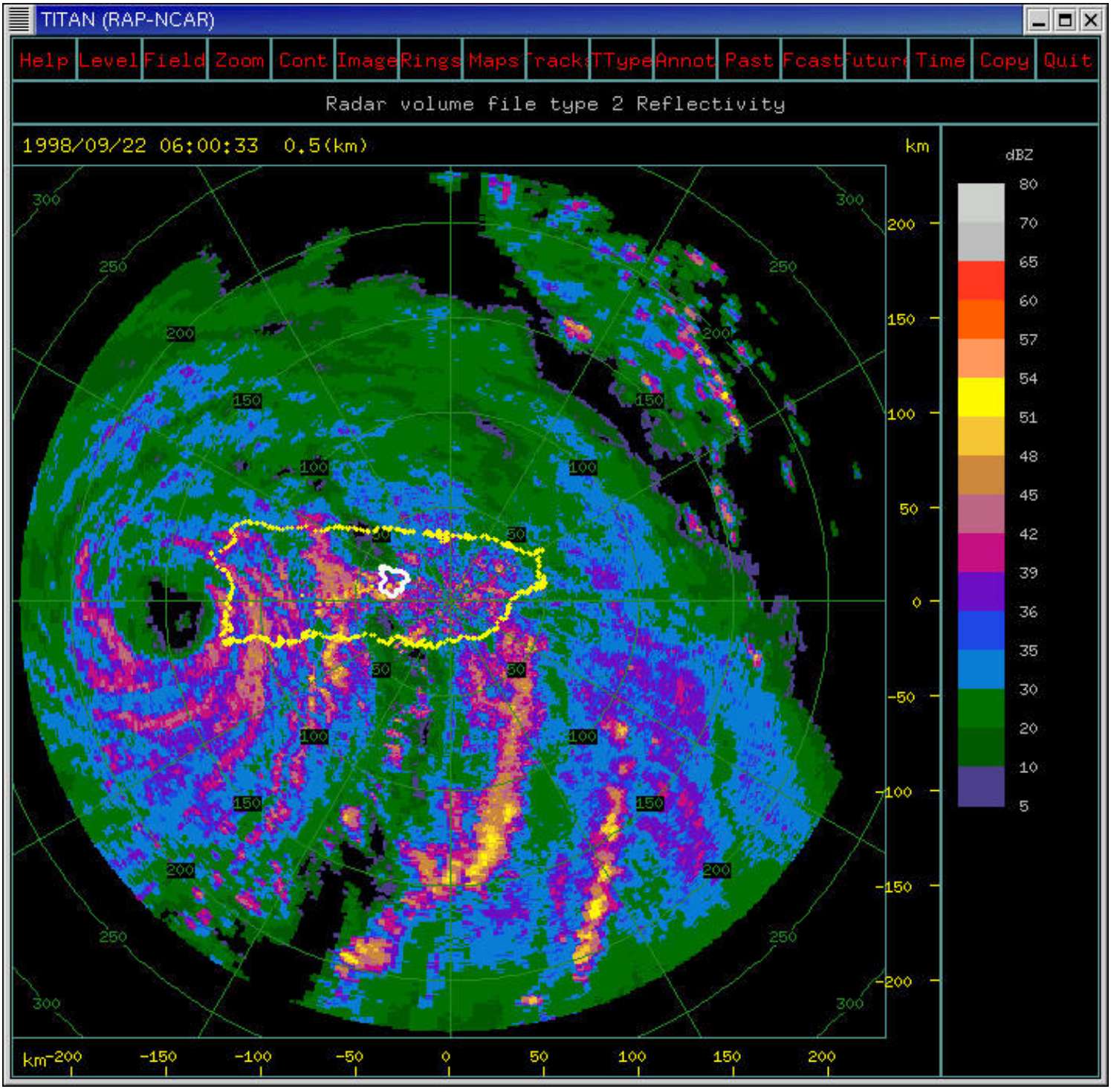

Figure 4.2f. Same as 2a, but 0600 UTC.

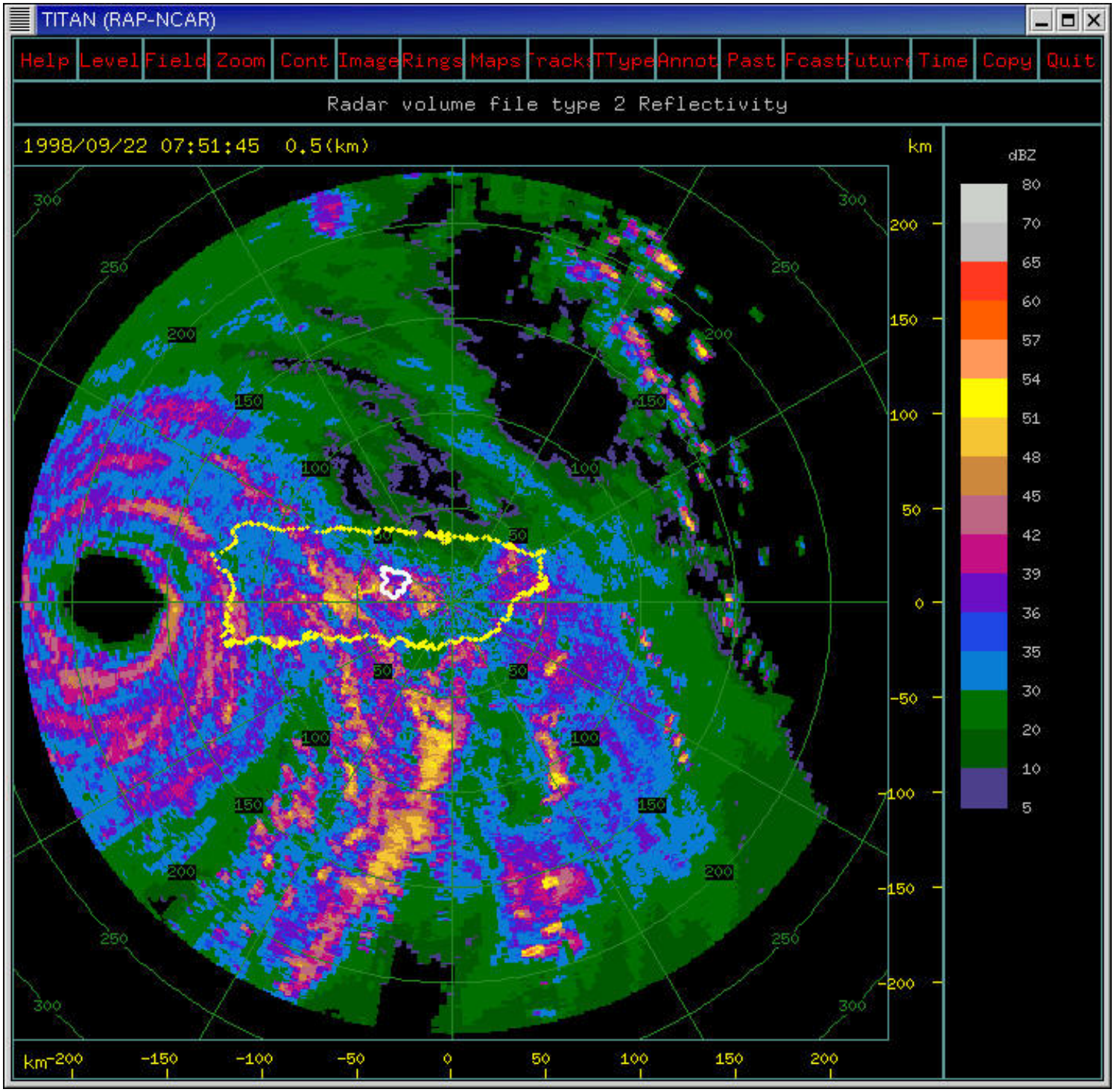

Figure 4.2g. Same as 2a, but 0751 UTC.

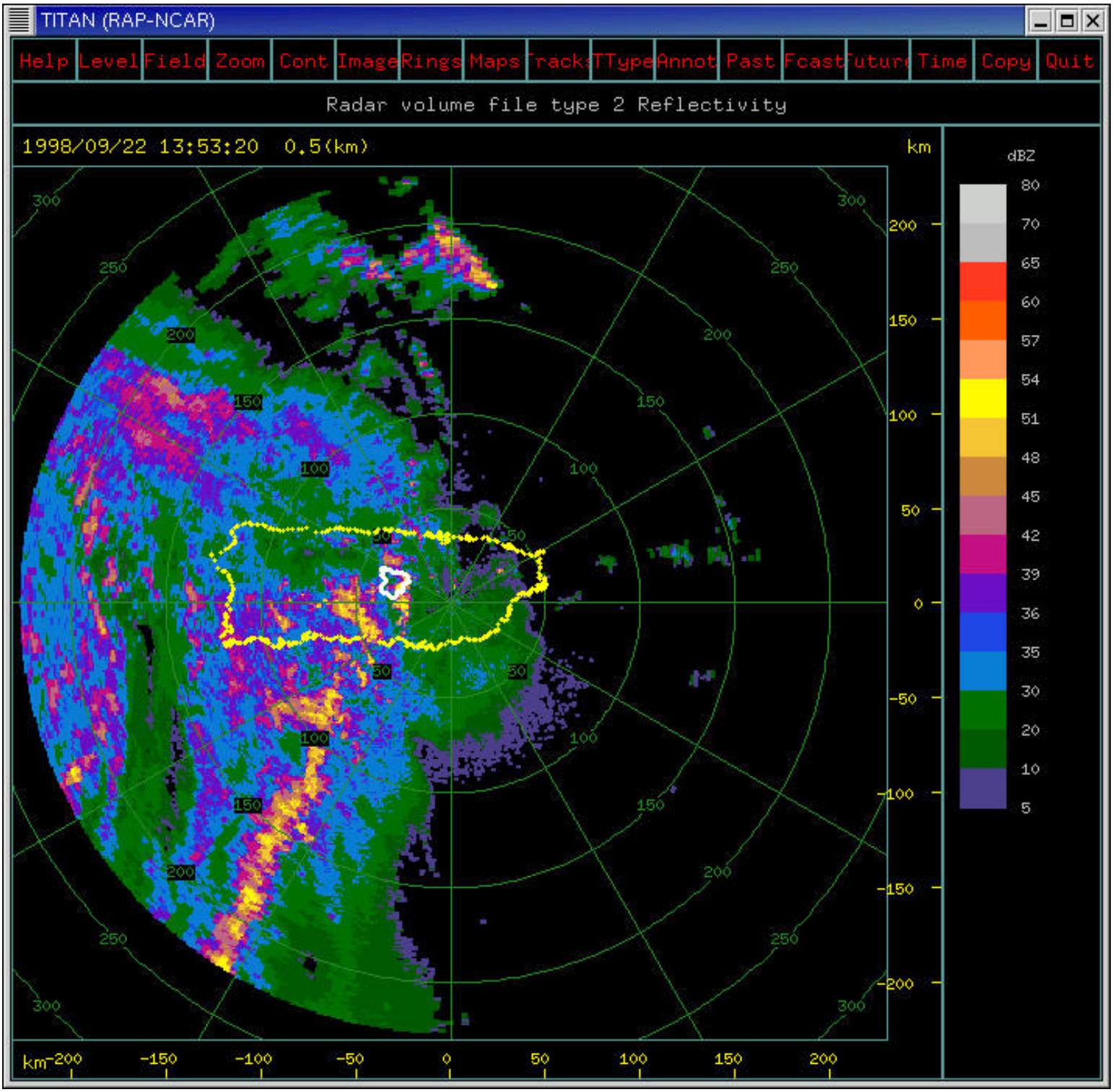

Figure 4.2h. Same as 2a, but 1353 UTC.

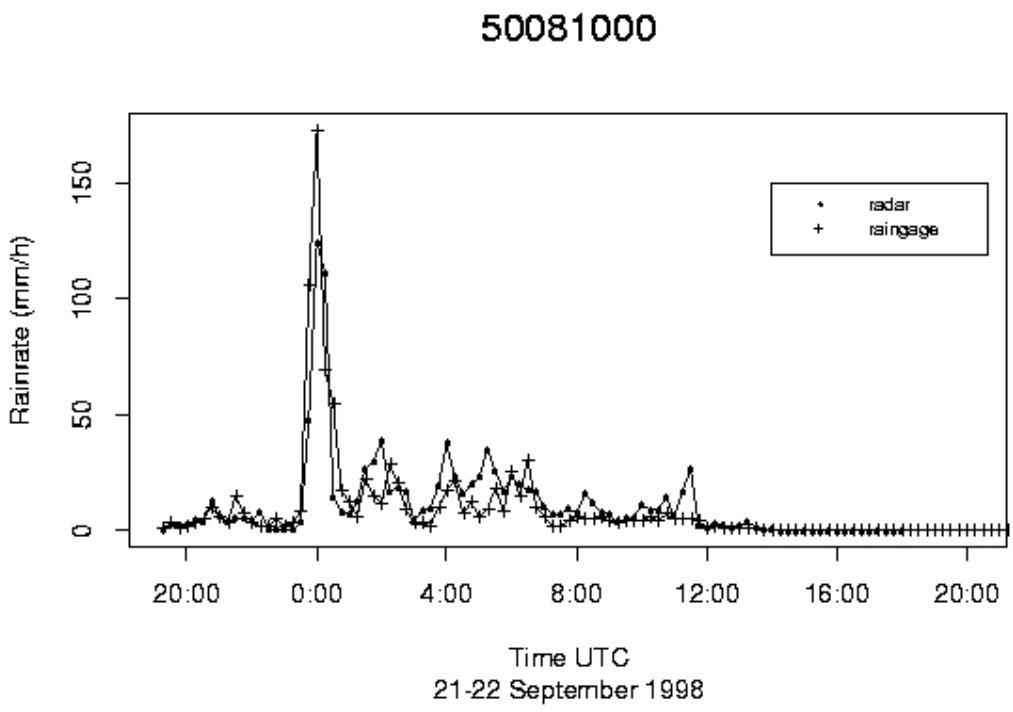

Figure 4.3a Time series of rain gage and radar rainfall estimate at 15 minute time interval for the Rio Humacao gage (USGS ID 50081000). Radar rainfall estimates were derived using the tropical Z-R relationship (see text for additional details)

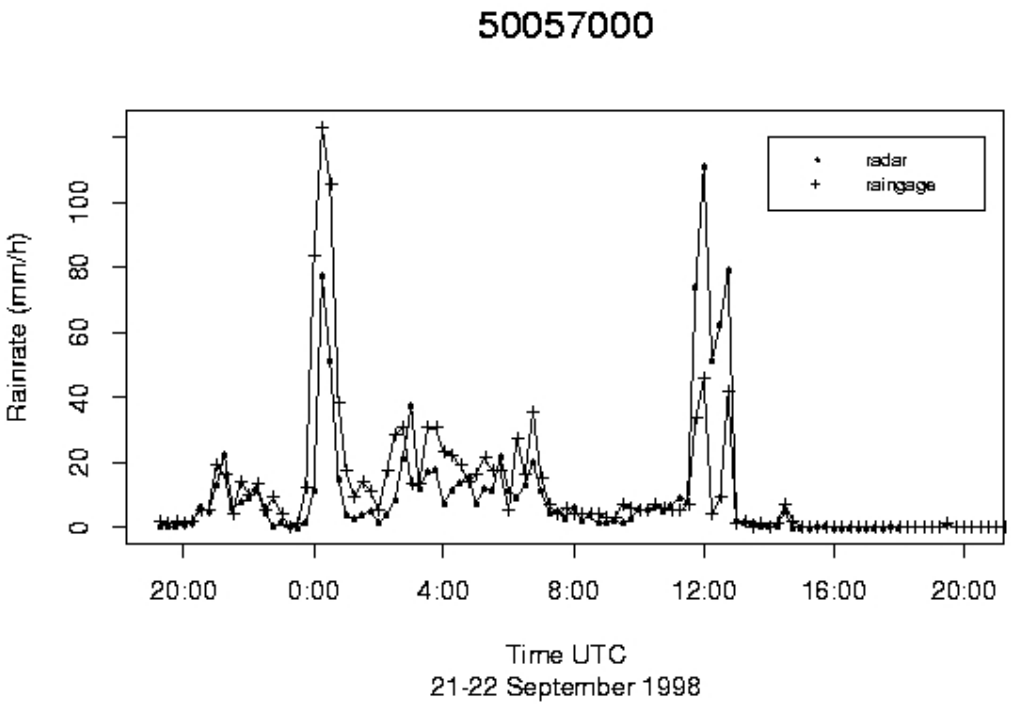

Figure 4.3b Time series of rain gage and radar rainfall estimate at 15 minute time interval for the Rio Gurabo gage (USGS ID 50057000). Radar rainfall estimates were derived using the tropical Z-R relationship (see text for additional details)

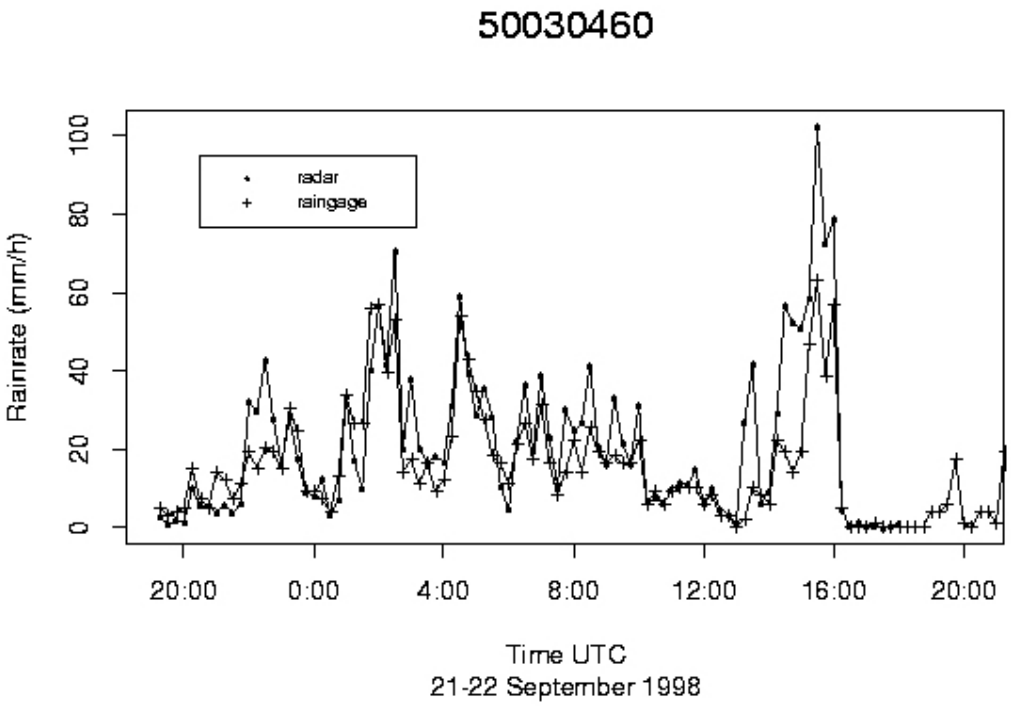

Figure 4.3c Time series of rain gage and radar rainfall estimate at 15 minute time interval for the Rio Orocovis gage (USGS ID 50030460). Radar rainfall estimates were derived using the tropical Z-R relationship (see text for additional details)

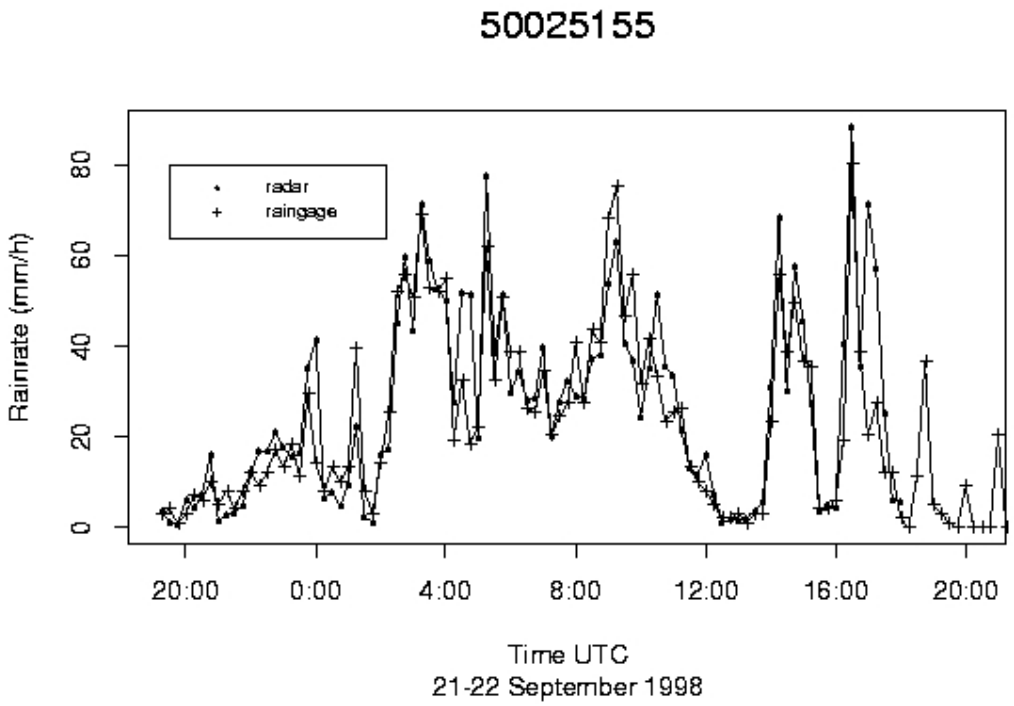

Figure 4.3d Time series of rain gage and radar rainfall estimate at 15 minute time interval for the Rio Saliente gage (USGS ID 50025155). Radar rainfall estimates were derived using the tropical Z-R relationship (see text for additional details)

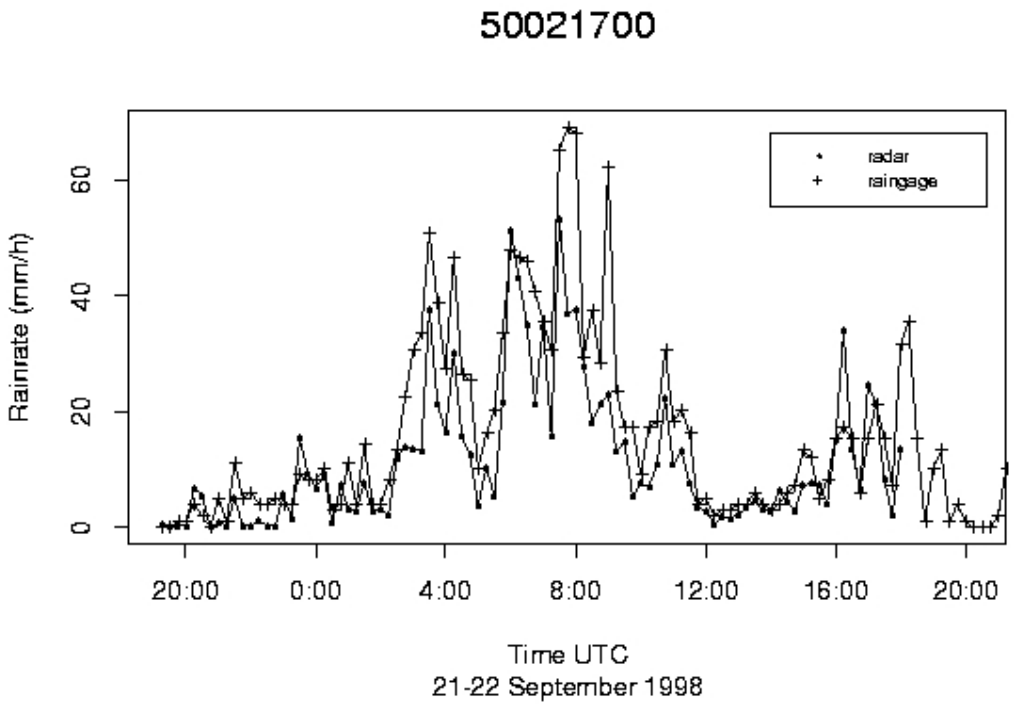

Figure4.3e Time series of rain gage and radar rainfall estimate at 15 minute time interval for the Rio Grande de Arecibo gage (USGS ID 50021700). Radar rainfall estimates were derived using the tropical Z-R relationship (see text for additional details)

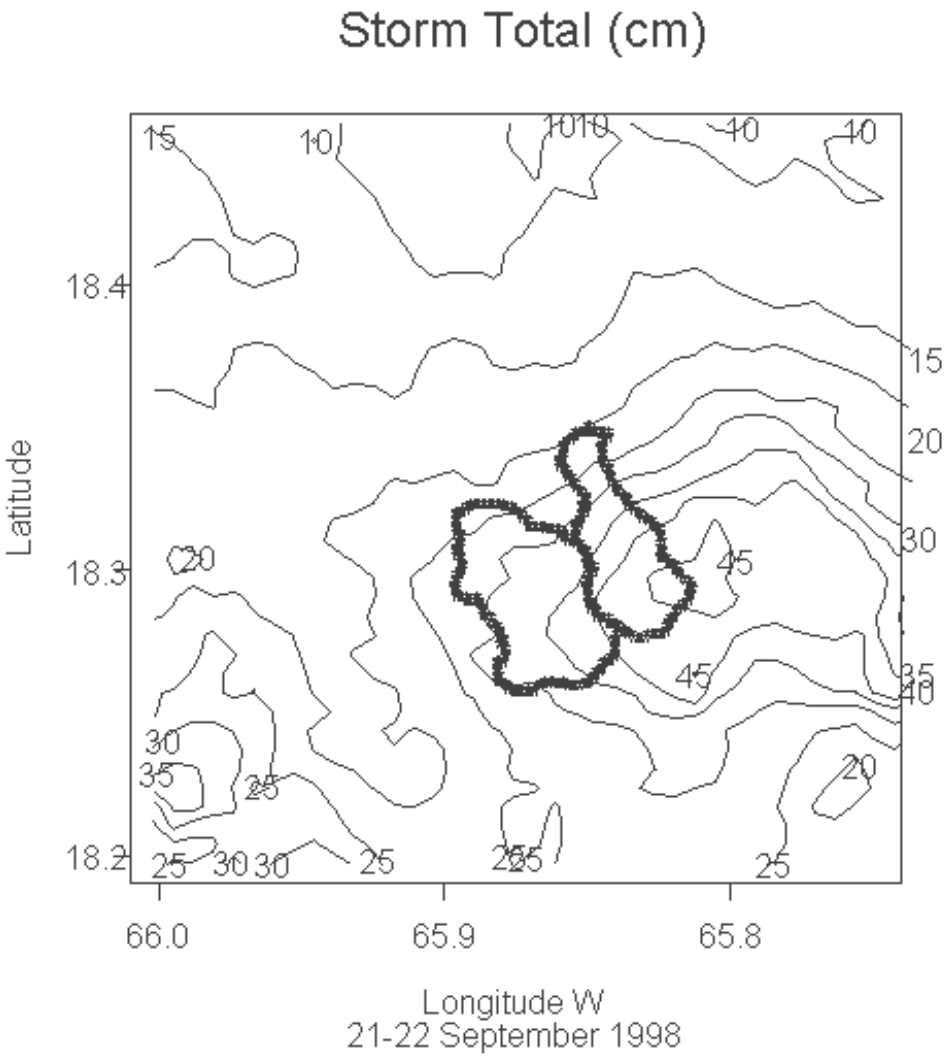

Figure 4.4.a Storm total rainfall estimates for the Rio Canovanas and Rio Grande el Verde basins. Tropical Z-R relationship was used to construct rainfall estimates.

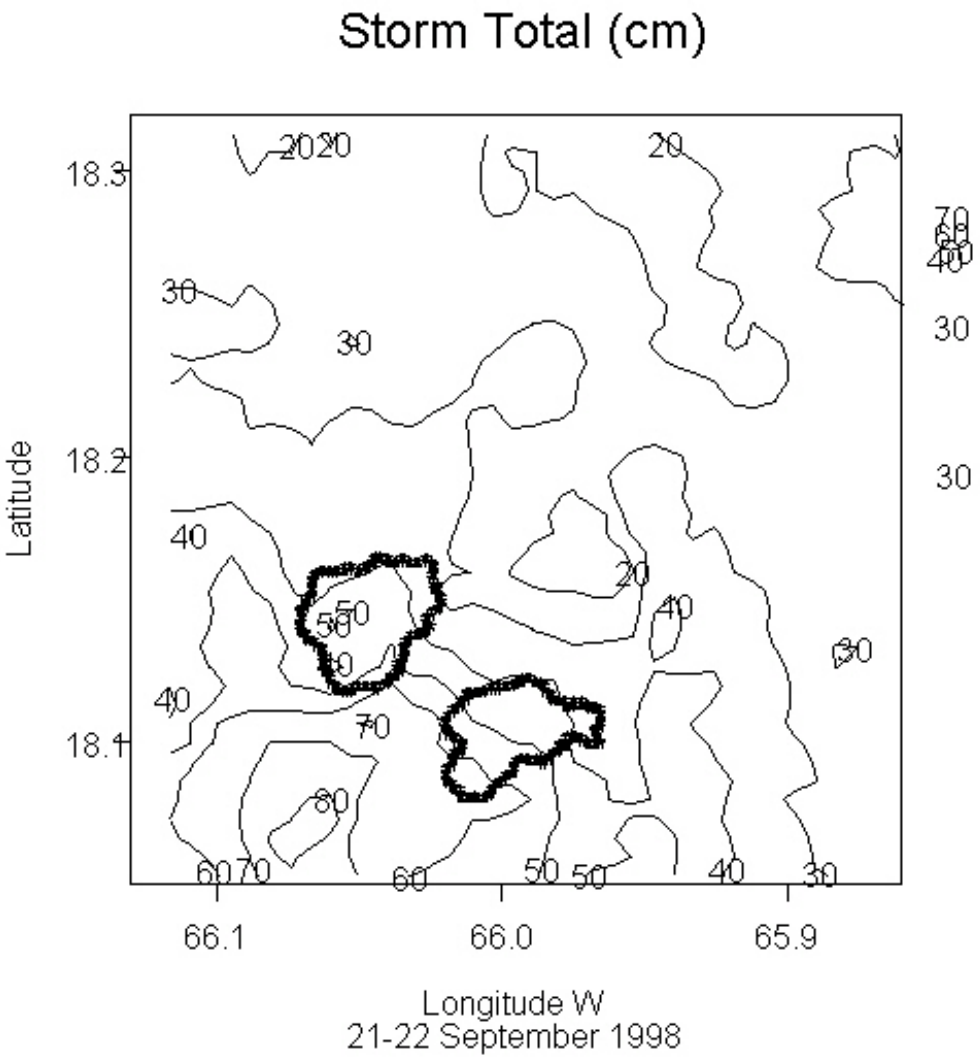

Figure 4.4.b Storm total rainfall estimates for the Rio Grande de Loiza and Rio Turabo basins. Tropical Z-R relationship was used to construct rainfall estimates

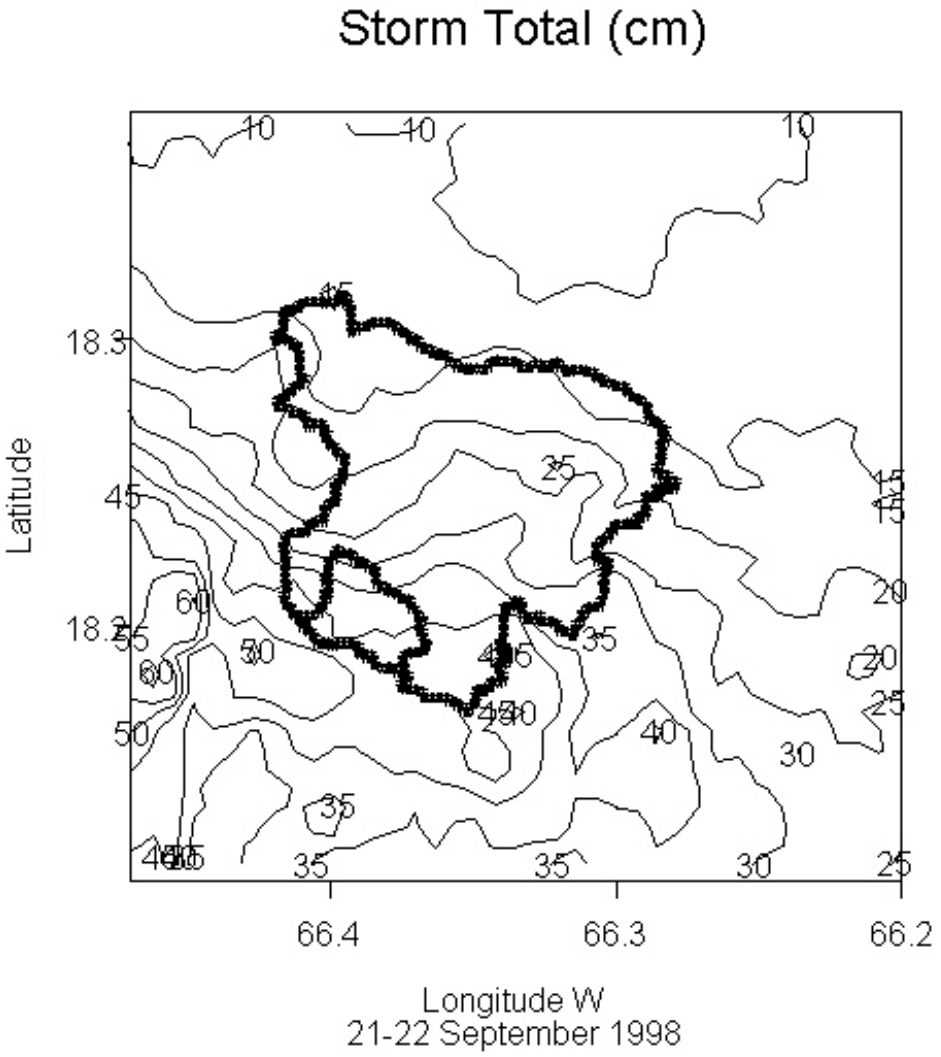

Figure 4.4 c. Storm total rainfall estimates for the Rio Orocovis and Rio Grande de Manati basins. Tropical Z-R relationship was used to construct rainfall estimates

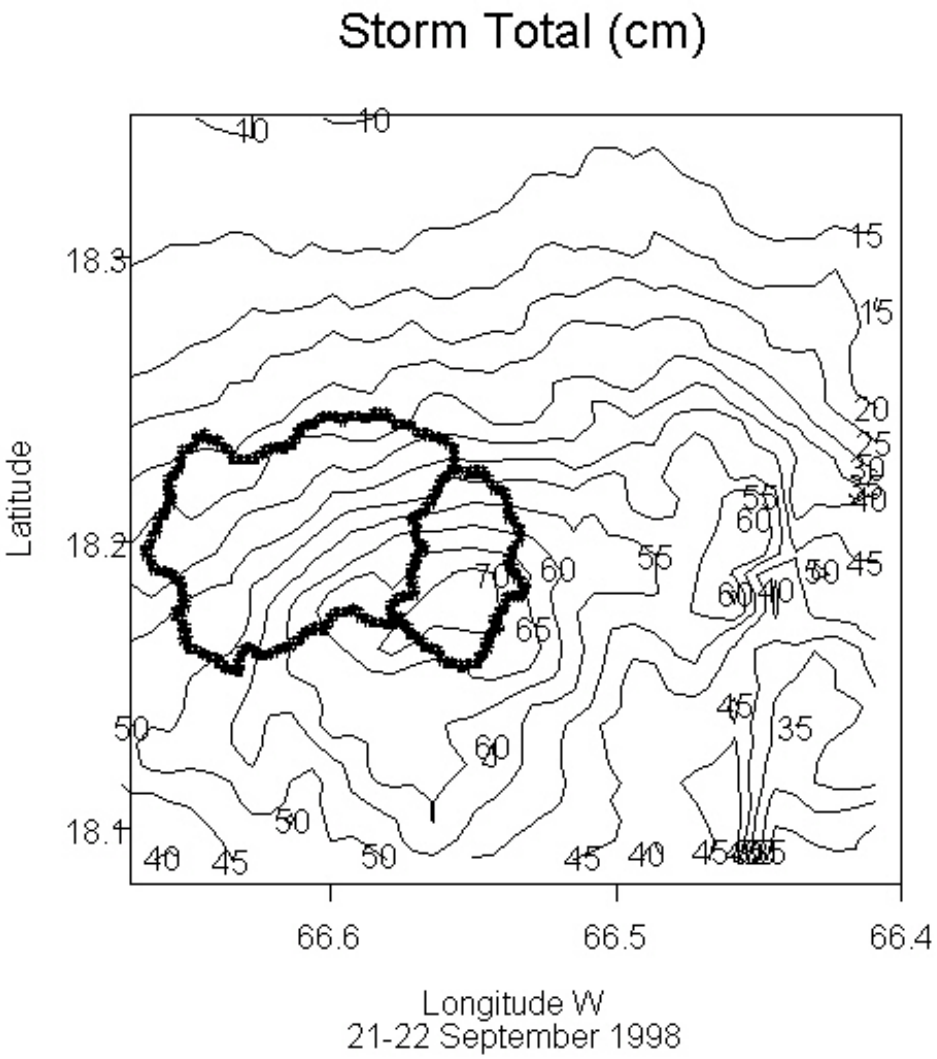

Figure 4.4 d. Storm total rainfall estimates for the Rio Saliente and Rio Caonillas basins. Tropical Z-R relationship was used to construct rainfall estimates

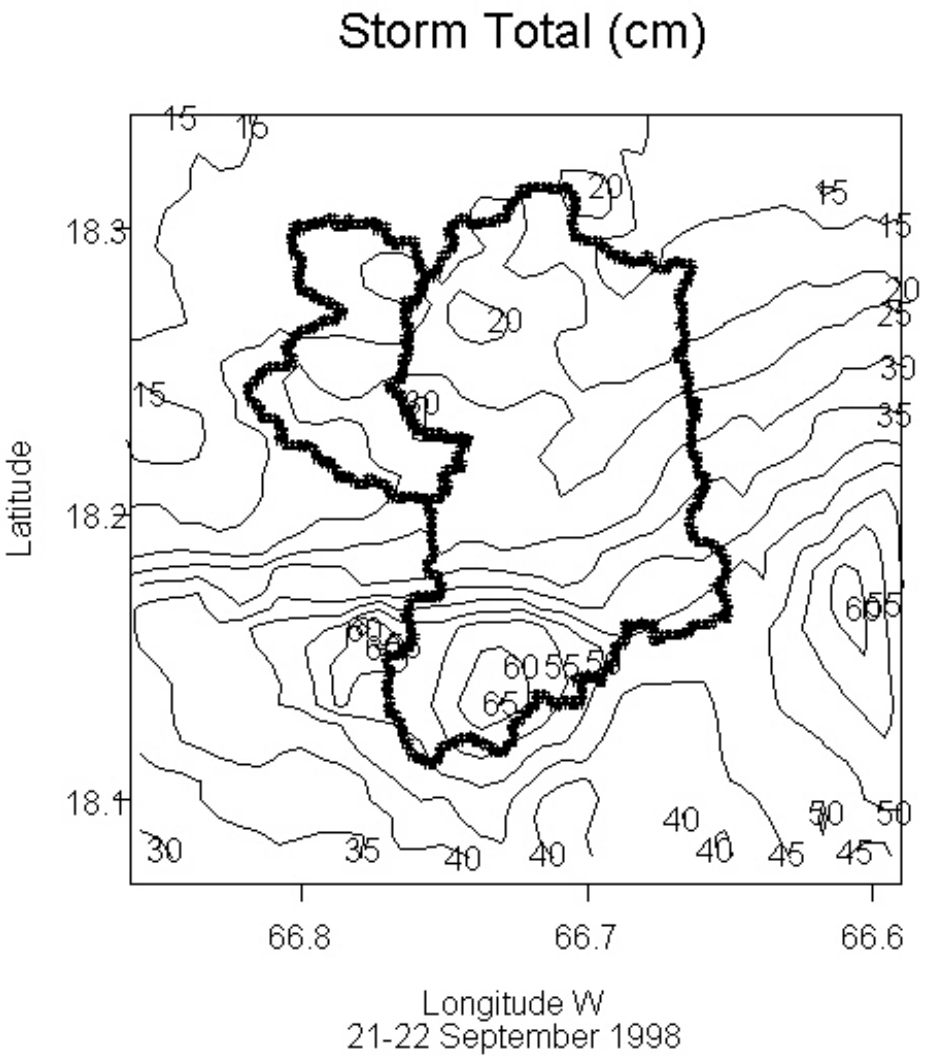

Figure 4.4 e. Storm total rainfall estimates for the Rio Grande de Arecibo and Rio Tanama basins. Tropical Z-R relationship was used to construct rainfall estimates

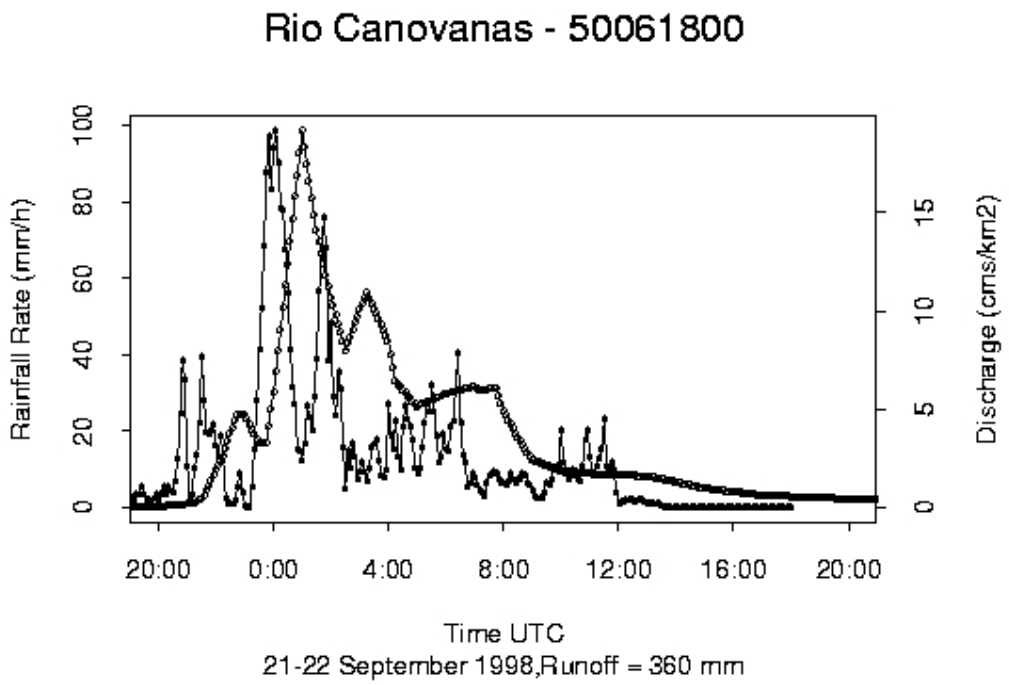

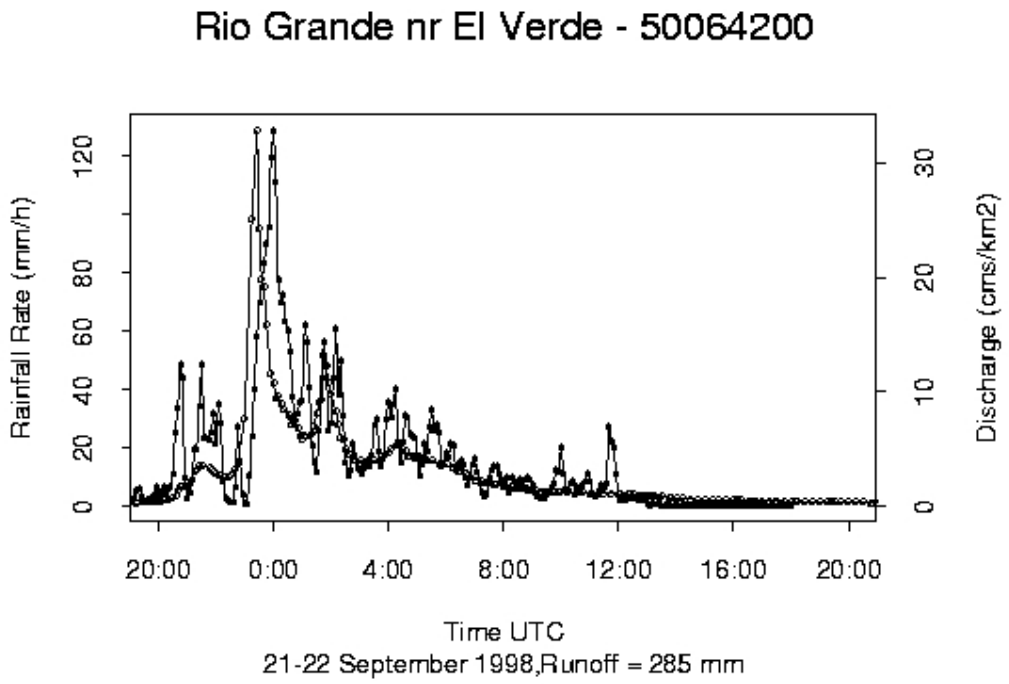

Figure 4.5a. Time series of basin-averaged rainfall and discharge for Rio Canovanas and Rio Grande El Verde.

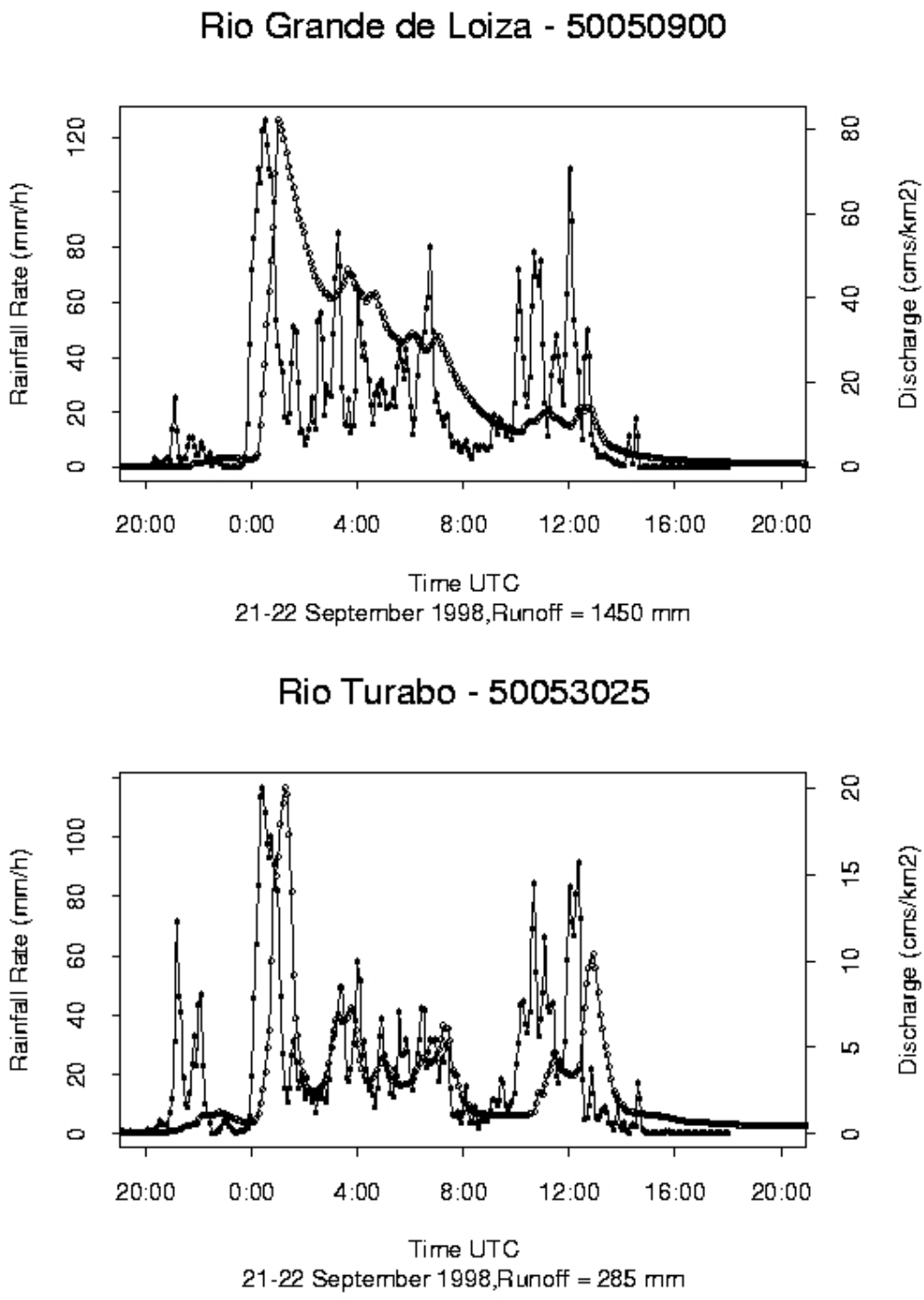

Figure 4.5b. Time series of basin-averaged rainfall and discharge for Rio Grande de Loiza and Rio Turabo.

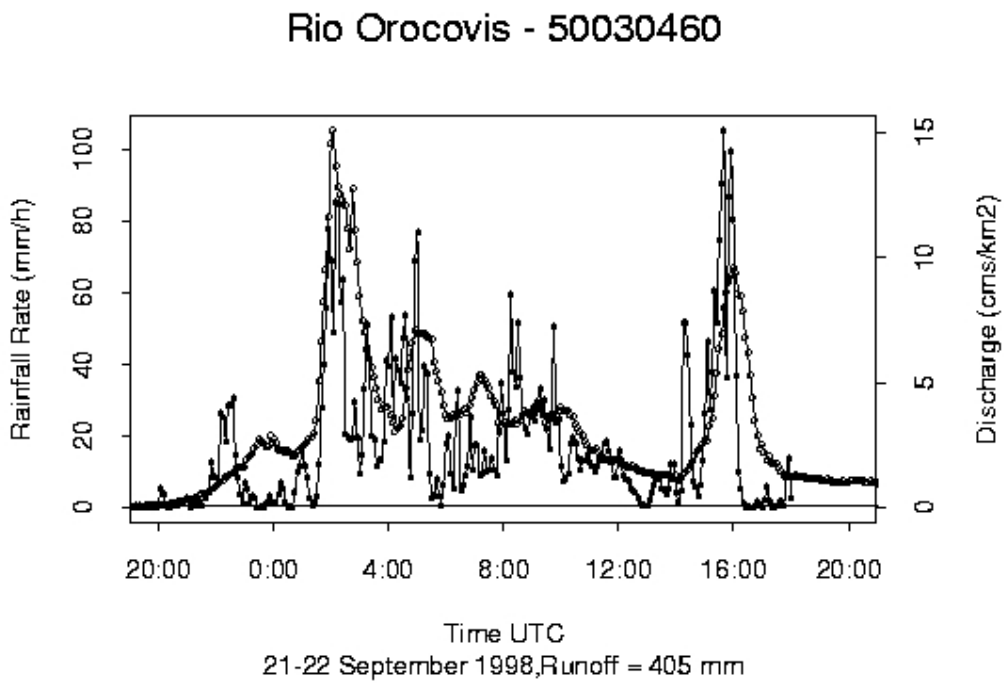

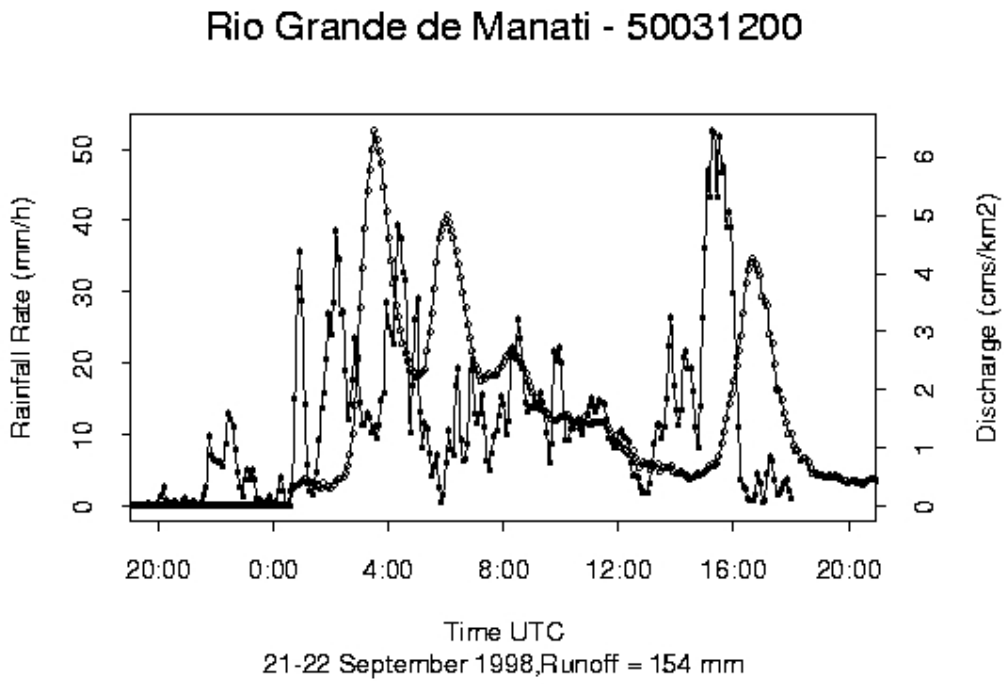

Figure 4.5c. Time series of basin-averaged rainfall rate and discharge for Rio Orocovis and Rio Grande de Manati.

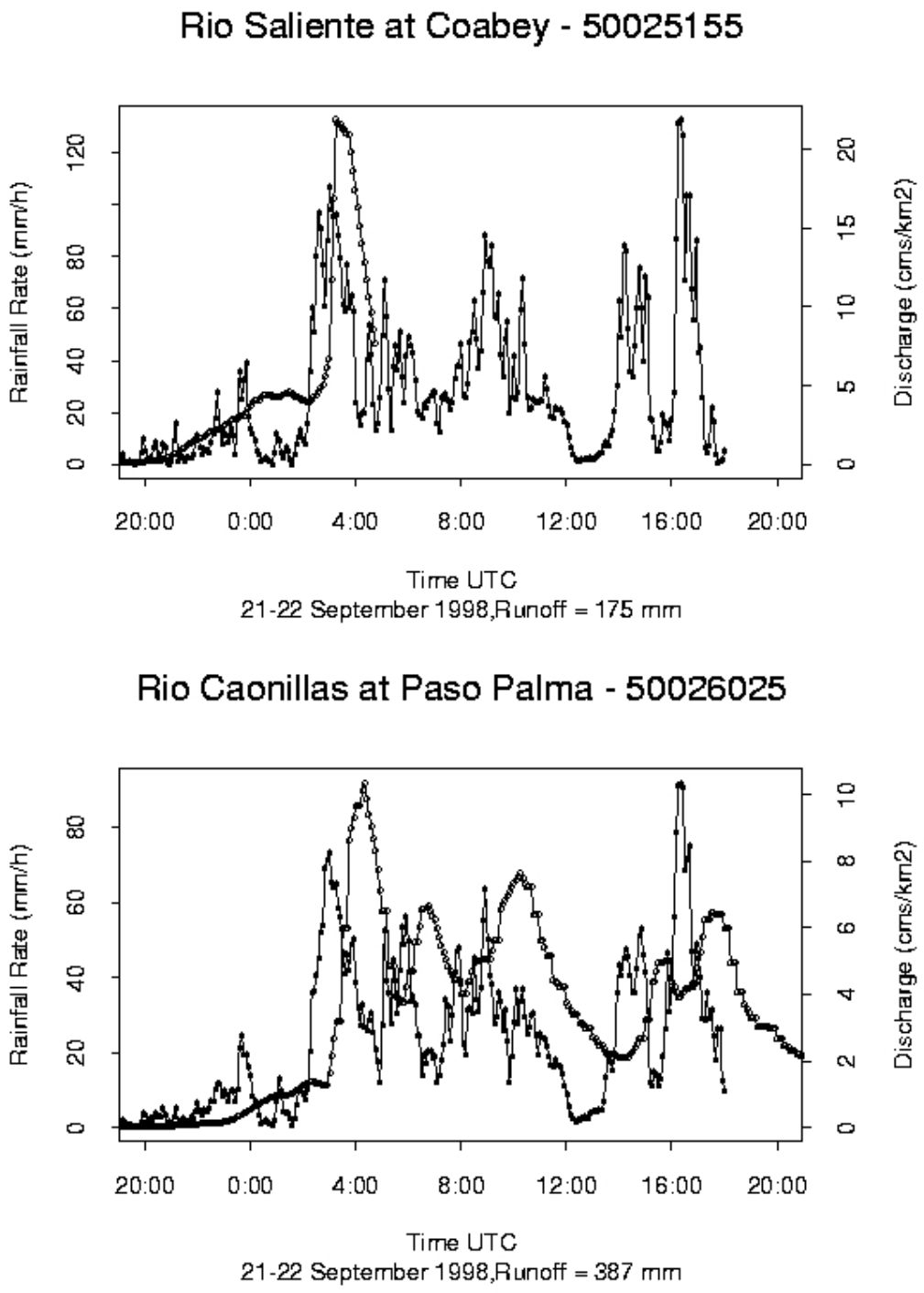

Figure 4.5d. Time series of basin-averaged rainfall rate and discharge for Rio Saliente and Rio Caonillas.

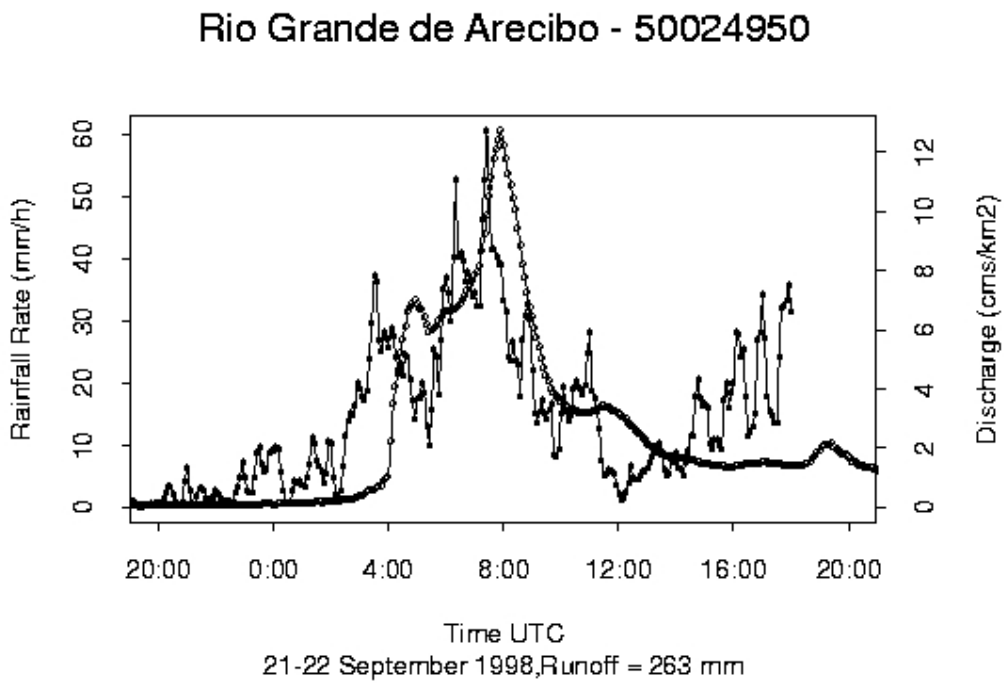

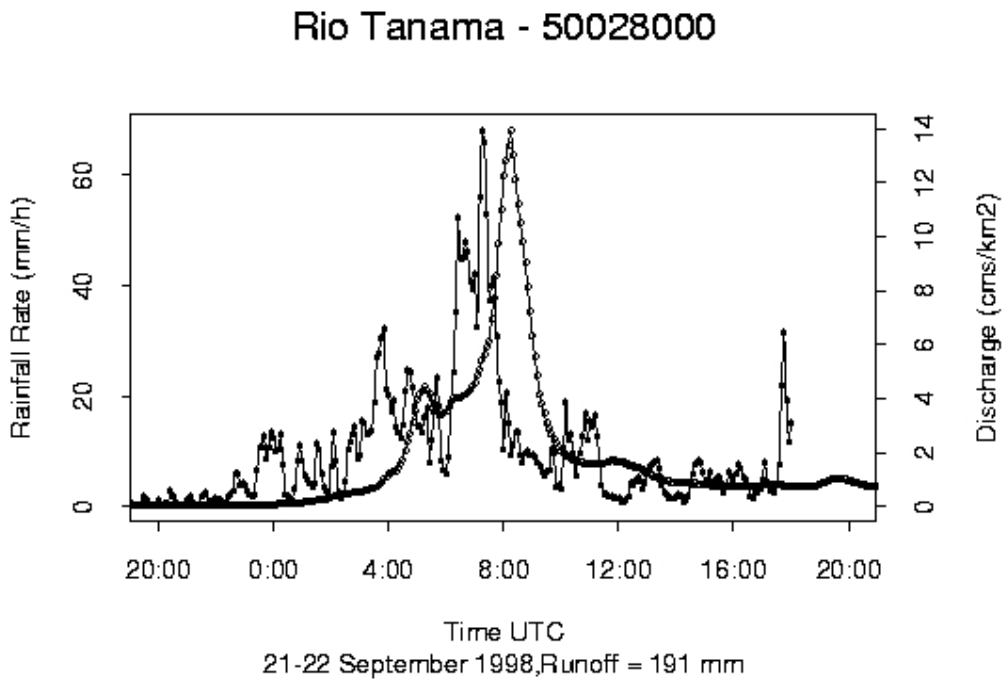

Figure 4.5e. Time series of basin-averaged rainfall rate and discharge for Rio Grande de Arecibo and Rio Tanama.

References

Baeck, M. L. and J. A. Smith, 1998, Estimation of heavy rainfall by the WSR-88D, Weather Forecasting, Weather and Forecasting, 13, 416-436.

Chappel, C., Quasistationary Convective Events in Mesoscale Meteorology, edited by P. Ray, AMS, Boston, 1989.

Ciach G. J. and W.F. Krajewski, Radar-rain gauge comparisons under observational uncertainties, Journal of Applied Meteorology, vol. 38 (10), pp. 1519-1525.

Fulton, R. A., J. P. Breidenbach, D.-J. Seo, D. A. Miller and T. O'Bannon, 1998, The WSR-88D rainfall algorithm, Weather and Forecasting, 13, 377 – 395.

Hazell, W. F. and J. D. Bales, 1997, Real-time rainfall measurements in the City of Charlotte and Mecklenburg County, North Carolina, U. S. Geological Survey Fact Sheet Fs-052-97.

Hazell, W.F., 2001, Personal Communication.

Krajewski, W. F. and J. A. Smith, 2002, Radar hydrology: rainfall estimation, Advances in Water Resources, to appear.

Larson, M. C., and A. Simon, 1993, Rainfall-threshold conditions for landslides in a humid-tropical system, Puerto Rico, Geogr. Ann. 75A (1-2), 13 – 23.

Larson, M. C., A. J. Torres-Sanchez, 1998, The frequency and distribution of recent landslides in three montane tropical regions of Puerto Rico, Geomorphology, 24, 309 – 331.

Robinson, J. B., W. F. Hazell, and W. S. Young, 1998, Effects of August 1995 and July 1997 storms in the City of Charlotte and Mecklenburg County, North Carolina, U.S. Geological Survey Fact Sheet FS-036-98.

Scatena, F. N. and M. C. Larson, 1991, Physical aspects of Hurricane Hugo in Puerto Rico, Biotropica, 23 (4A), 317 – 323.

Smith, J. A., M. L. Baeck, M. Steiner, and A. J. Miller, 1996, Catastrophic rainfall from an upslope thunderstorm in the Central Appalachians: the Rapidan Storm of June 27, 1995,Water Resources Research, 32(10), 3099 - 3113.

Smith, J. A., M. L. Baeck, J. E. Morrison, and P. Sturdevant Rees, 2000, Catastrophic rainfall and flooding in Texas, Journal of Hydrometeorology, 1(1), 5 – 25.

Smith, J. A., M. L. Baeck, P. Sturdevant-Rees, D. F. Turner-Gillespie and P. D. Bates, 2002, The regional hydrology of extreme floods in an urbanizing drainage basin, J. of Hydrometeorology, 3, pp. 267 – 281.

Smith, J. A. and W. F. Krajewski, 1993, A modeling study of rainfall rate reflectivity relationships, Water Resources Research, vol. 26 (8), pp. 2505-2514.

Smith, J. A., M. L. Baeck, J. E. Morrison, P. Sturdevant-Rees, D. F. Turner-Gillespie, and P. D. Bates, 2001, The regional hydrology of extreme floods in an urbanizing drainage basin, Journal of Hydrometeorology, 2002.

Sturdevant-Rees, P. L., J. A. Smith, J. E. Morrison, and M. L. Baeck, 2001, Tropical storms and the flood hydrology of the Central Appalachians, Water Resources Research, 37(8), 2143 – 2168.